



Universidad de Burgos

International Research Center in Critical Raw Materials for Advanced Industrial
Technologies (ICCRAM)

**Physicochemical and toxicological assessment
of commercial 2D nanomaterials**

Brixhilda Domi

Thesis for the degree of Doctor of Philosophy

2020



D. ROBERTO QUESADA PATO, Profesor Titular del Área de Química Orgánica del Departamento de Química de la Universidad de Burgos y D. JUAN ANTONIO TAMAYO RAMOS, investigador del International Research Center in Critical Raw Materials for Advanced Industrial Technologies (ICCRAM) de la Universidad de Burgos.

INFORMAN FAVORABLEMENTE:

Que la presente memoria titulada “Physicochemical and toxicological assessment of commercial 2D nanomaterials” ha sido realizada en el International Research Center in Critical Raw Materials for Advanced Industrial Technologies de la Universidad de Burgos, bajo su dirección, por la licenciada Brixhilda Domi y autorizan su presentación para que sea calificada como Tesis Doctoral.

Burgos, Noviembre 2020

Fdo.: Roberto Quesada Pato

Fdo.: Juan Antonio Tamayo Ramos



Brixhilda Domi received the MSc degree in biomedical and Molecular biology in October, 2017, with 110 cum laude (First class honours, 1st), recommendation for publication and academic mention at the "University of Amedeo Avogadro, Department of Science and Technological innovation", Alessandria, Italy. During the BSc degree and MSc degree she has been working in different Hospitals such as trainee in distinct fields: Microbiology, Cell biology and Medical Diagnosis of Allergies. In November 2017, Brixhilda won the Maria Skłodowska Curie-SOLUTION-ITN position as a PhD student supervised by Dr. Roberto Quesada Pato and co-supervised by Dr. Juan Antonio Tamayo-Ramos. The PhD project is focused on the evaluation of biocompatibility and nanotoxicity of 2D materials such as TMDs, using human tumor cell lines, bacteria and yeast.

To the Love of my Life...

"Life is not easy for any of us. But what of that?

We must have perseverance and above

all confidence in ourselves.

We must believe that we are gifted for something

and that this thing must be attained."

Marie Skłodowska Curie

Acknowledgments

The completion of this thesis has been possible thanks to the support of a great number of people who have given their intellectual and personal help throughout the last three years of my PhD thesis. Firstly, I would like to thank the “MSCA-ITN-2017 - Innovative Training Networks” and “SOLUTION” for the financial support without which this work would not have taken place. I would like to thank all the people that has been working at ICCRAM for the amazing moment spent together due to the beautiful job environment.

I am sincerely and heartily grateful to my supervisors Professor Roberto Quesada and Dr. Juan Antonio Tamayo-Ramos for selecting me to be a part of this innovative and exciting European project, and for providing me encouragement, independence, technically and scientific support in the research. I thank Dr. Carlos Rumbo Lorenzo for the laboratory help and theoretical knowledge in cell biology and his constant guidance and patience as a tutor. It was a great pleasure working for and with them. They are very good advisors and also nice colleagues. A very special thanks to Alfredo Bol, who helped me in several situations as a mentor.

Special thanks to another collaborator Professor Spyros Yannopolus’ group in FORTH-NET center, Patras, Greece for providing TMDs samples (fabricated by Kaphil Bhorkar, doctoral student) that I used for the in vitro assessment and also for inviting me for two months internship at his group.

I thank Sonia Martel and Mariluz Ortega, project manager and secretary at ICCRAM, who taught me all the little details of the administrative part at the beginning of my job contract and thesis. I also thank Loukia and Claudia for giving me emotional support for this difficult journey.

Last but not least, I thank my parents who continuously supported me throughout these three years of PhD, especially during the writing of this thesis. Special thanks to my boyfriend and future husband Salvatore, for helping and accompanying me in the most difficult moments. He has always been by my side encouraging me to never give up.

Brixhilda Domi

bdomi@ubu.es

brixhildadomi@gmail.com

688 473 093

ICCRAM-Universidad de Burgos

Resumen

Los nanomateriales bidimensionales (2D) han atraído una atención significativa como materiales de próxima generación. Las propiedades físico-químicas conferidas por una estructura en forma de capas con un espesor de átomos han dado lugar a su utilización en múltiples aplicaciones. En la última década se han realizado numerosos trabajos de investigación encaminados a evaluar la diferente toxicidad de estos nanomateriales. Sin embargo, la mayoría de estos trabajos se centran en nanopartículas sintetizadas en pequeña escala en laboratorio, sin ahondar en aspectos claves, como la caracterización físico-química de las nanopartículas, las dosis relevantes o la duración de la exposición. El objetivo principal de esta tesis es aumentar nuestra comprensión de las interacciones biológicas entre nanomateriales 2D y sistemas biológicos. Para ello se han utilizado diferentes nanomateriales disponibles comercialmente para evaluar la nanotoxicología asociada con los mismos en diferentes modelos celulares in vitro.

Palabras clave

Nanopartículas, nanotoxicidad, viabilidad celular, estrés oxidativo, análisis fisicoquímico

CODIGO UNESCO

BIOLOGIA MOLECULAR: 230221

COMPUESTOS DE AZUFRE: 230327

QUIMICA DEL ESTADO SOLIDO: 221028

CULTIVO CELULAR: 240701

Abstract

Two-dimensional nanomaterials (2D) have attracted significant attention as next generation materials. Multiple applications due to physico-chemical proprieties and the fascinating layered structure of a thickness of at least one atomic layer have emerged. However, concerns have been raised about the safety and biocompatibility of 2D nanomaterials due to contradictory results in several *in vitro* and *in vivo* nanotoxicological studies. Specifically, scientific data on the potential hazard of nanoparticles has underline the capability of layered nanomaterials to cross biological barriers, inducing reduction on cellular viability and increasing oxidative stress. In the last decade, the application of 2D nanomaterials has seen a rapid growing in the industrial field and, as a consequence, the safety assessment is necessary in order to develop biocompatible and safe nanotechnology. Notwithstanding numerous research efforts being made in the past decade to assess the different toxicity of nanomaterials, most of these scientific works focus on laboratory made nanoparticles, without tackling numerous aspects, such as apposite nanoparticle physico-chemical characterization, relevant doses and exposure duration. Therefore, the aim of this PhD thesis is to investigate the possible *in vitro* acute toxic effects of several 2D nanomaterials beyond graphene, considering the different physico-chemical proprieties of commercial graphene oxide, transition metal dichalcogenides (TMDs) and boron nitride, as well as the potential chemical degradation and oxidation in the environmental fate of TMDs, taking into consideration the possible differences in the toxicological responses of different eukaryotic and prokaryotic cells. The main goal of this thesis was to use different cellular models and *in vitro* cytotoxic assays to address several challenges in nanotoxicology, in order to increase our understanding of the biological interactions between 2D nanomaterials and biological systems.

Content

Chapter 1	1
General Introduction.....	1
Nanoparticles and Nanotechnology	2
Dimensionality	4
Morphology	6
Composition.....	7
Aggregation/Agglomeration.....	7
Physico-chemical properties of 2D materials and applications	8
Introduction to Graphene and Graphene Oxide	9
Synthesis.....	11
Applications	13
Graphene oxide	14
Synthesis.....	15
Applications	16
Introduction to Transition Metal Dichalcogenides	17
Synthesis.....	19
Applications	22
Introduction to Boron nitride	23
Synthesis.....	25
Applications	26
Potential hazards of 2D nanomaterials for human health and environment	27
Human exposure	27
Nanotoxicology of 2D materials	29
Toxicity of Graphene Oxide	32
Toxicity of Molybdenum Disulfide and Tungsten Disulfide.....	34
Toxicity of Boron Nitride	36
Aim of the research thesis.....	38
Chapter 2	42
Graphene Oxide Derivates	42
Interaction analysis of commercial graphene oxide nanoparticles with unicellular systems and biomolecules.....	43
Chapter 3	88
Transition Metal Dichalcogenides (TMDs)	88
Fate assessment of commercial 2D MoS ₂ aqueous dispersions at physicochemical and toxicological level.....	89

Toxicological assessment of commercial 2D WS ₂ aqueous suspensions using different eukaryotic models	128
Chapter 4	158
<i>Boron nitride nanosheets</i>	158
Low toxicity of commercial 2D boron nitride nanopowder and nanoplatelets towards eukaryotic cellular models	159
Chapter 5	188
<i>General Discussion and Conclusion</i>	188
General Discussion	189
Conclusion	213

Chapter 1

General Introduction

Nanoparticles and Nanotechnology

Nanotechnology and Nanoscience are described as an interdisciplinary discipline covering different scientific fields including biology, chemistry, physics, and material science¹. The specific term of “nanotechnology” was introduced by Taniguchi in 1974, indicating the possibility to use engineered materials at the nanometer level in several technological applications². For instance, nanotechnologies have an extensive use from electronics and computing to environmental applications, from agriculture, water purification to aerospace industry, among numerous others. Besides industrial and household uses, nanoparticles (NPs) can be used in the medicine field for the treatment of cancer, immunization purposes, infectious diseases and diagnostic procedures with new imaging agents and sensors. Specifically, the innovatory era on nanotechnology corresponds to the second half of the XX Century³. The development of new nanomaterials, through intensive research at different levels such as atomic, molecular and macro- molecular scales, has facilitated their new applications fields and physico-chemical proprieties⁴. The description of “nanoparticle” set by the European Commission include particles

¹ The Royal Society & The Royal Academy of Engineering, Nanoscience and Nanotechnologies: Opportunities and Uncertainties; July 2004.

² Bayda, S.; Adeel, M.; Tuccinardi, T.; Cordani, M.; Rizzolio F. The History of Nanoscience and Nanotechnology: From Chemical–Physical Applications to Nanomedicine. *Molecules*. 2020 Jan; 25(1): 112.

³ Ferreira, A. J.; Cemlyn-Jones, J.; Cordeiro, C. R. Nanoparticles, Nanotechnology and Pulmonary Nanotoxicology. *Fisioterapia* 2013, 19 (1), 28–37.

⁴ Jeevanandam, J.; Barhoum, A.; Chan, Y. S.; Dufresne, A.; Danquah, M. K. Review on Nanoparticles and Nanostructured Materials: History, Sources, Toxicity and Regulations. *Beilstein J. Nanotechnol.* 2018, 9, 1050–1074.

with size of 100 nm or smaller⁵. These nanoparticles have distinguishing properties different to those of the parent bulk material because of their small size and larger specific surface area. Moreover, at the nanoscale range, the impact of quantum effects can alter significant properties, such as electrical, magnetic and optical properties^{6,7}. Therefore, the intensive use of NPs could determine the nanoscience and nanotechnology a key element for the next industrial revolution⁸. For instance, the increased use of nanotechnology allowed the manipulations of several materials at the nanometer scale, follow-on in the production of instruments and technologies never visualized previously. Furthermore, the rising of new potential application fields, lead to new novel class of low dimensional systems of nanoscale sciences. Specifically, the global market for nanomaterials estimated by the European Commission excess €20 billion. Moreover, another interesting feature is the large typologies of nanoparticles present in the market⁹. Nanomaterials can be categorized based on their intrinsic proprieties such as dimensionality, morphology, composition and agglomeration state.

⁵ European commission, Nanomaterials.

⁶ Ferreira, A. J.; Cemlyn-Jones, J.; Cordeiro, C. R. Nanoparticles, Nanotechnology and Pulmonary Nanotoxicology. *Fisioterapia* 2013, 19 (1), 28–37.

⁷ Health Care Without Harm Europe. Nanomedicine New Solutions or New Problems? 2013.

⁸ Cappy, A.; Stievenard, D.; Vuillaume, D. Nanotechnology: The Next Industrial Revolution? Gallium Arsenide applications symposium. GAAS 2002, 23-27.

⁹ Nanomaterials | Internal Market, Industry, Entrepreneurship and SMEs.

Dimensionality

This categorization is centered on the number of dimensions of the material, which are outside the nanoscale (<100 nm) range. A representative image is shown in Figure 1.

0D nanomaterials:

The 0D materials, the three dimensions are in the nanoscale range, with a diameter less than 100 nm. In this category are included quantum dots, spheres, clusters and nanocrystals. Because of the intrinsic structural properties of 0D nanomaterials, such as high surface-to-volume ratios and ultra-small sizes, they have further active sites per unit mass. The quantum confinement effects of these nanomaterials provide them supplementary properties such as high photoluminescence (PL) quantum efficiency and chemiluminescence^{10,11}.

1D nanomaterials:

The materials in the nanometer scale with one dimension, are defined as materials with two dimensions at the nanoscale and one dimension at the macroscale. These materials exhibit several properties such as superior light absorption, excellent electronic conduction, high mechanical strength, and

¹⁰ Wang, Z.; Hu, T.; Liang, R.; Wei, M. Application of Zero-Dimensional Nanomaterials in Biosensing. *Frontiers in Chemistry*. Frontiers Media S.A. April 17, 2020, p 320.

¹¹ Cao, H. Synthesis, Characterization, and Applications of Zero-Dimensional (0D) Nanostructures. In *Synthesis and Applications of Inorganic Nanostructures*; Wiley-VCH Verlag GmbH & Co. KGaA: Weinheim, Germany, 2017; pp 21–146.

ultra-low thermal conductivity. In this category are present films and surface coatings, specifically used for decades in various fields, such as electronics, chemistry, and engineering^{12,13}.

2D nanomaterials:

Two-dimensional nanomaterials have one dimension at the macroscale range and two dimensions in the nanometer scale. In this category are included several 2D nanostructured films, nanopores, nanofibers and plate-like shapes particles¹⁴. Differing to their bulk materials, these 2D nanomaterials have a high aspect ratio (surface-area-to-volume ratio) and numerous atoms on their surface. Because of their excellent proprieties, they are utilized in different fields such as electronics, optoelectronics, solar cells, lithium batteries, composites, etc.¹⁵

3D nanomaterials:

Three-dimensional nanomaterials have all the dimensions in the macroscale range and no dimensions in the nanoscale range. This class can contain

¹² Xie, J. Le; Guo, C. X.; Li, C. M. Construction of One-Dimensional Nanostructures on Graphene for Efficient Energy Conversion and Storage. *Energy and Environmental Science*. Royal Society of Chemistry July 18, 2014, pp 2559–2579.

¹³ Garnett, E.; Mai, L.; Yang, P. Introduction: 1D Nanomaterials/Nanowires. *Chemical Reviews*. American Chemical Society August 14, 2019, pp 8955–8957.

¹⁴ Rafiei-Sarmazdeh, Z.; Morteza Zahedi-Dizaji, S.; Kafi Kang, A. Two-Dimensional Nanomaterials. In *Nanostructures*; IntechOpen, 2020.

¹⁵ Kim, S.; Kim, K. H.; Bark, C. W. Two-Dimensional Nanomaterials: Their Structures, Synthesis, and Applications. *Sci. Adv. Mater.* 2017, 9, 1441–1457.

dispersion of nanoparticles, bulk powders, nanowires, nanotubes as well as multi-nanolayers¹⁶.

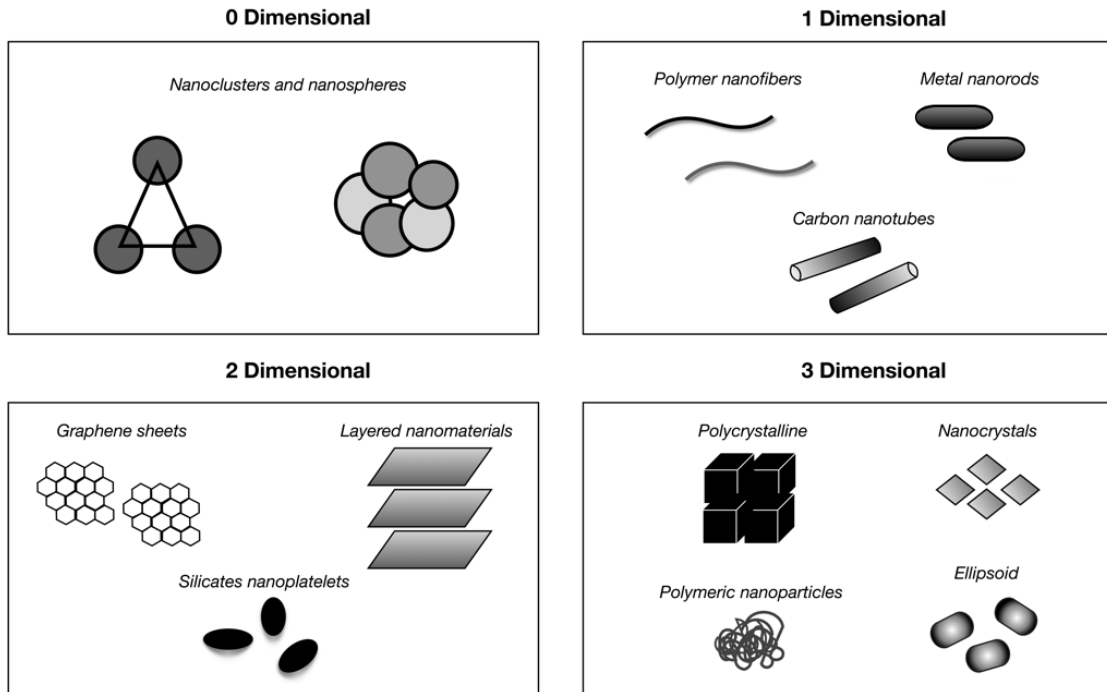


Figure 1: Schematic representation of the various dimensions of the nanomaterials (0D, 1D, 2D and 3D) and examples.

Morphology

Other aspects to take in consideration for the categorization of NPs are the morphological characteristics, including: sphericity, flatness and aspect ratio. For instance, the category of high aspect ratio nanoparticles is represented by nanotubes and nanowires, with various shapes. Instead, the small-aspect ratio morphologies include several shapes such as oval, spherical, prism, cubic and

¹⁶ Nanotechnology Introduction - new materials.

helical. Additionally, several commercial nanoparticles occur as powders, suspensions, or colloids¹⁷.

Composition

Nanoparticles can be made of several heterogeneous materials or of a single component material. The composition of a specific nanoparticle can be very complicated, differing on what interactions it has had with other particles and chemicals on its lifetime. For instance, the nanoparticles originated in nature are frequently agglomerations of materials with diverse compositions, whereas pure single-composition materials can be simply synthesized using a variety of physical and chemical methods¹⁸.

Aggregation/Agglomeration

Nanoparticles can exist as suspensions/colloids, dispersed aerosols or in an agglomerates state. The specific state depends on their chemistry and electromagnetic properties. Aggregation and agglomeration are two terms used for the description of the assemblage of particles in a sample¹⁹. Specifically, the aggregation process is reversible, whereas the agglomeration is irreversible. These two processes, such as other transformations in the environments, can alter important physico-chemical features such as nanoparticles' chemical

¹⁷ Buzea, C.; Pacheco, I. I.; Robbie, K. Nanomaterials and Nanoparticles: Sources and Toxicity. *Biointerphases* 2007, 2 (4), MR17–MR71.

¹⁸ Nanotechnologies: 3. What are the physical and chemical properties of nanoparticles?

¹⁹ Walter, D. *Contributions 1.1 Primary Particles-Agglomerates-Aggregates*.

reactivity, fate and biological interactions. For example, magnetic nanoparticles tend to aggregate and act as larger nanoparticles, depending on the size of the aggregate²⁰.

Physico-chemical properties of 2D materials and applications

The principal feature that distinguishes numerous classes of nanostructures is the dimension. As described before, the dimensionality is one of the principal parameters in material science, which not simply delineates the atomic structure of the material, but determines also the physico-chemical properties. One of the best-known and used nanomaterials are the family of the two-dimensional (2D) materials²¹. This class of single-atom thick materials represents the thinnest nanomaterials due to their dimensions and thickness on nanoscale and macroscale range²². These materials have a distinctive layered structure with weak van der Waals forces between layers and strong in-plane covalent bonds. This layered structure allows the possibility of being sliced into individual separate atomic layers determining outstanding physical and chemical properties very different to those of their bulk counterparts. Because of their exceptional properties, 2D nanostructures could have a

²⁰ Ashraf, M. A.; Peng, W.; Zare, Y.; Rhee, K. Y. Effects of Size and Aggregation/Agglomeration of Nanoparticles on the Interfacial/Interphase Properties and Tensile Strength of Polymer Nanocomposites. *Nanoscale Res. Lett.* 2018, 13 (1), 1–7.

²¹ Khan, K.; Tareen, A. K.; Aslam, M.; Wang, R.; Zhang, Y.; Mahmood, A.; Ouyang, Z.; Zhang, H.; Guo, Z. Recent Developments in Emerging Two-Dimensional Materials and Their Applications. *J. Mater. Chem. C* 2020, 8 (2), 387–440.

²² Choi, W.; Choudhary, N.; Han, G. H.; Park, J.; Akinwande, D.; Lee, Y. H. Recent Development of Two-Dimensional Transition Metal Dichalcogenides and Their Applications. *Mater. Today* 2017, 20 (3), 116–130.

significant impact on multiple applications, ranging from electronics, catalyst, high performance sensors, support membranes, biomedicine, drug delivery etc.²³ As practical applications of these materials became widespread, further research efforts are put in the development of proficient techniques to produce 2D nanosheets with definite number of layers and tune their properties as well as investigating heterogeneous 2D nanomaterials, combining different layers from different materials²⁴. At present, the 2D nanomaterials family includes graphene and other layered materials such as transition metal dichalcogenides (TMDs), mono-elemental 2D semiconductors (silicene, germanene, stanene, and phosphorene), MXenes, 2D oxide/hydroxide materials and hexagonal boron nitride²⁵. The physico-chemical properties and methods of synthesis/preparation of the specific categories of the nanomaterials used in this thesis for the evaluation of their potential cytotoxic effects will be detailed explained in the follow paragraph.

Introduction to Graphene and Graphene Oxide

Graphene

The most prominent two-dimensional material is graphene, a carbon structure composed of a single atomic layer sp^2 -bonded carbon atom hexagonal

²³ Banerjee, A. N. Graphene and Its Derivatives as Biomedical Materials: Future Prospects and Challenges. *Interface Focus*. Royal Society Publishing June 6, 2018.

²⁴ Tyagi, D.; Wang, H.; Huang, W.; Hu, L.; Tang, Y.; Guo, Z.; Ouyang, Z.; Zhang, H. Recent Advances in Two-Dimensional-Material-Based Sensing Technology toward Health and Environmental Monitoring Applications. *Nanoscale*. Royal Society of Chemistry February 14, 2020, pp 3535–3559.

²⁵ Agarwal, V.; Chatterjee, K. Recent Advances in the Field of Transition Metal Dichalcogenides for Biomedical Applications. *Nanoscale* 2018, 10 (35), 16365–16397.

framework. The connection between the carbon atoms is strong enough to tolerate external force by a twisting lattice plane to prevent the reconfiguration of atoms²⁶. The famous discovery of this compound in 2004 fascinated a lot of consideration and led to the detection of several properties such as electronic properties, unprecedented impermeability, high mechanical strength, excellent thermal and electrical conduction²⁷. Furthermore, graphene is a semimetal or a semiconductor with a bandgap of zero and has very high electron mobility at room temperature. For instance, single-layer graphene has an unexpected high degree of transparency in UV-Vis and IR radiation and it is also considered as one of the strongest materials²⁸. Different improvements of the synthesis and functionalization of graphene have amplified the application of these materials in many fields, such as composite materials, energy technology, catalyst and sensors²⁹. For example, graphene shows great ability to be functionalized with several functional groups in the form of covalent and noncovalent which leads to its solubility in different solvents³⁰. Moreover, the potential biocompatibility of graphene has encouraged investigations toward applications in the

²⁶ Yang, G.; Li, L.; Lee, W. B.; Ng, M. C. Structure of Graphene and Its Disorders: A Review. *Science and Technology of Advanced Materials*. Taylor and Francis Ltd. December 31, 2018, pp 613–648.

²⁷ Novoselov, K. S.; Morozov, S. V.; Mohinddin, T. M. G.; Ponomarenko, L. A.; Elias, D. C.; Yang, R.; Barbolina, I. I.; Blake, P.; Booth, T. J.; Jiang, D.; et al. Electronic Properties of Graphene. In *Physica Status Solidi (B) Basic Research*; John Wiley & Sons, Ltd, 2007; Vol. 244, pp 4106–4111.

²⁸ Xia, F.; Yan, H.; Avouris, P. The Interaction of Light and Graphene: Basics, Devices, and Applications. *Proc. IEEE* 2013, 101 (7), 1717–1731.

²⁹ Chen, H.; Gao, Q.; Li, J.; Lin, J. M. Graphene Materials-Based Chemiluminescence for Sensing. *Journal of Photochemistry and Photobiology C: Photochemistry Reviews*. Elsevier B.V. January 19, 2016, pp 54–71.

³⁰ Georgakilas, V.; Otyepka, M.; Bourlinos, A. B.; Chandra, V.; Kim, N.; Kemp, K. C.; Hobza, P.; Zboril, R.; Kim, K. S. Functionalization of Graphene: Covalent and Non-Covalent Approaches, Derivatives and Applications. *Chem. Rev.* 2012, 112 (11), 6156–6214.

biomedical field³¹. Given these extraordinary mechanical properties, further potential applications in nanocomposite and coating industries are estimated to be opened.

Synthesis

There are several synthesis methods for graphene, including advantages and disadvantages:

Mechanical exfoliation

Mechanical exfoliation is a top-down technique and it's the scarcest utilized methods for the extraction single layer graphene flakes from graphite on chosen substrates. The principal source is graphite, made of mono-atomic graphene layers stacked together by weak van der Waals forces. Hence, the exfoliation process is the opposite of the stacking process, where due to the weak bonding it is possible to separate the layers. Several graphene sheets can be obtained throughout mechanical exfoliation or by peeling off layers from graphitic materials such as highly ordered pyrolytic graphite (HOPG), single-crystal graphite, or natural graphite. This method can be completed using a multiplicity of agents like scotch tape, ultrasonication, electric field etc.³²

³¹ Wang, K.; Wang, K.; Ruan, J.; Song, H.; Zhang, J.; Wo, Y.; Guo, S.; Cui, D. Biocompatibility of Graphene Oxide Biocompatibility of Graphene Oxide. *Nanoscale Res Lett* 2010, 6 (1), 8.

³² Gong, J. R. *Graphene-Synthesis, Characterization, Properties and Applications Edited*; 2011.

Chemical exfoliation

One of the best appropriate method for synthesis of graphene is the chemical method. In the follow process, the use of intercalation compound allows the production of colloidal suspension of graphene from graphite. Basically, the chemical exfoliation is a two-step process. Firstly, there is the reduction of the interlayer van der Waals forces to expand the interlayer spacing. Consequently, the formation of graphene-intercalated compounds occurs. Secondly, the method proceeds with the exfoliation of graphene with single to few layers by rapid heating or sonication³³.

Chemical vapor deposition (CVD)

Chemical vapor deposition includes chemical reaction where molecules are heated and transformed to a gaseous state and that is the so-called precursor. In this specific CVD process a substrate is spread on thermally fragmented precursors in high temperature. Then, it deposits on thin films, solid, liquid or gaseous precursors on the surface of the substrate. The deposition of high-quality graphene from CVD process is usually done onto various transition-metal substrates like as Nickel (Ni) and Copper (Cu)³⁴.

³³ Yi, M.; Shen, Z. A Review on Mechanical Exfoliation for the Scalable Production of Graphene. *Journal of Materials Chemistry A*. Royal Society of Chemistry June 14, 2015, pp 11700–11715.

³⁴ Kalita, G.; Tanemura, M. Fundamentals of Chemical Vapor Deposited Graphene and Emerging Applications. In *Graphene Materials - Advanced Applications*; InTech, 2017.

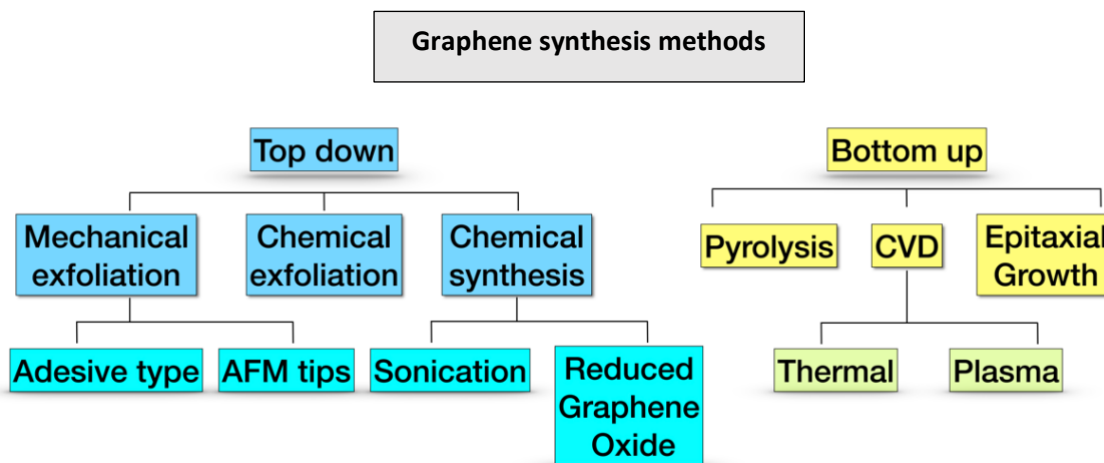


Figure 2: Schematic representation of the different methods used for the graphene synthesis.

Applications

The optimal physico-chemical properties of graphene allow its use in several applications, including:

- Semiconductor silicons in transistors³⁵
- Conductive transparent coating for solar cells³⁶
- Reinforcement in composites for the creation of lighter and stronger satellites and aerocrafts³⁷

³⁵ Liu, C.; Ma, W.; Chen, M.; Ren, W.; Sun, D. A Vertical Silicon-Graphene-Germanium Transistor. *Nat. Commun.* 2019, 10 (1), 1–7.

³⁶ Parvez, K.; Li, R.; Müllen, K. Graphene as Transparent Electrodes for Solar Cells; 2015; pp 249–280.

³⁷ Carbon nanotube ‘stitches’ make stronger, lighter composites: Method to reinforce these materials could help make airplane frames lighter, more damage-resistant - ScienceDaily.

- Stronger medical implants³⁸
- Cancer therapy³⁹
- Drug delivery⁴⁰

Graphene oxide

Because of the unique proprieties of graphene, its potential application in the biomedical field led to an increased research interest. Moreover, chemical modifications such as the oxidation of graphite leads to graphite oxide, which contains multiple stacked layers of graphene oxide (GO). Specifically, GO has a comparable hexagonal carbon structure to graphene but also contains hydroxyl (OH), alkoxy (COC), carbonyl (CO), carboxylic acid (COOH) and other oxygen-based functional groups⁴¹. One particular propriety, is the easily functionalization of GO (Figure 3), showing a better-off surface chemistry due to the existence of the oxygenated groups. Another advantage of GO, is the outstanding hydrophilicity, however this nanomaterial shows electrical and mechanical proprieties poorer than graphene⁴². Thus, it has been discovered

³⁸ Podila, R.; Moore, T.; Alexis, F.; Rao, A. Graphene Coatings for Biomedical Implants. *J. Vis. Exp.* 2013, No. 73, 50276.

³⁹ Eskiizmir, G.; Baskin, Y.; Yapici, K. Graphene-Based Nanomaterials in Cancer Treatment and Diagnosis. In *Fullerenes, Graphenes and Nanotubes: A Pharmaceutical Approach*; Elsevier, 2018; pp 331–374.

⁴⁰ Liu, J.; Cui, L.; Losic, D. Graphene and Graphene Oxide as New Nanocarriers for Drug Delivery Applications. *Acta Biomaterialia*. Elsevier December 1, 2013, pp 9243–9257.

⁴¹ Smith, A. T.; LaChance, A. M.; Zeng, S.; Liu, B.; Sun, L. Synthesis, Properties, and Applications of Graphene Oxide/Reduced Graphene Oxide and Their Nanocomposites. *Nano Mater. Sci.* 2019, 1 (1), 31–47.

⁴² Syama, S.; Mohanan, P. V. Comprehensive Application of Graphene: Emphasis on Biomedical Concerns. *Nano-Micro Letters*. SpringerOpen December 1, 2019, pp 1–31.

that the chemical modification such as thermal or chemical reduction of GO, could improve its properties, proving that the reduced graphene oxide (rGO) can maintain properties of both graphene and GO nanomaterials⁴³.

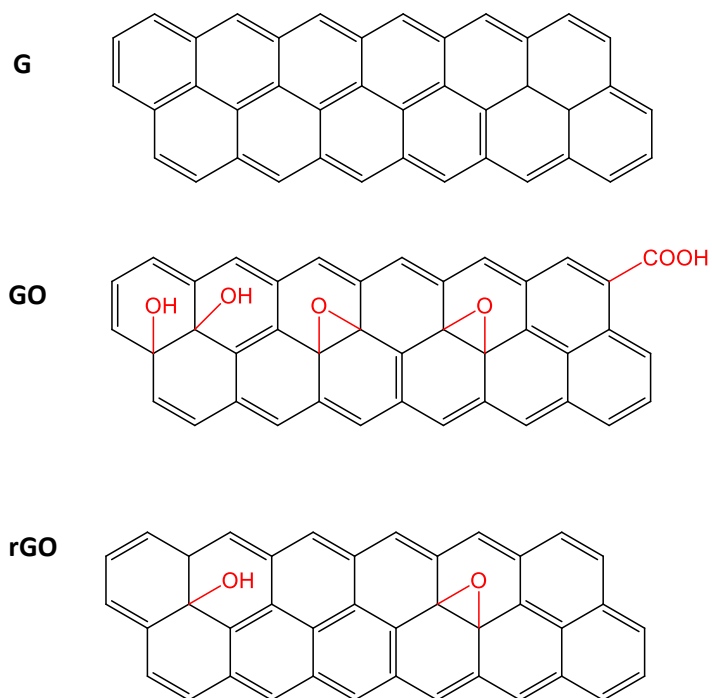


Figure 3: Structure of Graphene (G), Graphene Oxide (GO) and Reduced Graphene Oxide (rGO).

Synthesis

Graphene oxide synthesis can principally be differed into two principal categories: “bottom-up” methods (carbon molecules are utilized for the construction of pristine graphene), and “top-down” methods (extraction of graphene’ layers from a carbon source). Bottom-up synthesis are scarcely

⁴³ Fisher, C.; Rider, A. E.; Jun Han, Z.; Kumar, S.; Levchenko, I.; Ostrikov, K. Review Article Applications and Nanotoxicity of Carbon Nanotubes and Graphene in Biomedicine. *J. Nanomater.* 2012.

used due to the time-consuming and include: chemical vapor deposition⁴⁴. Thus, the top-down methods are the most utilized preparation methods. The first synthesis of GO is the oxidation of graphite using various techniques (attributed to Brodie, Staudenmaier, Hummers and Offeman). Because of the safer and more scalable process, the Hummers' method is the most used to generate GO. Specifically, Hummers and Offeman made an amount of advances on the original top-down techniques to make them harmless, such as the addition of sodium nitrate rather than using nitric acid as a solvent and the use of potassium permanganate (KMnO₄) as an oxidizer, instead of using potassium chlorate (KClO₃), which changes in the toxic chlorine dioxide (ClO₂) gas⁴⁵.

Applications

The unique properties of graphene oxide have produced researchers and companies to consider using this material in several fields including:

- Electronics, such as graphene-based effect transistor and chemical sensors⁴⁶
- Biomedical, such as component in drug delivery systems¹⁶

⁴⁴ Tour, J. M. Top-Down versus Bottom-Up Fabrication of Graphene-Based Electronics. *Chem. Mater.* 2014, 26 (1), 163–171.

⁴⁵ Poh, H. L.; Šaněk, F.; Ambrosi, A.; Zhao, G.; Sofer, Z.; Pumera, M. Graphenes Prepared by Staudenmaier, Hofmann and Hummers Methods with Consequent Thermal Exfoliation Exhibit Very Different Electrochemical Properties. *Nanoscale* 2012, 4 (11), 3515–3522.

⁴⁶ Zhan, B.; Li, C.; Yang, J.; Jenkins, G.; Huang, W.; Dong, X. Graphene Field-Effect Transistor and Its Application for Electronic Sensing. *Small* 2014, 10 (20).

- Batteries⁴⁷
- Supercapacitors⁴⁸
- Radiant heat material, such as LED lighting, cell phone and PC⁴⁹ and so on.

Introduction to Transition Metal Dichalcogenides

The discovery of graphene and its applications, prompted the study of other two-dimensional materials. Another interesting class of the 2D nanomaterials family are the transition metal dichalcogenides (TMDs), with a similar layered structure of graphene. These include molybdenum disulfide (MoS_2), molybdenum diselenide (MoSe_2), tungsten disulfide (WS_2), and tungsten diselenide (WSe_2) etc.⁵⁰. The general structure representation is MX_2 , where M is a transition metal typically from groups 4–7 (Mo, W, Ta, Nb, Re and Mn) sandwiched between X, parts of chalcogenides (S, Se, Te) as shown in Figure 4. In a TMD monolayer, the atoms of the transition metal and chalcogen are bonded covalently, allowing numerous polymorphs like 1T, 2H, and 3R, which refer to one, two, and three layers per unit cell stacking in the tetragonal (T),

⁴⁷ Ye, M.; Gao, J.; Xiao, Y.; Xu, T.; Zhao, Y.; Qu, L. Metal/Graphene Oxide Batteries. *Carbon N. Y.* 2017, 125, 299–307.

⁴⁸ Down, M. P.; Rowley-Neale, S. J.; Smith, G. C.; Banks, C. E. Fabrication of Graphene Oxide Supercapacitor Devices. *ACS Appl. Energy Mater.* 2018, 1 (2), 707–714.

⁴⁹ Jiang, G.; Tian, H.; Wang, X. F.; Hirtz, T.; Wu, F.; Qiao, Y. C.; Gou, G. Y.; Wei, Y. H.; Yang, J. M.; Yang, S.; et al. An Efficient Flexible Graphene-Based Light-Emitting Device. *Nanoscale Adv.* 2019, 1 (12), 4745–4754.

⁵⁰ Lv, R.; Robinson, J. A.; Schaak, R. E.; Sun, D.; Sun, Y.; Mallouk, T. E.; Terrones, M. Transition Metal Dichalcogenides and beyond: Synthesis, Properties, and Applications of Single- and Few-Layer Nanosheets. *Acc. Chem. Res.* 2015, 48 (1), 56–64.

hexagonal (H), and rhombohedral (R) symmetry, respectively⁵¹. The consideration about TMDs has been attributed to their excellent optical, mechanical and electronic properties resultant from their ultrathin atomic single-layer or few-layer structure⁵². Their unique properties depend from the quantum confinement and surface effects that appear during the transition of an indirect bandgap (bulk form) to a direct bandgap (monolayers form). This tunable bandgap establishes a strong photoluminescence, making TMDs a promising candidate for a range of opto-electronic devices, involving photo-detectors, photo-transistors, solar cells, and light-emitting diodes. Moreover, TMDs, which are almost as thin and flexible as graphene, have attracted huge research attention in other application fields including catalysis, solid lubrication, and more recently biomedicine⁵³. Moreover, TMD nanosheets present large specific surface area, facility of modification and easy exfoliation, which make them ideal nanomaterials for biomedical applications. For instance, their potential for use in multimodal imaging, antimicrobial agents and tissue engineering is being studied. However, despite the promise biomedical applications, the commercial translation of exfoliated TMDs has been reduced because of the low aqueous solubility of these materials⁵⁴. Nevertheless, a

⁵¹ Shi, Y.; Zhang, H.; Chang, W.-H.; Shin, H.; Li, L. Synthesis and Structure of Two-Dimensional Transition-Metal Dichalcogenides. *MRS Bull.* 2015, 40, 566–576.

⁵² Chia, X.; Pumera, M. Characteristics and Performance of Two-Dimensional Materials for Electrocatalysis. *Nat. Catal.* 2018, 1 (12), 909–921.

⁵³ Agarwal, V.; Chatterjee, K. Recent Advances in the Field of Transition Metal Dichalcogenides for Biomedical Applications. *Nanoscale* 2018, 10 (35), 16365–16397.

⁵⁴ Eftekhari, A. Tungsten Dichalcogenides (WS₂, WSe₂, and WTe₂): Materials Chemistry and Applications. *J. Mater. Chem. A* 2017, 18299–18325.

major and very significant research field of TMDs is the consistent production of atomically thin 2D layers and the manipulation of the electronic properties via scalable methodologies. Specifically, two main approaches have been used to obtain TMD monolayers: one is the chemical or mechanical exfoliation from the bulk crystals/material and another one is the bottom-up growth method⁴³.

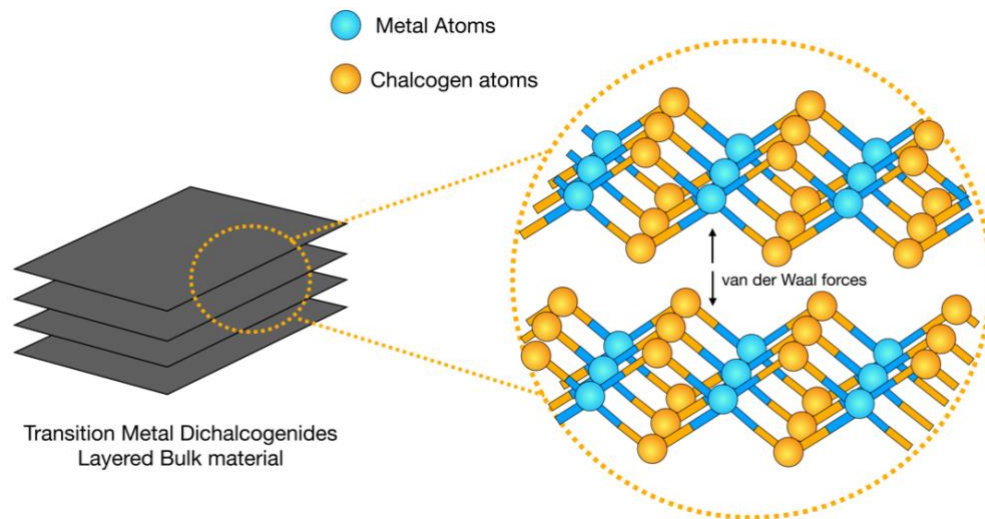


Figure 4: Layered structure of transition metal dichalcogenides (TMDs).

Synthesis

TMDs Monolayers can be synthesized employing several approaches, for instance one of the most used method is the exfoliation such as mechanical and chemical exfoliation. However, different methods have been developed and could be utilized such as chemical vapor deposition (CVD) as shown in Figure 5 and atomic layer deposition (ALD)⁴².

Mechanical exfoliation method

This specific procedure allows the production of various layers of TMDs from their bulk materials (scotch-tape method) and it is typically utilized to obtain single layers. However, the quality of the size of the layers is small (around tens of micron) causing a limitation in real device purposes⁵⁵.

Chemical exfoliation

This procedure is a solution-based synthetic method in which TMD precursors (typically in the form of powder) is dissolved in certain solutions, followed by ultra-sonication. This method is used for the production of several widely used TMDs such as MoS₂, WS₂, MoSe₂ and WSe₂ and so on. Usually, as a solvent in this method dimethylformamide and N-methyl-2-pyrrolidone are utilized, to overcome the cohesive energy present between each layer. However, this procedure shows some difficulties to maintain the integrate layer/film due to the ultra-sonication. An improvement of this method has been developed, such as the lithium intercalation method, specially used at the industrial/commercial level. In the follow procedure, N-Butyl lithium is used as the lithiation agent and hexane is used as the solvent to delete the residuals. The final thickness of the TMD layer could be around 1 nm, which is comparable to the mechanically exfoliated samples⁵⁶.

Chemical vapor deposition (CVD)

⁵⁵ Han, S. A.; Bhatia, R.; Kim, S.-W. Synthesis, Properties and Potential Applications of Two-Dimensional Transition Metal Dichalcogenides. *Nano Converg.* 2015, 2 (1), 17.

⁵⁶ Zhang, Q.; Mei, L.; Cao, X.; Tang, Y.; Zeng, Z. Intercalation and Exfoliation Chemistries of Transition Metal Dichalcogenides. *J. Mater. Chem. A* 2020, 8 (31), 15417–15444.

Another commonly performed method for the synthesis of the TMDs is the chemical vapor deposition (CVD). One of the possible routes of TMDs growth by CVD is detailed explained in You et al work. For example, for the synthesis of MoS₂, one possible approach is the thermal composition of precursors such as ammonium tetrathiomolybdate, (NH₄)₂MoS₄, in specific conditions like inert and reductive ambient and in the presence of hydrogen H₂ at low temperature to avoid oxidation and to convert (NH₄)₂MoS₄ into MoS₂. Usually, it is a two-step thermolysis procedure. Firstly, (NH₄)₂MoS₄ is dip-coated on substrates and Ar/H₂ mix flow is introduced and kept at low temperature of 500 °C and low pressures of 1 Torr for an hour. Secondly, after the annealing step, high temperature (1000 °C) and supplementary sulfur is applied to increase the crystallinity and electrical performance⁵⁷.

⁵⁷ You, J.; Hossain, M. D.; Luo, Z. Synthesis of 2D Transition Metal Dichalcogenides by Chemical Vapor Deposition with Controlled Layer Number and Morphology. *Nano Convergence*. Korea Nano Technology Research Society December 1, 2018, pp 1–13.

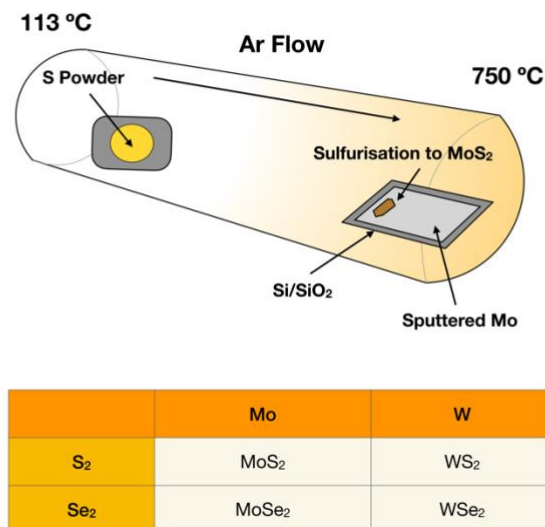


Figure 5: Chemical Vapor Deposition (CVD) of TMDs.

Applications

TMDs are increasingly studied worldwide and they can be used in several fields and applications like:

- DNA⁵⁸ and glucose sensor⁵⁹
- Photonic⁶⁰ and electronic devices⁶¹

⁵⁸ Lan, L.; Yao, Y.; Ping, J.; Ying, Y. Ultrathin Transition-Metal Dichalcogenide Nanosheet-Based Colorimetric Sensor for Sensitive and Label-Free Detection of DNA. *Sensors Actuators, B Chem.* 2019, 290, 565–572.

⁵⁹ Lee, C. W.; Suh, J. M.; Jang, H. W. Chemical Sensors Based on Two-Dimensional (2D) Materials for Selective Detection of Ions and Molecules in Liquid. *Frontiers in Chemistry.* Frontiers Media S.A. November 15, 2019, p 708.

⁶⁰ Datta, I.; Chae, S. H.; Bhatt, G. R.; Tadayon, M. A.; Li, B.; Yu, Y.; Park, C.; Park, J.; Cao, L.; Basov, D. N.; et al. Low-Loss Composite Photonic Platform Based on 2D Semiconductor Monolayers. *Nat. Photonics* 2020, 14 (4), 256–262.

⁶¹ Ko, T. J.; Wang, M.; Yoo, C.; Okogbue, E.; Islam, M. A.; Li, H.; Shawkat, M. S.; Han, S. S.; Oh, K. H.; Jung, Y. Large-Area 2D TMD Layers for Mechanically Reconfigurable Electronic Devices. *Journal of Physics D: Applied Physics.* Institute of Physics Publishing July 29, 2020, p 313002.

- Bioimaging⁶²
- Antibacterial agent⁶³
- Cancer therapy⁶⁴

Introduction to Boron nitride

Another member of the 2D nanomaterials class is boron nitride (BN). Boron nitride is an inorganic compound with a flat, hexagonal framework similar to graphite, where the carbon atoms are substituted by boron and nitrogen atoms⁶⁵. The alternating boron and nitrogen atoms are bonded forming hexagonal rings composed of three boron atoms and three nitrogen atoms, and the layers are held together by van der Waals forces (Figure 5). Similar to carbon, boron nitride additionally can be produced in amorphous and crystalline forms. Specifically, BN occurs in three different allotropes: hexagonal boron nitride (h-BN), sphalerite boron nitride (β -BN) and wurtzite boron nitride (γ -BN)⁶⁶. Moreover, BN shows interesting physico-chemical properties, like high electrical resistivity, resistance to thermal shock and

⁶² Yadav, V.; Roy, S.; Singh, P.; Khan, Z.; Jaiswal, A. 2D MoS₂ -Based Nanomaterials for Therapeutic, Bioimaging, and Biosensing Applications. *Small* 2019, 15 (1), 1803706.

⁶³ Kaur, J.; Valadan, M.; Nebbioso, A.; Vergara, A.; Montone, A. M. I.; Benedetti, R.; Rossi, M.; Giardina, P.; Cutarelli, A.; Altucci, L.; et al. Biological Interactions of Biocompatible and Water-Dispersed MoS₂ Nanosheets with Bacteria and Human Cells. *Sci. Rep.* 2018.

⁶⁴ Zhou, R.; Zhu, S.; Gong, L.; Fu, Y.; Gu, Z.; Zhao, Y. Recent Advances of Stimuli-Responsive Systems Based on Transition Metal Dichalcogenides for Smart Cancer Therapy. *Journal of Materials Chemistry B*. Royal Society of Chemistry April 17, 2019, pp 2588–2607.

⁶⁵ Perevislov, S. N. Structure, Properties, and Applications of Graphite-Like Hexagonal Boron Nitride. *Refract. Ind. Ceram.* 2019, 60 (3), 291–295.

⁶⁶ Ribeiro, H.; Adriane Luciano, M.; Von Randow C, P.; N. Vilela, D.; M. Andrade, L. Functionalized Boron Nitride Applications in Biotechnology. In *Recent Advances in Boron-containing Materials*; *IntechOpen*, 2019.

inertness to most chemical compounds. Specifically, the allotrope of hexagonal boron nitride is used in the electronic industry as an electrical insulating and dielectric material working in an extensive temperature range at high-frequencies⁶⁷. Furthermore, its decomposition temperature is around 3000°C, allowing the application of BN in several numbers of industries such as nuclear, chemical and precision metallurgy⁶⁸. Considering the similarity with the graphene structure, this material has also attracted a significant attention in the biomedical field in the latest years.

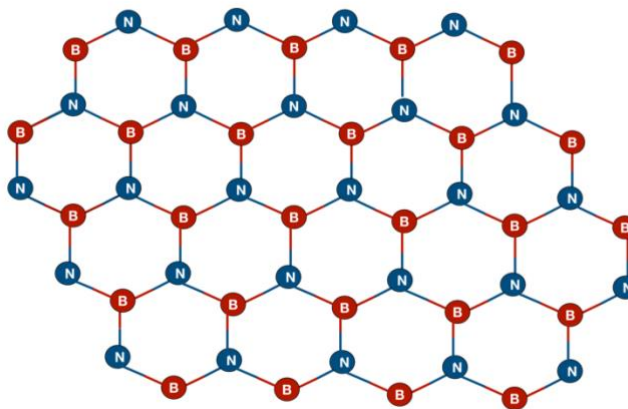


Figure 6: structure of boron nitride (BN).

⁶⁷ Izyumskaya, N.; Demchenko, D.; Das, S.; Özgür, Ü.; Avrutin, V.; Morkoç, H. Recent Development of Boron Nitride towards Electronic Applications. *Adv. Electron. Mater.* 2017, 3, 1600485.

⁶⁸ Merlo, A.; Mokkapati, V. R. S. S.; Pandit, S.; Mijakovic, I. Biomaterials Science REVIEW Boron Nitride Nanomaterials: Biocompatibility and Bio-Applications. *Biomater. Sci.* 2018, 6.

Synthesis

Similar to graphene and TMDs, BN can be synthesized via top-down (typical exfoliation-type approaches) or bottom-up approaches (usually CVD or other deposition techniques).

Mechanical Exfoliation

The procedure is similar to the previous mechanical exfoliation of other 2D nanomaterials, also identified as the “scotch tape method,” or micromechanical cleavage method. Within this procedure, it is possible to isolate the layers in a controlled way down to monolayers, maintaining big flake size⁶⁹.

Solvent-Assisted Ultrasonication

In this method boron nitride is dispersed in a solvent following sonication, the sample tends to exfoliate because of the energy that is generated by the sonication process⁷⁰.

⁶⁹ Island, J. O.; Steele, G. A.; Can Der Zant, H. S. J.; Castellanos-Gomez, A. *Mechanical Manipulation and Exfoliation of Boron Nitride Flakes by Micro-Plowing with an AFM Tip*.

⁷⁰ Nie, X.; Li, G.; Jiang, Z.; Li, W.; Ouyang, T.; Wang, J. Co-Solvent Exfoliation of Hexagonal Boron Nitride: Effect of Raw Bulk Boron Nitride Size and Co-Solvent Composition. *Nanomaterials* 2020, 10 (6).

Acid Exfoliation

Usually, boron nitride is normally neutral when reacting to acids, however it has been reported that using a strong protic acid such as methyl sulfonic acid (MSA) exfoliation of BN it is possible.⁷¹

Chemical Vapor Deposition

CVD is another typical method and it is reliant on the use of reactive precursors such as gaseous, liquid, and solid precursors. As reported by et al the gaseous precursors are more toxic (for example BF_3/NH_3 , BCl_3/NH_3 , and $\text{B}_2\text{H}_6/\text{NH}_3$) and necessitate meticulous ratios of gases to preserve a 1:1 B/N stoichiometry. Moreover, the borazine liquid precursor, shows equivalent amounts of boron and nitrogen atoms, and do not produce highly toxic side products. Finally, for solid precursors, it is used the stable borazane (1:1 B/N stoichiometry)⁷².

Applications

Similar to the other class of 2D nanomaterials, boron nitride has attracted tremendous attention and investigation research regarding its potential use, including:

- Dielectrics in Next-Generation nano-electronic devices⁷³

⁷¹ Bhimanapati, G. R.; Glavin, N. R.; Robinson, J. A. 2D Boron Nitride: Synthesis and Applications. In *Semiconductors and Semimetals*; Academic Press Inc., 2016; Vol. 95, pp 101–147.

⁷² Mercan, Ö. *Production of boron nitride using chemical vapor deposition method a thesis submitted to the graduate school of Nature and Applied sciences of Middle East Technical University*; 2014.

⁷³ Glavin, N.; Muratore, C.; Jespersen, M.; Hu, J.; Hagerty, P.; Hilton, A.; Blake, A.; Grabowski, C.; Durstock, M.; McConney, M.; et al. Amorphous Boron Nitride: A Universal, Ultrathin Dielectric For 2D Nanoelectronics. *Adv. Funct. Mater.* 2016, 26.

- Protective Coatings⁷⁴
- Cosmetics⁷⁵
- Gas sensing such as ammonia⁷⁶ and ethanol⁷⁷
- Functionalized BN as a candidate for imaging and cancer therapy⁷⁸
- Piezoelectric devices⁷⁹ and so on.

Potential hazards of 2D nanomaterials for human health and environment

Understanding the toxicity of nanoparticles toward human health and their potential toxicological impact into the environment it is crucial because of the high potential exposure. Thus, several authors raised concerns about their safety. Specifically, it is very unlikely that 2D nanoparticles could be introduced into humans in sufficient concentrations to trigger adverse effects. However, some of them might be inhaled in certain workplaces in significant amounts.

Human exposure

The main access of NPs to the human body can occur essentially through the lungs, the skin or the intestinal tract. The first target organs are the lungs, where

⁷⁴ Husain, E. A. M.; Narayanan, T.; Taha-Tijerina, J.; Vinod, S.; Vajtai, R.; Ajayan, P. Marine Corrosion Protective Coatings of Hexagonal Boron Nitride Thin Films on Stainless Steel. *ACS Appl. Mater. Interfaces* 2013, 5.

⁷⁵ Fiume, M. M.; Bergfeld, W. F.; Belsito, D. V.; Hill, R. A.; Klaassen, C. D.; Liebler, D. C.; Marks, J. G.; Shank, R. C.; Slaga, T. J.; Snyder, P. W.; et al. Safety Assessment of Boron Nitride as Used in Cosmetics.

⁷⁶ Feng, P. X.; Chavez, E.; Malca, C. Super Stable Pollution Gas Sensor Based on Functionalized 2D Boron Nitride Nanosheet Materials for High Humidity Environments. *Chemosensors* 2018, 6 (4).

⁷⁷ Sajjad, M.; Feng, P. Study the Gas Sensing Properties of Boron Nitride Nanosheets. *Mater. Res. Bull.* 2014, 49, 35–38.

⁷⁸ Sharker, S. M. Hexagonal Boron Nitrides (White Graphene): A Promising Method for Cancer Drug Delivery. *International Journal of Nanomedicine*. Dove Medical Press Ltd. 2019, pp 9983–9993.

⁷⁹ Ares, P.; Cea, T.; Holwill, M.; Wang, Y. B.; Roldán, R.; Guinea, F.; Andreeva, D. V.; Fumagalli, L.; Novoselov, K. S.; Woods, C. R. *Piezoelectricity in Monolayer Hexagonal Boron Nitride*.

small particles can be blocked and removed by the rhythmical beating action of microscopic protrusions (cilia). However, particles in the nanoscale, can overstep this barrier and reach the gas-exchanging tissues and be phagocytized by macrophages. Consequently, these cells then transport the particles from the lungs to the lymphatic vessels and could cause excessive inflammation and thus destruction of lung tissue⁸⁰. Another important human barrier is the skin, formed by the epidermis, protected by a hydrophobic lipid layer. Usually, the epidermis is impermeable to several particles, however in damaged conditions such as abrasions, cuts and perforations it could be less effective as a protective barrier against NPs⁸¹. The last human barrier from NPs is the gut, where its epithelium is impermeable to large molecules. However, the small size of NPs allows them to translocate into the bloodstream and access each organ upon crossing the gut epithelium⁸².

Environment exposure

The biocompatibility and degradation of 2D layered nanomaterials and their effect on living organisms or at the larger level of ecosystems is an important area of study as these materials find increasing applications and uses⁸³.

⁸⁰ Fröhlich, E.; Salar-Behzadi, S. Toxicological Assessment of Inhaled Nanoparticles: Role of in Vivo, Ex Vivo, in Vitro, and in Silico Studies. *Int. J. Mol. Sci.* 2014, *15* (3), 4795–4822.

⁸¹ Schneider, M.; Stracke, F.; Hansen, S.; Schaefer, U. F. Nanoparticles and Their Interactions with the Dermal Barrier. *Dermatoendocrinol.* 2009, *1* (4), 197–206.

⁸² Bergin, I. L.; Witzmann, F. A. Nanoparticle Toxicity by the Gastrointestinal Route: Evidence and Knowledge Gaps. *Int. J. Biomed. Nanosci. Nanotechnol.* 2013, *3* (1–2).

⁸³ Seaton, A.; Tran, L.; Aitken, R.; Donaldson, K. Nanoparticles, Human Health Hazard and Regulation. *Journal of the Royal Society Interface. Royal Society* February 6, 2010, p S119.

Likewise, it is indispensable to close knowledge-gaps across the potential human exposure and the life cycle analysis of 2D nanomaterials, in order to correctly assess and manage the risks of these materials. Additionally, due to the wide-ranging spectrum of applications, 2D nanomaterials could be exposed to agricultural soil and water. For instance, the release into water could determine transformation in the form of aggregation, oxidation, or changes in the chemical state⁸⁴. Thus, understanding the interaction between these nanomaterials and the environment and assessing their biological effects on several organisms is urgently needed⁸⁵.

Nanotoxicology of 2D materials

The principal purpose of nanotoxicological studies is to define the toxic/hazardous effects of nanomaterials on living organisms and on the environment. The potential toxicity of these systems is closely related on several factors including the physico-chemical properties of nanomaterials such as size, shape, surface area, purity etc. (Figure 7)⁸⁶ It is well-known that size plays a central role for the reactivity of the 2D nanomaterials and thus in their nanotoxicology. Reducing size results in an increase of the specific surface. In addition, size determines the cellular uptake mechanisms. For

⁸⁴ Fadeel, B.; Bussy, C.; Merino, S.; Va, E.; Flahaut, E.; Mouchet, F.; Evariste, L.; Gauthier, L.; Koivisto, A. J.; Vogel, U.; et al. Safety Assessment of Graphene-Based Materials: Focus on Human Health and the Environment. 2018

⁸⁵ Guiney, L. M.; Wang, X.; Xia, T.; Nel, A. E.; Hersam, M. C. Assessing and Mitigating the Hazard Potential of Two-Dimensional Materials. *ACS Nano* 2018, 12 (7), 6360–6377.

⁸⁶ Ganguly, P.; Breen, A.; Pillai, S. C. Toxicity of Nanomaterials: Exposure, Pathways, Assessment, and Recent Advances. *ACS Biomater. Sci. Eng.* 2018, 4 (7), 2237–2275.

instance, regarding the active uptake mechanisms, nanoparticles up to 100 nm can be taken up by pinocytosis, caveolin and clathrin molecular pathways, although larger nanoparticles are taken up by phagocytosis and macropinocytosis⁸⁷. Other physico chemical factors can influence the possible toxicological responses of 2D nanomaterials. For example, particle agglomeration and sedimentation can influence the uptake and consequently the toxicity of nanoparticles⁸⁸. Moreover, the morphological characteristics including nanotubes and nanowires, and various shapes, such as spherical, oval, cubic exist as powders, suspension, or colloids. Another important factor to take into consideration is the dose and concentration of the nanoparticles exposed to living systems. There are numerous conflicting results correlated to the toxic effects of NPs at different concentrations. In addition, it has been demonstrated that also the number of layers can influence the toxicity⁸⁹.

⁸⁷ Zhang, S.; Li, J.; Lykotrafitis, G.; Bao, G.; Suresh, S.; Zhang, P. S. Size-Dependent Endocytosis of Nanoparticles. *Adv Mater* 2009, 21, 419–424.

⁸⁸ Lewinski, N.; Colvin, V.; Drezek, R. Cytotoxicity of Nanoparticles. *Small*. 2008.

⁸⁹ Chng, E. L. K.; Sofer, Z.; Pumera, M. MoS₂ Exhibits Stronger Toxicity with Increased Exfoliation. *Nanoscale* 2014.

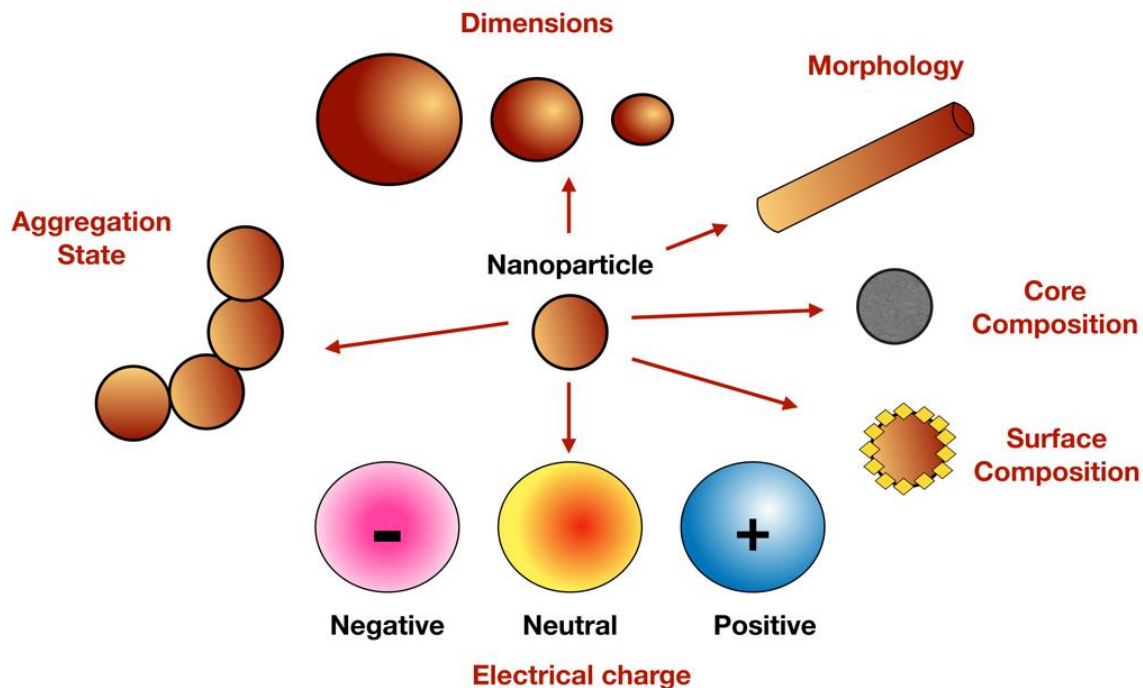


Figure 7: Physico chemical properties of nanomaterials.

Layered nanomaterials can adsorb different molecules upon contact with biological medium or abiotic environments, making for instance the so-called protein corona. Specifically, the biophysical properties of nanoparticles covered by a protein corona might change drastically from those of pure particles and thus, alter notably their biological responses⁹⁰. Hence, taking in consideration these several physico chemical factors, numerous *in vivo* and *in vitro* studies have been done for the evaluation of the potential safety of 2D nanomaterials, due to the applications and future additional prospective in the

⁹⁰ Corbo, C.; Molinaro, R.; Parodi, A.; Toledano Furman, N. E.; Salvatore, F.; Tasciotti, E. The Impact of Nanoparticle Protein Corona on Cytotoxicity, Immunotoxicity and Target Drug Delivery. *Nanomedicine* (Lond). 2016, 11 (1), 81–100.

biomedical field. In the follow paragraph, the scientific knowledge and gaps regarding the *in vitro* toxicological studies of the selected 2D nanomaterials used in this thesis are briefly discussed.

Toxicity of Graphene Oxide

A great amount of toxicological studies, both *in vitro* and *in vivo* have evaluated the interaction of graphene-based nanomaterials with various living systems such as mammalian cells, prokaryotic cells and animal models. For instance, Lv et al⁹¹ studied the specific interaction of graphene oxide within neuroblastoma cells (SH-SY5Y) showing that the viability was affected in a dose and time dependent. Moreover, Yuan et al⁹² showed the less toxic effects of GO in comparison to single-walled carbon nanotubes (SWCNTs), inducing less mitochondrial damage, ROS generation, apoptotic cell toward human liver carcinoma cells (HepG2). In addition, the dose and time toxicity of GO was confirmed by Horváth et al where the it was possible to observe the cellular internalization of GO inside phago-endosomes toward lung epithelial cells (A549) and murine macrophage cells (RAW 264.7)⁹³. These and more similar studies indicate that toxicity of graphene could be dependent on several factors such as dose and time of exposure, shape and size, purity and synthesis

⁹¹ Lv, M.; Zhang, Y.; Liang, L.; Wei, M.; Hu, W.; Li, X.; Huang, Q. Effect of Graphene Oxide on Undifferentiated and Retinoic Acid-Differentiated SH-SY5Y Cells Line. *Nanoscale* 2012, 4 (13), 3861.

⁹² Yuan, J.; Gao, H.; Sui, J.; Duan, H.; Chen, W. N.; Ching, C. B. Cytotoxicity Evaluation of Oxidized Single-Walled Carbon Nanotubes and Graphene Oxide on Human Hepatoma HepG2 Cells: An ITRAQ-Coupled 2D LC-MS/MS Proteome Analysis. *Toxicol. Sci.* 2012, 126 (1), 149–161.

⁹³ Horváth, L.; Magrez, A.; Burghard, M.; Kern, K.; Forró, L.; Schwaller, B. Evaluation of the Toxicity of Graphene Derivatives on Cells of the Lung Luminal Surface. *Carbon N. Y.* 2013, 64, 45–60.

methods etc. For instance, the morphology of GO could strongly influence the potential cellular uptake whereas the presence of the functional groups can alter the interactions with several biomolecules, micronutrients and proteins. Another important feature, is that even though there are various forms of graphene nanoparticles, GO has been the greatest commonly used for biomedical applications⁹⁴. Moreover, in that regard, several works have been conducted to investigate the potential antimicrobial activity of GO toward prokaryotic cells. For instance, Chen et al shown the extremely prominent dose-dependent antibacterial activity of GO and reduced graphene oxide, inducing strong cell membrane damages and oxidative stress in *Xanthomonas oryzae*⁹⁵. Moreover, the potential use of GO as an antibacterial agent has been showed also by Hu et al, where cellular viability of *Escherichia coli* was strongly affected by the presence of the nanomaterial⁹⁶. Furthermore, in another similar work, the size and shape of GO could strongly influence the grade of the toxic effects toward bacteria. Specifically, Liu et al demonstrated the size-dependent antibacterial activity of GO sheets (larger sheets induced higher antibacterial effects) in the bacteria *E. coli*⁹⁷. However, very few studies compared the potential adverse effects of commercial GO using different eukaryotic and

⁹⁴ Lalwani, G.; D'Agati, M.; Khan, A. M.; Sitharaman, B. Toxicology of Graphene-Based Nanomaterials. *Adv. Drug Deliv. Rev.* 2016, 105 (Pt B), 109–144.

⁹⁵ Chen, J.; Wang, X.; Han, H. A New Function of Graphene Oxide Emerges: Inactivating Phytopathogenic Bacterium *Xanthomonas Oryzae* Pv. *Oryzae. J. Nanoparticle Res.* 2013, 15 (5), 1658.

⁹⁶ Hu, W.; Peng, C.; Luo, W.; Lv, M.; Li, X.; Li, D.; Huang, Q.; Fan, C. Graphene-Based Antibacterial Paper. *ACS Nano* 2010, 4 (7), 4317–4323.

⁹⁷ Liu, S.; Hu, M.; Zeng, T. H.; Wu, R.; Jiang, R.; Wei, J.; Wang, L.; Kong, J.; Chen, Y. Lateral Dimension-Dependent Antibacterial Activity of Graphene Oxide Sheets. *Langmuir* 2012, 28 (33), 12364–12372.

prokaryotic cellular models. More detailed studies are needed to examine and fully understand the toxicity of commercial graphene oxide nanomaterials and to properly associate the biological phenomenon with their chemical, structural, and morphological variations. Consequently, the focus of Chapter 2 of this thesis, is to provide new source of nanotoxicological results, data and approaches for graphene-oxide materials.

Toxicity of Molybdenum Disulfide and Tungsten Disulfide

Molybdenum disulfide (MoS_2) and Tungsten disulfide (WS_2) nanomaterials, which appertain to the TMDs family, have recently originate various applications in the biomedical and environmental fields due to their outstanding physicochemical properties. However, little is known about their specific interactions with biological systems. Few works have investigated the potential impact of these 2D layered materials toward mammalian cells. For instance, Moore et al explored the cytotoxicity, cellular uptake and inflammatory responses in A549 cells, adenocarcinoma of the stomach cells (AGS) and leukemic monocytes cells (THP-1) succeeding incubation with MoS_2 flakes of varying sizes. The results indicated that the three different MoS_2 sizes did not induce any toxic effects on all the cell-lines⁹⁸. Moreover, a similar no cytotoxic effects was observed with WS_2 nanoparticles. In this study, et al showed in a series of biocompatibility tests, that WS_2 did not induce any adverse effects on

⁹⁸ Moore, C.; Movia, D.; Smith, R. J.; Hanlon, D.; Lebre, F.; Lavelle, E. C.; Byrne, H. J.; Coleman, J. N.; Volkov, Y.; McIntyre, J. Industrial Grade 2D Molybdenum Disulphide (MoS_2): An in Vitro Exploration of the Impact on Cellular Uptake, Cytotoxicity, and Inflammation. *2D Mater.* 2017, 4 (2).

human epithelial kidney cells (HEK293f)⁹⁹. Additionally, cytotoxicity examinations of fullerene-like MoS₂ and WS₂ on human cell-lines, salivary gland cells and A549, showed the non-toxicity due to the high cell viability after prolonged exposure to TMDs¹⁰⁰. Furthermore, both MoS₂ and WS₂ were also investigated to understand their potential antibacterial effects toward several prokaryotic cells. Specifically, in this work it has been demonstrated the antimicrobial behavior of MoS₂ toward *E. coli* due to the physical damage of the cellular membrane and over production of oxidation stress such as superoxide anion (O₂⁻)¹⁰¹. In another similar work, the antibacterial activities of WS₂ nanosheets against *E. coli* and *Staphylococcus aureus* was evaluated studying the cellular vitality. The results showed the time and concentration dependent antibacterial activity (retardation of bacterial growth) for both bacterial strains¹⁰². However, the potential toxicity of these two TMDs nanomaterials toward the cellular model *S. cerevisiae* is very scares. Moreover, the majority of the works have been focused on the use of laboratory made MoS₂ and WS₂. Consequently, in Chapter 3 we discuss the potential impact and adverse effects of the selected commercial TMDs, with different physico-

⁹⁹ Appel, J. H.; Li, D. O.; Podlevsky, J. D.; Debnath, A.; Green, A. A.; Wang, Q. H.; Chae, J. Low Cytotoxicity and Genotoxicity of Two-Dimensional MoS₂ and WS₂. *ACS Biomater. Sci. Eng.* 2016, 2 (3), 361–367.

¹⁰⁰ Goldman, E. B.; Zak, A.; Tenne, R.; Kartvelishvily, E.; Levin- Zaidman, S.; Neumann, Y.; Stiubea-Cohen, R.; Palmon, A.; Hovav, A.- H.; Aframian, D. J. Biocompatibility of tungsten disulfide inorganic nanotubes and fullerene-like nanoparticles with salivary gland cells. *Tissue Eng. Part A* 2015, 21, 1013–1023

¹⁰¹ Yang, X.; Li, J.; Liang, T.; Ma, C.; Zhang, Y.; Chen, H.; Hanagata, N.; Su, H.; Xu, M. Antibacterial Activity of Two-Dimensional MoS₂ Sheets. *Nanoscale* 2014, 6 (17), 10126–10133.

¹⁰² Liu, X.; Duan, G.; Li, W.; Zhou, Z.; Zhou, R. Membrane Destruction-Mediated Antibacterial Activity of Tungsten Disulfide (WS₂). *RSC Adv.* 2017, 7 (60), 37873–37880.

chemical proprieties such as size, shape and method of synthesis, toward A549 cells and yeast.

Toxicity of Boron Nitride

Conflicting results have been described in the scientific literature on the cytotoxicity of boron nitride. It is well known in nanotoxicology how several physico-chemical factors can alter the biocompatibility of a particular noncompound. It is possible to observe a similar situation for BN nanocomposites and the strong alterations on biological responses of living systems in relation to shape, size and concentration of BN materials¹⁰³. For instance, et al showed the high biocompatibility of functionalized boron nitride nanotubes (G-chitosan-coated) toward human neuroblastoma SH-SY5Y cells. The boron nitride nanotubes did not affect the DNA concentration, cell viability, apoptosis, or ROS formation¹⁰⁴. Similar studies, where BN did not induce any toxic effects, were performed using other mammalian cells such as HEK293 cells and Chinese hamster ovary (CHO) cells¹⁰⁵. However, the results presented above contradict other toxicological studies. For example, in this work, boron nitride nanotubes are cytotoxic toward lung epithelial cells (A549), alveolar macrophages (RAW 264.7), and fibroblast cells (3T3-L1) and in

¹⁰³ Ray, P. C.; Yu, H.; Fu, P. P. Toxicity and Environmental Risks of Nanomaterials: Challenges and Future Needs. *J. Environ. Sci. Health. C. Environ. Carcinog. Ecotoxicol. Rev.* 2009, 27 (1), 1–35.

¹⁰⁴ Ciofani, G.; Danti, S.; D'Alessandro, D.; Moscato, S.; Menciassi, A. Assessing Cytotoxicity of Boron Nitride Nanotubes: Interference with the MTT Assay. *Biochem. Biophys. Res. Commun.* 2010, 394 (2), 405–411.

¹⁰⁵ Chen, X.; Wu, P.; Rouseas, M.; Okawa, D.; Gartner, Z.; Zettl, A.; Bertozzi, C. R. Boron Nitride Nanotubes Are Noncytotoxic and Can Be Functionalized for Interaction with Proteins and Cells. *J. Am. Chem. Soc.* 2009, 131, 3, 890–891

human embryonic kidney cells (HEK 293). Specifically, after 48-h the toxicity of BN nanotubes was time-, dose-, and cell type-dependent, where the maximum cytotoxic effect was detected in macrophages (high phagocytic activity) and the lowest toxic effect was observed in HEK293 cells with the lowest endocytic activity¹⁰⁶. Hence, the biocompatibility is an important property for future biomedical applications of BN, but the conflicting results need more investigation and research. Thus, in Chapter 4, we investigated the potential toxicity of amorphous nano compounds of two different commercial BN toward A549 cells. In addition, several authors investigated whether BN, a nanomaterial with extensive similarities to graphene, might exhibit similar antibacterial properties. For example, in this study, the antimicrobial activity of BN composites was evaluated against *Escherichia coli*, *Pseudomonas aeruginosa*, *Staphylococcus epidermidis* and *Staphylococcus aureus* by the colony forming units (CFUs) counting method¹⁰⁷. The authors showed that the BN composites physically interact with the bacterial cellular envelope, causing irreversible physical damage. Moreover, another work demonstrated via experimental and simulation-based approaches that BN nanosheets trigger degradation of bacterial cell membranes (outer and inner membranes)¹⁰⁸. However, few works investigated the potential antimicrobial and antifungal

¹⁰⁶ Horváth, L.; Magrez, A.; Golberg, D.; Zhi, C.; Bando, Y.; Smajda, R.; Horváth, E.; Forró, L.; Schwaller, B. In Vitro Investigation of the Cellular Toxicity of Boron Nitride Nanotubes. *ACS Nano* 2011, 5 (5), 3800–3810.

¹⁰⁷ Pandit, S.; Gaska, K.; Mokkalpati, V. R. S. S.; Forsberg, S.; Svensson, M.; Kádár, R.; Mijakovic, I. Antibacterial Effect of Boron Nitride Flakes with Controlled Orientation in Polymer Composites. *RSC Adv.* 2019, 9 (57), 33454–33459.

¹⁰⁸ Zhang, Y.; Chan, C.; Li, Z.; Ma, J.; Meng, Q.; Zhi, C.; Sun, H.; Fan, J. Nanotoxicity of Boron Nitride Nanosheet to Bacterial Membranes. *Langmuir* 2019, 35 (18), 6179–6187.

activity of BN. Hence, in Chapter 4 we focused on the study of the cell viability and oxidative stress production of *S. cerevisiae* after the exposure to BN nanoparticles, demonstrating high biocompatibility toward the selected cellular model in the condition selected.

Aim of the research thesis

This research thesis is focused on the evaluation of the potential toxicological effects of different 2D nanomaterials such as graphene oxide (GO), TMDs like molybdenum disulfide (MoS_2) and tungsten disulfide (WS_2) and boron nitride (BN). Because of the increased use of these materials and the contradictory results in the scientific literature, the need of understanding their toxicological potential and environmental fate it is crucial. In addition, there is a lack in the literature regarding the toxicological impact of the degradation products of TMDs and the comparison of the biological effects of 2D nanomaterial toward different cellular models. Hence, commercially available materials were selected and studied in order to shed light into the correlation of their physico-chemical properties with their nanotoxicology effects. Using different *in vitro* approaches, we investigated the biological responses to the exposure to various concentrations and time of the selected nanomaterials. Several cellular models were used, specifically adenocarcinomic human alveolar basal epithelial cells (A549 cells), the yeast *Saccharomyces cerevisiae*, the bacteria *Vibrio fischeri* and prokaryotic enzymes. Consequently, to evaluate the percentage of living cells after incubation with the nanomaterials, specific assays were performed such as Neutral Red, MTT (tetrazolium assay),

cytofluorimetry, CFU (Colony Forming Unit) and bioluminescence inhibition. Moreover, the percentage of ROS (reactive oxygen species) production was evaluated using the DCFDA assay and in addition the potential inhibition of the activity of several prokaryotic enzymes was studied. The discussion of the observed results enhances our knowledge about the hazards associated to the use of these 2D nanomaterials which present a bright future in real world applications. Specifically, in Chapter 2, we focused on the investigation of the ability of commercial monolayer graphene oxide (GO) and graphene oxide nanocolloids (GOC) to interact with different unicellular systems and biomolecules. Human alveolar carcinoma epithelial cells, the yeast *S. cerevisiae* and the bacteria *V. fischeri* were exposed to the presence of different nanoparticle concentrations and the toxicological results are deeply explained. Moreover, the binding affinity of different microbial enzymes, like the α -L-rhamnosidase enzyme RhaB1 from the bacteria *Lactobacillus plantarum* and the AbG β -D-glucosidase from *Agrobacterium* sp. with these materials were studied. In Chapter 3, we focused on the study of the physicochemical properties and the toxicological potential of commercially available MoS₂ nanoparticles with different lateral size and degradation stage were studied. The structure and stoichiometry of fresh and aged aqueous suspensions of micro-MoS₂ and nano-MoS₂ was analyzed by Raman spectroscopy, while X-ray photoelectron spectroscopy (XPS) allowed to identify more quantitatively the nature of the formed oxidized species. We used similar techniques to those described in Chapter 2, to investigate the toxicological effects toward A549 cells and the unicellular fungus *Saccharomyces cerevisiae*. The toxicological

results indicated that all the MoS₂ nanoparticles induced sublethal damage on the A549 cells though the increase of intracellular ROS levels, while comparable concentrations reduced the viability of yeast cells. In addition, another work focused on the potential toxicity of WS₂ is introduced in this chapter. In this study, we performed a similar research study to the MoS₂ work. Specifically, the physico-chemical characteristics and the in vitro toxicological potential of different commercial WS₂ nanoforms was assessed. The two samples, present in particles suspension stocks, such as micro WS₂ and nano WS₂ and the two other samples present in powders form were analyzed using TEM, Raman and XPS analysis to study physico-chemical proprieties such as the structure and stoichiometry. The toxicological potential of all the WS₂ nanoforms was evaluated performing the cellular viability and the oxidative stress assays, in two different eukaryotic cellular models: A549 cells and the yeast *Saccharomyces cerevisiae*. The toxicological results indicate different biological responses in relation to the commercial WS₂ products, showing significant differences in the toxicological impact. In Chapter 4, the potential toxicity of two different commercial boron nitride (BN) nanomaterials have been explored evaluating the physicochemical properties, to identify possible alterations in the toxicological behavior in relation to the size and the shape of the particles selected and comparing the biological responses toward different cellular models (always A549 cells and yeast). Both the commercial selected nanomaterials did not induce any toxicity in the two cellular models. Overall, in this research thesis we investigated whether existing commercial 2D products could affect several biological parameters of living cells, at different

concentrations and exposure times. In addition, we explored the potential environmental fate of 2D nanomaterials providing new information of their risk assessment dealing with the complex physico-chemical factors that could influence the safety.

Chapter 2

Graphene Oxide Derivates

Interaction analysis of commercial graphene oxide nanoparticles with unicellular systems and biomolecules

Brixhilda Domi¹, Carlos Rumbo¹, Javier García-Toja², Livia Sima³, Gabriela Negroiu³, Juan Antonio Tamayo-Ramos¹

¹ International Research Centre in Critical Raw Materials-ICCRAM, University of Burgos, Plaza Misael Banuelos s/n, 09001 Burgos, Spain

² Department of Chemistry, University of Burgos, Plaza Misael Bañuelos s/n., 09001 Burgos, Spain

³ Molecular Cell Biology, Institute of Biochemistry of the Romanian Academy, 060031 Bucharest, Romania

Abstract

The ability of commercial monolayer graphene oxide (GO) and graphene oxide nanocolloids (GOC) to interact with different unicellular systems and biomolecules was studied by analyzing the response of human alveolar carcinoma epithelial cells, the yeast *Saccharomyces cerevisiae* and the bacteria *Vibrio fischeri* to the presence of different nanoparticle concentrations, and by studying the binding affinity of different microbial enzymes, like the α -L-rhamnosidase enzyme RhaB1 from the bacteria *Lactobacillus plantarum* and the AbG β -D-glucosidase from *Agrobacterium* sp. (strain ATCC 21400). An analysis of cytotoxicity on human epithelial cell line A549, *S. cerevisiae* (colony forming units, ROS induction, genotoxicity) and *V. fischeri* (luminescence inhibition) cells determined the potential of both nanoparticle types to damage the selected unicellular systems. Also, the protein binding affinity of the graphene derivatives at different oxidation states was analyzed. The reported results highlight the variability that can exist in terms of toxicological potential and binding affinity depending on the target organism or protein and the selected nanomaterial.

Keywords

Graphene, unicellular organisms, toxicity, binding capacity, ATR-FTIR, TEM, ICP-MS

Introduction

The interest in the immobilization of microorganisms and microbial enzymes for biotechnological applications has been continuously rising during the last decades because of several factors, including the increased availability of microbial strains and biocatalysts tailored to new applications, the development of new immobilization supports with improved properties, and the need of a shift toward the use of more sustainable processes in different industrial fields [1,2,3,4,5]. The immobilization of microorganisms and enzymes on solid carriers leads to a number of benefits. Immobilized biocatalysts facilitate the efficient recovery and separation of the reaction product, the reutilization of the biocatalyst, and enhance the safety of the material handling (i.e., preventing the appearance of allergies). The use of solid supports of microbial cells for the production of high-value compounds (chemicals, enzymes, etc.) and transformation processes in multiple fields (e.g., agricultural, environmental, food, medical, etc.) has been explored as well to enhance the microbial biological activity, to facilitate their delivery and to separate them more easily from the fermentation broth [3,5,6,7,8]. Therefore, during the last years there has been an emerging interest in biocompatibility studies for interfacing biological systems with artificial materials. Unicellular microorganisms, such as bacteria, fungi, and algae, have been utilized extensively for the encapsulation of whole single cells as well as for the introduction of nanomaterials onto the living cells.

During the last 40 years, a range of different materials have been investigated as enzyme and microbial immobilization matrices: from organic compounds, like natural alginate or carrageenan or synthetic polymers, to inorganic compounds, such as processed or natural minerals, like silica [3,9]. In the last decade, the focus has been put in the use of nanocomposites as promising immobilization matrices. This is, in part, due to the enormous functional surface area they provide, which increases the microbial and enzyme loading. Metal and carbon derived nanomaterials, as well as electrospun nanofibers have taken the lead in this area [5,8,10,11]. Regarding the use of nanoparticles, an extensive number of studies have described the properties of different nanomaterials such as magnetic nanoparticles, including iron oxide (Fe_3O_4 and $\gamma\text{-Fe}_2\text{O}_3$), alloy-based (CoPt_3 and FePt), pure metal (Fe and Co), and spinel-type ferromagnets (MgFe_2O_4 , MnFe_2O_4 , and CoFe_2O_4)[12], or carbon derived nanoparticles, namely single and multiwall carbon nanotubes, graphene, graphene oxide, fullerene, etc.[4,13,14,15], as suitable carriers for enzymes of industrial interest. Similarly, applications for the use of these types of nanomaterials for the immobilization of prokaryotic and eukaryotic microorganisms have been investigated [11,16,17,18].

Among the different carbon-derived nanomaterials, graphene oxide has received a particular focus for biological applications because of its vast surface area, electroconductivity, superflexibility, and thermal stability, which makes this type of nanomaterial a suitable biological carrier [19,20]. Currently, it is possible to find in the market a portfolio of graphene oxide derivatives,

expanding the availability of possible microbial and biomolecule immobilization materials for different applications. The use of distinct commercial graphene oxide nanoparticles can influence dramatically the biocatalyst loading, biochemical properties, and stability. For this reason, the selection of an optimal biocatalyst-carrier combination makes advisable a thorough screening of the available options⁴. Also, in regard to the suitability of graphene oxide derivatives as support for microbial immobilization, conflicting results relating biocompatibility and cytotoxicity induced by these nanomaterials have been reported in the literature[21], which could be in part due to their heterogeneity in functional groups composition, the presence of different amounts of trace elements, their size and morphology, etc. The fact that the materials used in most biocompatibility and toxicology studies are mostly homemade makes it challenging to achieve highly reproducible results. According to previous reports, graphene oxide nanoparticles have dose- and size-dependent toxicity toward different cell lines, such as human fibroblast, human hepatocellular carcinoma, human skin keratinocyte, etc. [22,23,24,25,26]. However, the amount of literature available focusing on the biocompatibility analysis of graphene with microbial cells is much scarcer.

In this research study we selected two graphene derivatives: monolayer graphene oxide (GO; supplied by Graphenea) and graphene oxide nanocolloids (GOC; supplied by Sigma-Merk), and both their toxicological potential against different unicellular organisms and their binding affinity toward different industrial enzymes was compared.

Results and Discussion

Characteristics of the Selected Commercial Graphene Oxide Derivatives

The physical-chemical properties of the graphene oxide derivatives selected for this study were recently determined [4]. Microscopy analyses using AFM and TEM instruments showed that GO and GOC flakes were mostly in monolayer state and had a different size, while the analysis of their composition revealed a high similarity between both nanomaterials. In the present study, the same commercial nanomaterials' suspensions were selected, but a new batch of the GOC material was used (for more details see the Materials and Methods section). Therefore, we decided to perform a new microscopy and spectroscopy analysis to confirm the physico-chemical properties of the new GOC sample. Surprisingly, new AFM and TEM analyses revealed that the nanoparticles of the new GOC batch were morphologically very different to the older GOC batch (GOC_o), showing instead a high similarity in morphology and size to that observed on the monolayer GO particles (Figure 1).

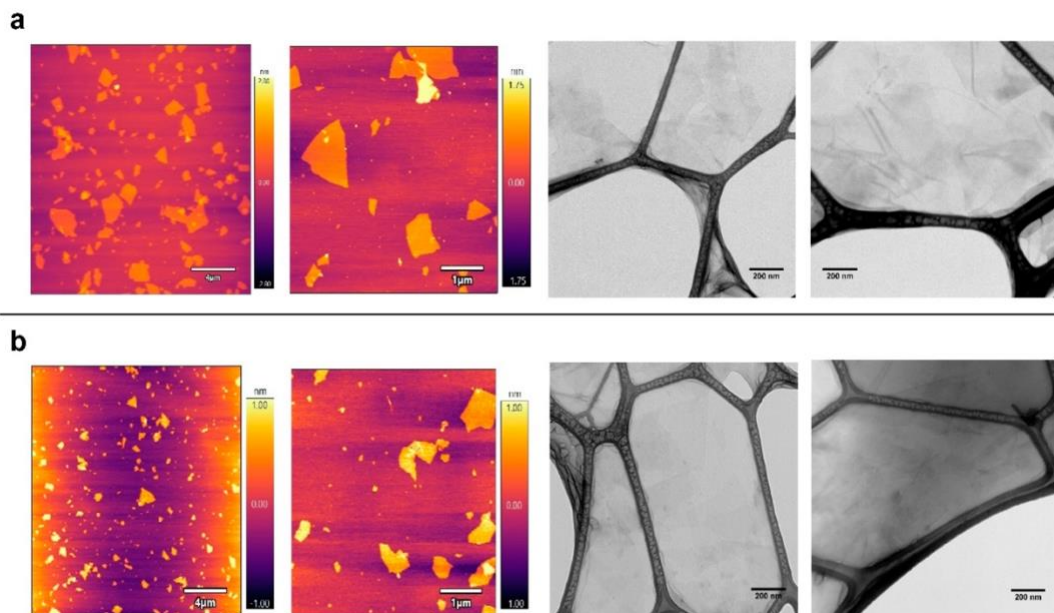


Figure 1. AFM and TEM analysis of graphene oxide (GO) (a) and graphene oxide nanocolloids (GOC) (b). Graphene suspensions with a final concentration of 20 mg L^{-1} were deposited by drop casting on a mica surface and carbon-coated copper grids respectively.

AFM topography imaging showed that both nanomaterial types have a wide lateral size distribution, ranging from the nanometric to the micrometric scale, while the flakes thickness is around 1–2 nm. Graphene oxide nanomaterials of similar characteristics have been reported to produce membrane-damaging activity in different unicellular systems [25,27,28].

The FTIR spectra of GO and the new GOC batch was determined as well, and both nanomaterials showed to be very similar in their oxygen functional groups content (Figure 2). Following the tentative assignments given in the figure, the most significant difference found between GO and GOC was that the former showed a slightly greater content in ether/alcoxy groups than the latter, which

could be related with the increase in the intensity of $\nu(\text{C-O})$ stretching modes reported by other authors [29].

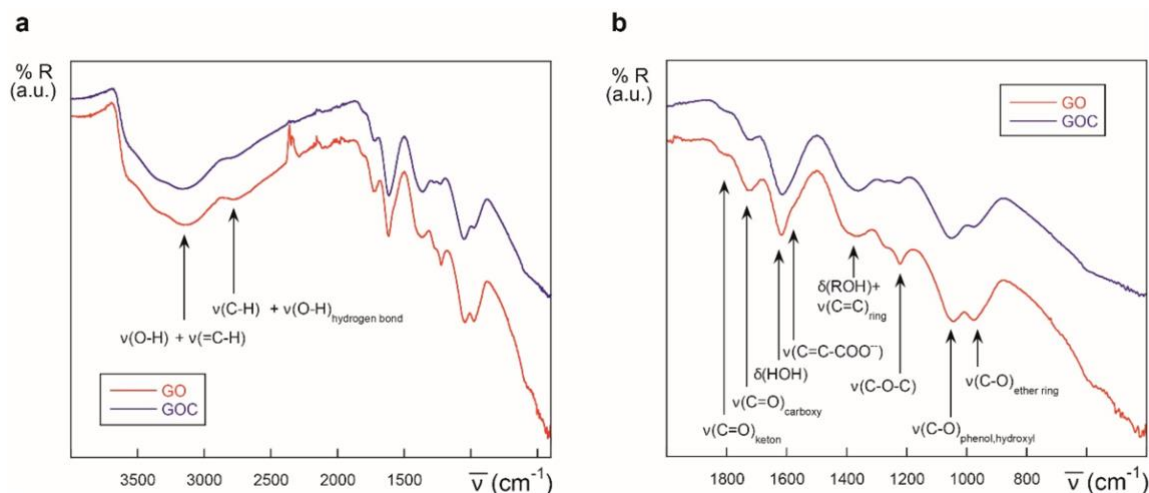


Figure 2. ATR-IR spectra of different graphene derivatives: GO (red) and GOC (blue), in the $4000\text{--}400\text{ cm}^{-1}$ (a) and $2000\text{--}400\text{ cm}^{-1}$ regions (b).

The results obtained indicate that the reproducibility in the production of commercial graphene oxide may still have relevant issues, making essential for the end user to confirm that the purchased product matches with the expected characteristics.

Since the presence of trace metal impurities in graphene derivatives, either contained in the graphite precursor or transferred by reactants used in the nanomaterial preparation, has been previously described, a trace element analysis of GO and GOC was done by inductively coupled plasma mass spectrometry (ICP-MS). As shown in Table 1, the presence of different metallic elements was observed in GO and GOC, although the concentration of most of them was found to be low. Nevertheless, significant differences in the

concentration of some of the identified metals and metalloids were observed between both nanomaterials.

Table 1. Inductively coupled plasma mass spectrometry (ICP-MS) analysis of GO and GOC. Values below the detection limit of the ICP-MS procedure are also shown.

	GO (ppm)	GOC (ppm)
Al	0,160 ± 0,113	1,445 ± 0,106
B	<0,004	1,600 ± 0,255
Ba	0,006 ± 0,008	0,214 ± 0,006
Ca	0,063 ± 0,088	0,835 ± 0,035
Cu	0,052 ± 0,039	0,581 ± 0,030
Fe	0,379 ± 0,067	1,899 ± 0,033
Ga	0,004 ± 0,006	0,047 ± 0,000
K	3,770 ± 0,184	2,628 ± 0,252
Mg	0,350 ± 0,028	2,000 ± 0,113
Mn	34,700 ± 0,156	62,405 ± 0,233
Mo	0,029 ± 0,002	0,017 ± 0,001
Na	1,240 ± 0,509	4,810 ± 0,057
Ni	0,027 ± 0,020	0,027 ± 0,007
Pb	0,054 ± 0,023	0,152 ± 0,009
Sn	0,003 ± 0,003	0,034 ± 0,001

Sr	0,008 ± 0,001	0,034 ± 0,001
V	<0,0001	0,006 ± 0,001
W	0,004 ± 0,001	0,006 ± 0,001
Zn	0,068 ± 0,061	1,069 ± 0,740

Overall, the concentration of metallic elements was higher in GOC than in GO. Both nanomaterials showed to have a high content of Mn (GO: 34.700 ppm; GOC: 62.405 ppm) and K (GO: 3.770; GOC: 2.628 ppm), which suggests they were obtained through the Hummer's method, which is the most common oxidation method currently used for GO production and known to result in residual manganese accumulation because of the use of permanganate oxidant (KMnO_4)[30]. Additionally, ICP-MS data suggested the possible presence of S in both nanomaterials, which can be present as well in graphene oxide prepared through the Hummer's method, being its content significantly higher in GO. However, the obtained results in case of GOC were close to the background noise. For this reason, to get further insight into the possible presence of sulfur species and the differences in their content between GO and GOC, XPS analysis was performed. Again, the obtained results indicated that S species were higher in GO (relative atomic percentage: 0.6%) than in GOC, where a reliable quantitative value could not be determined. The presence of organosulfate groups in graphene oxide is described, and suggested to be responsible for part of the reactivity of this nanomaterial, such as in the

immobilization of adsorbed species [31]. However, we could not get insights on the type of S species (e.g., organic or inorganic) present in GO or GOC.

Determination of Human Cancer Cell Line A549 Response to GO and GOC

The viability of the human cell line A549 after 24 h of exposure to 40, 80, and 160 mg L⁻¹ of GO and GOC was analyzed using the neutral red uptake and MTT assays. The neutral red assay is based on the ability of healthy cells to incorporate and retain the neutral red dye in their lysosomes, which is an indicator of the cell's capacity to maintain pH gradients through the production of ATP, and thus a viability indicator. In Figure 3, the results obtained for neutral red assay are presented. No negative effects on cell viability was observed in any of the concentrations tested for both nanomaterials, showing all the studied conditions (negative control and exposed cells) a similar percentage of viable cells.

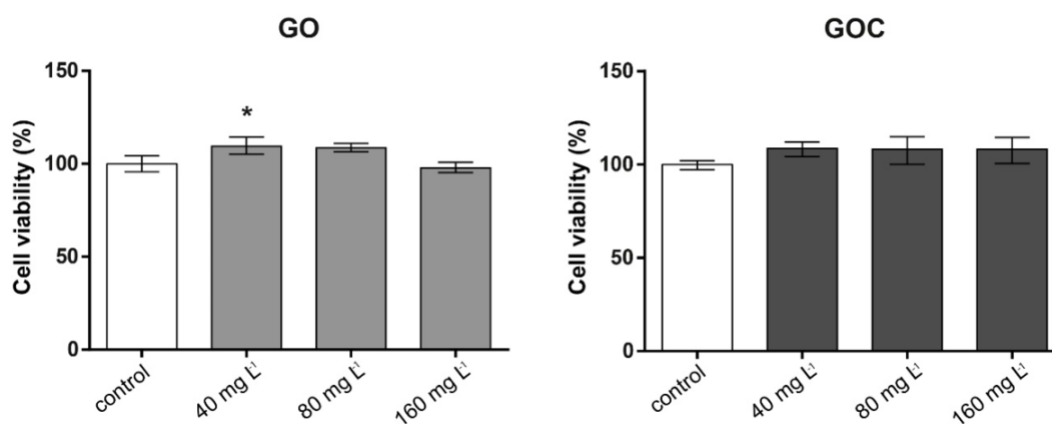


Figure 3. Viability of A549 cells (neutral red assay) treated with different concentrations of GO (left) and GOC (right). Results are expressed as % of control (untreated cells). Data represent the mean (\pm standard deviation, SD) of

three independent replicates. Differences were established using a one-way ANOVA followed by Dunnett post hoc test to compare every mean with the control, and considered significant at $p \leq 0.05$. * $p \leq 0.05$.

The MTT assay is based on the ability of viable cells with active metabolism to convert MTT into a purple colored formazan product that can be measured at OD 590 nm, being this color formation a useful marker to assess cells viability. The cytotoxicity studies conducted using this assay (Figure 4) revealed that cells exposed to GOC presented a slight decline in viability at the higher concentrations tested, being statistically significant in the case of cells exposed to 160 mg L^{-1} , whereas in cells incubated with GO, no significant differences were found between controls and samples.

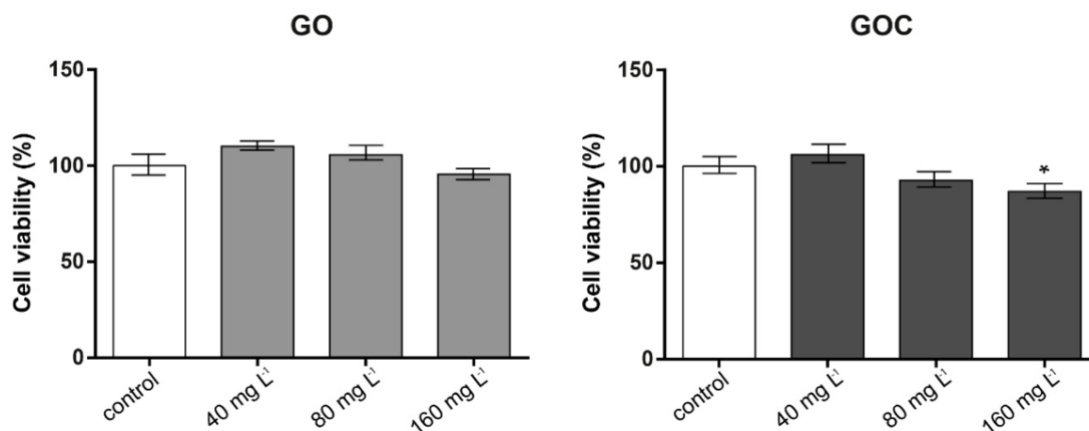


Figure 4. Viability of A549 cells (MTT assay) treated with different concentrations of GO (left) and GOC (right). Results are expressed as % of control (untreated cells). Data represent the mean (\pm standard deviation, SD) of three independent replicates. Differences were established using a one-way

ANOVA followed by Dunnett post hoc test to compare every mean with the control, and considered significant at $p \leq 0.05$. * $p \leq 0.05$.

The toxicity of graphene oxide in human cell lines has been widely investigated in different studies. However, the results and conclusions reached by them are apparently inconsistent, as evidenced by some of the recent reviews [21,32]. Several factors, such as the size, the surface chemistry, or the levels of impurities, critically affect the physico-chemical properties of the nanoparticles and, subsequently, the interactions with cells, which lead to differences in their inherent cytotoxicity. Moreover, the toxicity of GO varies greatly depending on the cell line and cell type exposed [33]. In our experiments, only a slight statistically significant decrease in viability was detected in A549 cells treated with 160 mg L^{-1} of GOC (less than 15% of decrease) performing the MTT assay, whereas no negative effect was detected in the NR assay. It is also important to mention that in both assays a different number of cells per well were used, being six times lower in the MTT assay. Even in this case, where the nanoparticle/cell exposure ratio was higher, both GO and GOC demonstrated to be safe in terms of cell viability. These results are in concordance with the work of Chang et al. [34], which was performed using the same cell line. These authors described the good biocompatibility of GO, describing only a slight decrease in the viability after an exposure to high doses. In contrast, other authors observed a negative effect on the viability caused by these nanoparticles on A549 cells. Gies et al. described a size and dose dependent effect, showing a high decrease in the percentage of viable cells

after 24 h of exposure to high concentrations of GO (100 and 200 mg L⁻¹) [33]. Likewise, Reshma et al. showed a dose-dependent decrease in viability of cells treated with reduced GO (rGO) and PEGylated GO [35]. These authors observed a significant reduction from concentrations of, at least, 25 mg L⁻¹. Mittal et al. analyzed the interaction between three graphene oxide derivatives with A549 cells [36], observing a significant reduction of viability over 48 h of exposure even at low concentrations, whereas Hu et al. described only a mild effect in cytotoxicity of A549 cells exposed during 24 h to GO and rGO, being significantly higher in the case of the latter [37]. This variability between the results obtained using the same cell line could be attributed to the factors explained above, such as the levels of impurities present in the nanoparticles, or even the oxidative method through which the nanoparticles were prepared, which influence their toxicological behavior [38].

In relation to the possible induction of oxidative stress by GO and GOC, the DCFH-DA assay was used to measure the reactive oxygen species (ROS) levels on the A549 cells after contact with different concentrations of the nanomaterials. Figure 5 shows that the ROS levels were significantly increased in A549 cells after 1 h of exposure to both nanoparticles, being this induction much higher in the case of the cells incubated with GO.

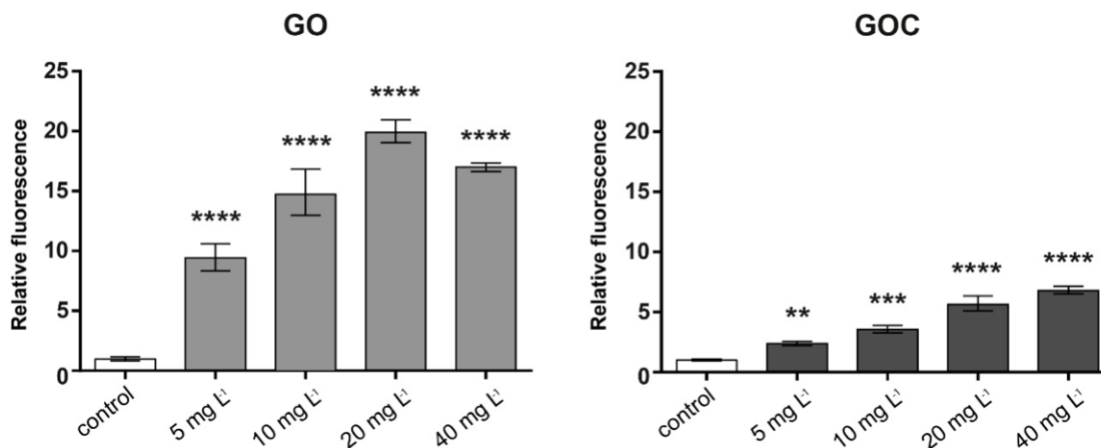


Figure 5. Reactive oxygen species (ROS) production of A549 cells treated with different concentrations of GO (left) and GOC (right). The reported values are expressed in arbitrary units and correspond to the averages of two biological replicates per culture condition. Data represent the mean of three replicates (\pm standard deviation, SD). Differences were established using a one-way ANOVA followed by Dunnett post hoc test to compare every mean with the control, and considered significant at $p \leq 0.05$. ** $p \leq 0.01$, *** $p \leq 0.001$, **** $p \leq 0.0001$.

Our assays were performed using concentrations of both nanoparticle types up to 40 mg L⁻¹. From that concentration, we have observed that in our experimental procedure the fluorescent response may be masked by both GO and GOC, leading to an underestimation of the ROS production. Either way, our results demonstrate that the low concentrations tested in our assays are enough to produce statistically significant levels of oxidative stress after 1 h of incubation, being this much higher in the case of GO. The induction of oxidative stress after interaction with graphene oxides and their derivatives have been

reported in several works using different cell lines [39,40,41]. These nanomaterials can induce cellular damage through the formation of ROS by their interaction with cellular membranes. In the specific case of A549 cell line, several works have demonstrated their ability to induce ROS release. For example, Chang et al. found that GO exposure can induce oxidative stress at low concentrations [34]. Mittal et al. observed an overproduction of ROS in A549 cells in contact with GO and their derivatives, as well as in other human lung cells such as the BEAS-2B cell line [36]. In both studies, the times of exposure tested were longer than the times used in the present work. In any case, based on our results and in previous reports, it has been evidenced that an acute exposure of human cells to graphene oxide can induce high oxidative stress levels.

High levels of ROS can cause damage to different biomolecules of the cell, such as proteins or nucleic acids, which can lead to activation of apoptosis. In order to assess whether the levels of ROS produced by A549 cells after being exposed to GO and GOC can induce an apoptotic response, we quantified the percentages of apoptotic and necrotic cells using flow cytometry, upon the addition of different nanoparticles concentrations for 24 h. The obtained results have shown that cells treated with different GO concentrations (Figure 6b; 40, 80, 160 mg L⁻¹) showed a constant 93–95% of viable cells, similar to the untreated control sample (Figure 6a). In the case of GOC, we evidenced a stable 6–10% cell death, irrespective of the administered dose (Figure 6b). As

a positive control for the assay, we used cisplatin (a common chemotherapeutic agent) which induced over 40% cell death (Figure 6a).

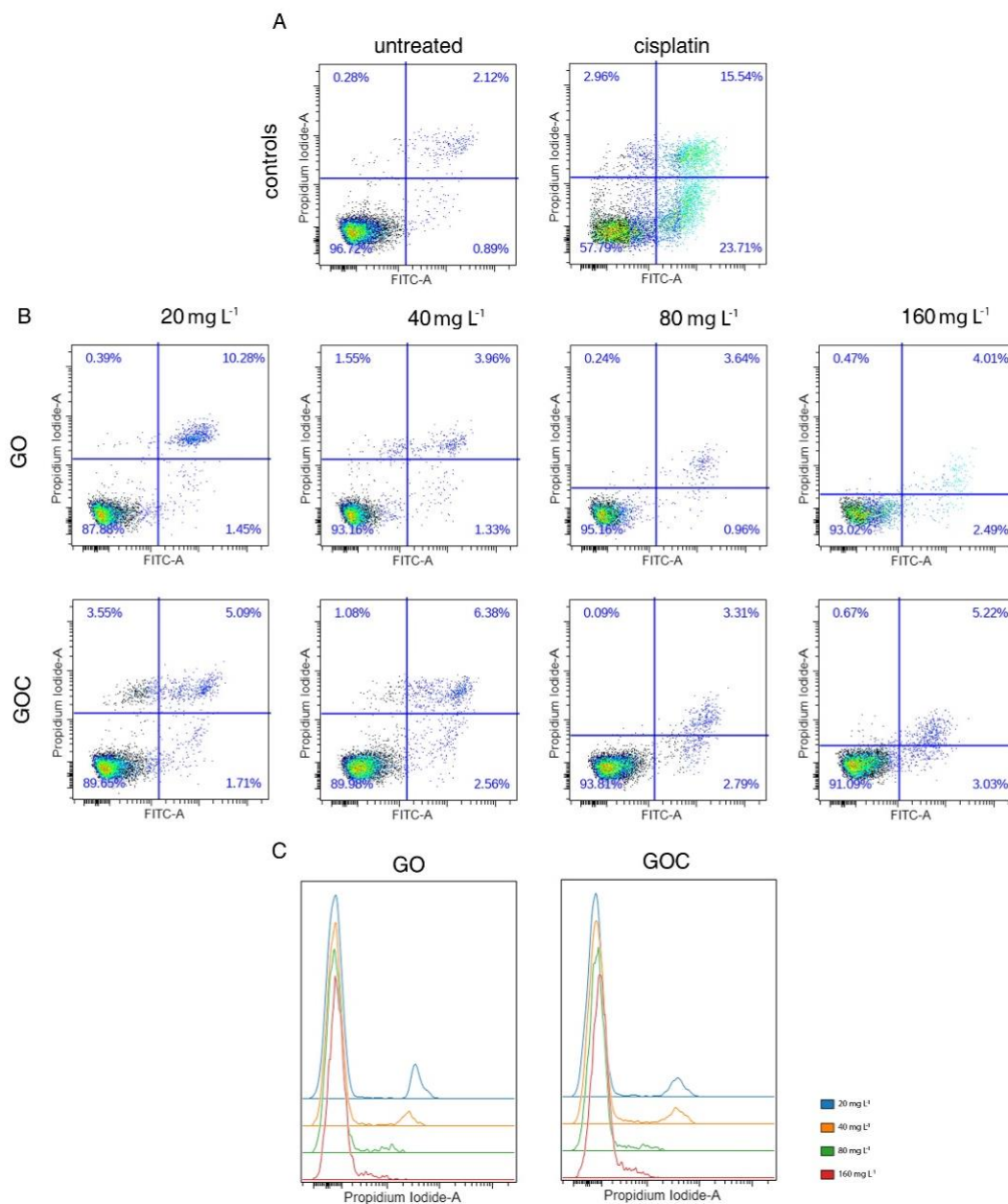


Figure 6. Flow cytometry analysis of apoptosis response of A549 cells treated with different concentrations of GO (top) and GOC (bottom) upon double

staining with Annexin V-FITC and propidium iodide (PI). Results are displayed as density plots and expressed as percent (%) live (low left quadrants), apoptotic (low right quadrants), and necrotic (upper right quadrants) cells (a,b) of the total cell population excluding doublets. Histograms (c) show distribution of PI signal in cells treated with increased doses of GO and GOC.

Interestingly, we found that the PI signal was decreasing in a dose-dependent manner in GO- and GOC-treated cells (Figure 6c). However, despite the signal to noise ratio diminution for the PI staining, this did not impede the quantification of the PI⁺ cell subpopulation. The PI signal decrease is probably caused by the quenching of the dye by the nanoparticles, as previously reported [42,43]. The quenching could be due to the energy transfer from the fluorophore to the metal [42] or in the case of graphenes, it could be due to the excitation of an exciton too [43]. Wu et al. found that the quenching efficiency of GO was still around 30% when the distance between dyes and GO was increased to more than 30 nm [44].

Several studies have described the impact of graphene-based materials on different types of programmed cell death, including apoptosis [45], in diverse cell lines, through distinct mechanisms such as caspase activation or DNA fragmentation [46,47]. For example, in the A549 cell line, the implication of graphene nanopores in the induction of early apoptosis was described and, at concentrations higher than 250 mg L⁻¹, late apoptosis was observed too [48]. In addition, Adil et al. observed that apoptosis can be triggered by green synthesized nanocomposites of silver-decorated highly reduced graphene

oxide [49], while Mbeh et al. described that high concentrations of graphene oxide nanoribbons (100 mg L^{-1}) can also cause cell apoptosis [50]. However, other authors did not find any evidence of apoptosis induction in A549 cells after treatment with GO derivatives. For instance, Chang et al. observed that, independently of dose and size, GO did not induce any apoptosis or necrosis in A549 cells [34]. Moreover, Hu et al. described that apoptosis did not occur in A549 cells treated with GO nanosheets after a 24-h exposure with 20 and 85 mg L^{-1} [37]. Finally, Yang et al. found that the exposure to different graphene quantum dots, even at high concentration (200 mg L^{-1}), did not result in apoptosis induction [51]. The results described in these latter works are in concordance with our observations, since, in spite of the fact that both GO and GOC produced oxidative stress in A549 cells, no significant increase in apoptosis was detected at concentrations up to 160 mg L^{-1} .

Determination of *Saccharomyces Cerevisiae* Cells Response to GO and GOC

The viability of *S. cerevisiae* cells exposed to two different GO and GOC concentrations (160 and 800 mg L^{-1}) and exposure times (2 and 24 h) was assessed through colony forming units (CFU) determination. As displayed in Figure 7, no significant differences in viability were observed in the selected exposure conditions after 2 h of exposure, except for the condition where a high GOC concentration was used. However, after 24 h, viability issues could be observed after a longer exposure time. In case of GO, the nanomaterial reduced *S. cerevisiae* CFUs after an exposure of 24 h, provoking a viability loss

of 36.5% when the material was present at the lower concentration and 49.7% when the material was present at the higher concentration. In contrast, GOC showed no significant influence on the yeast viability at 160 mg L⁻¹, although the viability loss observed at the higher concentration was very similar for both nanomaterials. The effect on *S. cerevisiae* viability of non-commercial grade graphene oxide nanoparticles was also tested in a recent study, and the fungus mortality was found to be close to 20% in the presence of 600 mg L⁻¹ [52]. Also, the toxicological potential of other carbon nanomaterials toward *S. cerevisiae* was reported, such as multi-walled carbon nanotubes (MWCNTs) or oxidized single-walled carbon nanotubes (O-SWCNTs), which induced significant yeast mortality at 400 mg L⁻¹ (6.1%) and 188.2 mg L⁻¹ (approximately 11%) respectively [53,54].

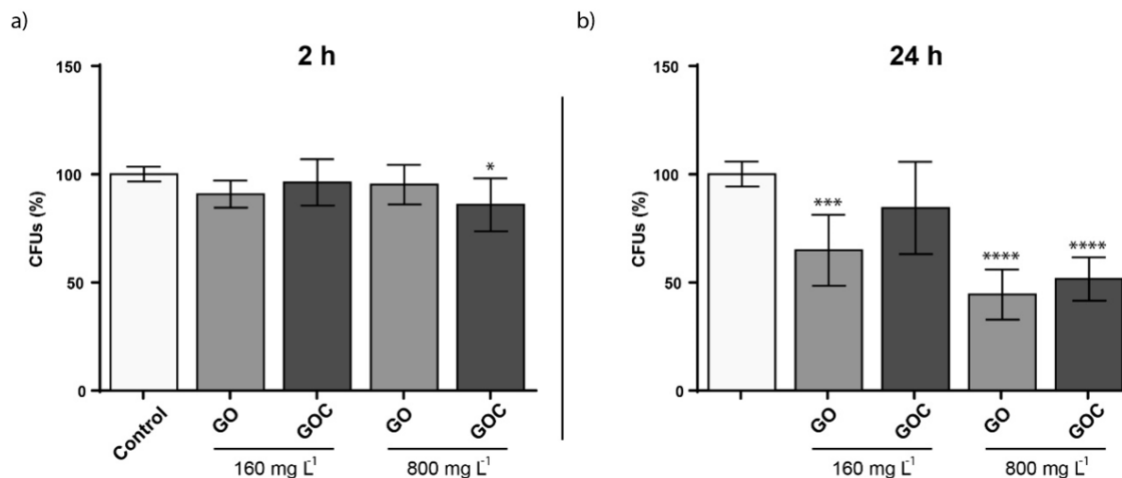


Figure 7. Colony forming units (CFUs) determination of *S. cerevisiae* cells exposed to 160 and 800 mg L⁻¹ of GO and GOC during 2 h (a) and 24 h (b). The reported values are the averages of three biological replicates per culture

condition. Differences were established using a one-way ANOVA followed by Dunnett post hoc test to compare every mean with the control, and considered significant at $p \leq 0.05$. * $p \leq 0.05$, *** $p \leq 0.001$, **** $p \leq 0.0001$.

To evaluate whether GO and GOC were able to induce oxidative stress in *S. cerevisiae*, cells growing at exponential phase were exposed to 160 and 800 mg L⁻¹ of the nanomaterials, for 24 h. As shown in the Figure 8, the oxidative stress levels were significantly increased in *S. cerevisiae* in the presence of both carbon nanoparticles. Carbon derived nanomaterials have shown previously to induce oxidative stress in yeast. Non-commercial grade GO and O-SWCNT, also induced ROS with a similar concentration to the one tested here, although the exposure time tested in both cases was 24 h instead of 2 h [52,54]. However, the oxidative stress provoked by MWCNT in yeast seem to be lower than that observed in the present study for GO and GOC or that previously observed for other carbon derived nanoparticles [53].

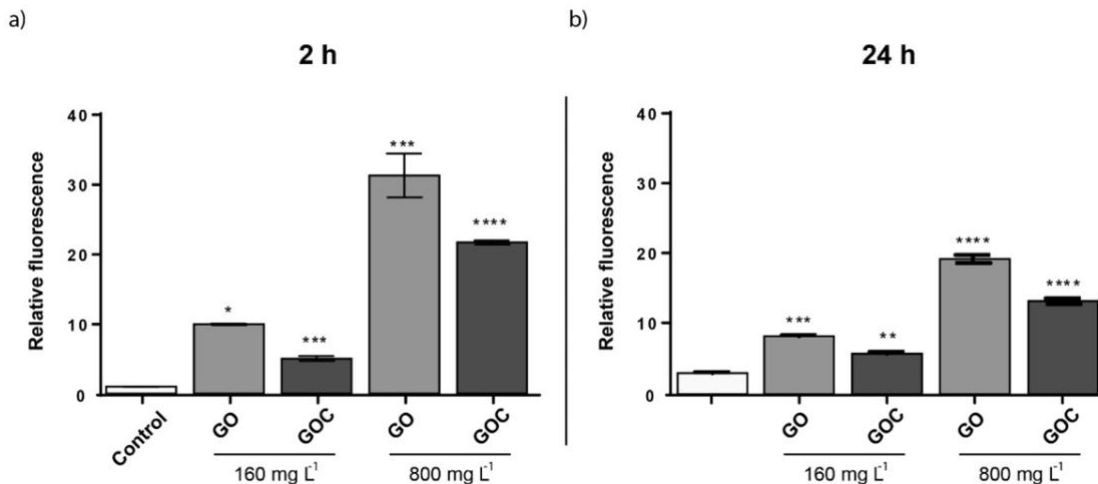


Figure 8. Oxidative stress (ROS) determination of *S. cerevisiae* cells exposed to 160 mg L⁻¹ of GO and GOC during 2 h. The reported values are expressed in arbitrary units and correspond to the averages of two biological replicates per culture condition. Differences were established using a one-way ANOVA followed by Dunnett post hoc test to compare every mean with the control, and considered significant at $p \leq 0.05$. * $p \leq 0.05$, ** $p \leq 0.01$, *** $p \leq 0.001$, **** $p \leq 0.0001$.

We also aimed to determine the possible genotoxic effect of the selected graphene oxide nanomaterials on *S. cerevisiae* using the comet assay protocol previously described [55]. However, because of the nanomaterials' morphology, graphene oxide concentrations higher than 20 mg L⁻¹ prevented the proper visualization and analysis of the cell nuclei under the fluorescence microscope, making the comet assay an unsuitable method for the determination of genotoxicity in yeast with two dimensional nanoparticles of a big lateral size.

Determination of *Vibrio Fischeri* Bioluminescence Inhibition to GO and GOC

The marine bacteria *Vibrio fischeri* was also used to compare the toxicological potential of both graphene oxide suspensions. The *V. fischeri* luminescence assay is an environmental monitoring tool to determine the toxicity in sediments and leachates that may be a source of contamination in aquatic ecosystems. The ability of the nanomaterials to inhibit the microorganism luminescence was measured at two concentrations (160 and 800 mg L⁻¹) and exposure times (10 and 30 min). When the lower concentration of GO and GOC was present in the media, we did not observe a *V. fischeri* significant luminescence inhibition. The bacteria luminescence decreased in the presence of a higher concentration of the nanomaterials, with significant difference between both nanomaterial types (Figure 9). In case of GO, the presence of 800 mg L⁻¹ induced a 100% of luminescence inhibition, already after 10 min of exposure. In contrast, the same concentration of GOC showed a significantly lower luminescence inhibition capacity at both exposure times ($p < 0.001$ and $p < 0.01$ respectively).

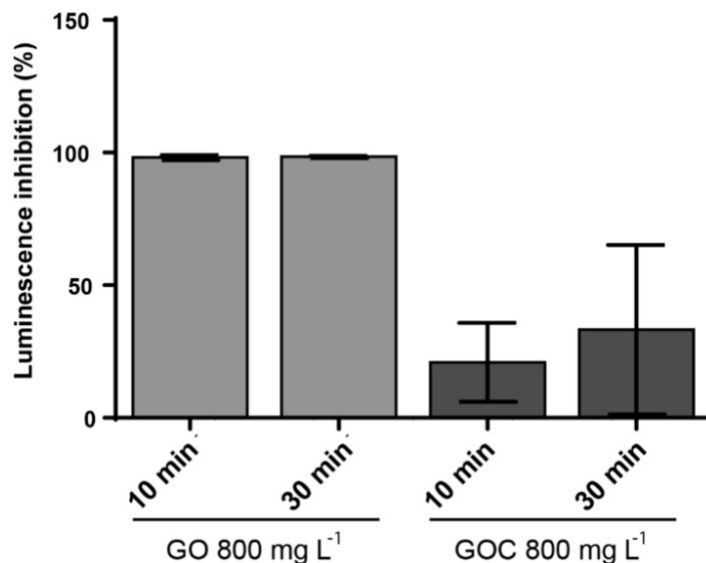


Figure 9. Luminescence inhibition assay of *V. fischeri* cells exposed to 800 mg L⁻¹ of GO and GOC during 30 min. The reported values are the averages of four biological replicates per culture condition.

Previous studies have evaluated the luminescence inhibition of *V. fischeri* promoted by nanomaterials, such as nano-metal oxides, nanoscale cationic polymers, silica nanoparticles, catechol-based submicron particles or functionalized reduced graphene oxide nanoparticles [56,57,58,59]. Interestingly, the toxicity of reduced graphene oxide functionalized with Fe₃O₄ [57], was similar to that observed for GOC in the present study.

Determination of GO and GOC Binding Efficiency on Different Microbial Enzymes

Biotechnological and biomedical applications of graphene oxide rely on nanomaterial-biomolecule interactions. The protein binding capacity of nanomaterials determines possible biological applications and their

toxicological potential too [60,61]. In case of commercial GO and GOC, both nanomaterial suspensions showed a high protein loading capacity and a good potential as enzyme immobilization supports [4]. However, their maximum protein binding capacity was not determined, and their polypeptide binding properties were determined using a single enzyme. Also, having into account that the protein binding efficiency of the new GOC lot (MKCD9594) was unknown, we decided to characterize the nanomaterial-enzyme binding efficiency of GO and GOC. In addition, to assess whether a variation on the GO and GOC oxidation state could further increase their enzyme loading capacity, the nanomaterials were partially reduced and their protein binding capacity was compared with that of the untreated nanomaterials. The partial reduction of GO and GOC was performed using a concentrated solution (50 mM) of the mild reductant mercaptoethylamine-HCl (further details are described in the Materials and Methods section). The reduction of the nanocarbon derivatives was confirmed by ATR-FTIR analysis (Figure 10). The spectrum of GOC exhibited drastic changes after the nanomaterials' treatment with the mercaptoethylamine-HCl. Basically, the intensity of the absorptions sharply decreased, in good agreement with the reduction of the described functional groups. In the case of rGO, an analogous trend to that shown by the rGOC spectrum was observed.

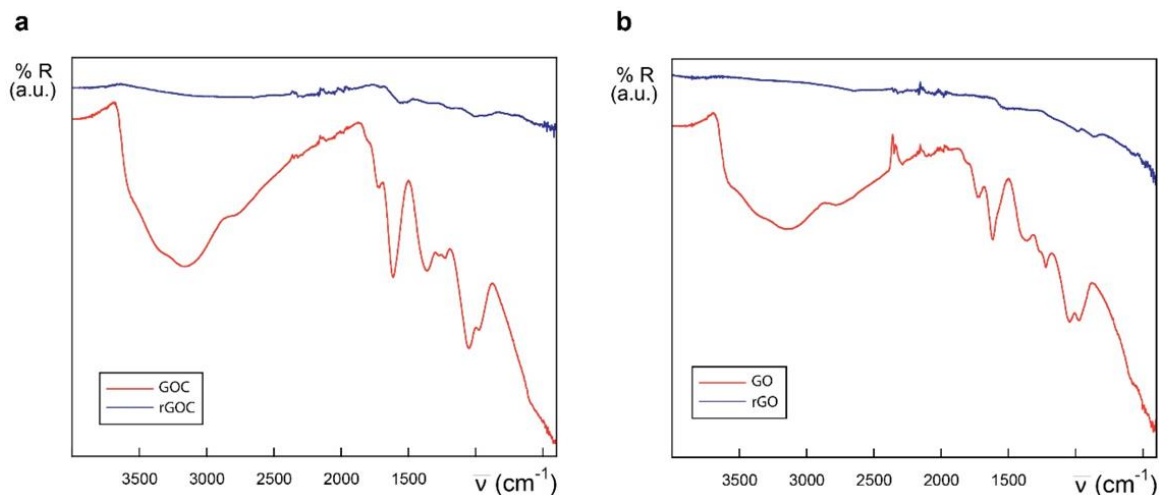


Figure 10. IR spectra of GOC and rGOC (a) and GO and rGO (b) in the 4000–400 cm^{-1} region.

The maximum enzyme loading capacity of chemically reduced GO (rGO) and GOC (rGOC) was analyzed and compared with that of the non-modified nanoparticles, using the bacterial enzymes α -L-rhamnosidase enzyme RhaB1, from *Lactobacillus plantarum*, and the β -D-glucosidase AbG, from *Agrobacterium* sp. (strain ATCC 21400), following the immobilization protocol described previously [4]. As displayed in Table 2, the binding capacity of GO and GOC was different for both enzymes and significantly higher than that observed in the reduced versions of the nanoparticles.

Table 2. Maximum binding capacity (%) of GO, GOC, rGO, and rGOC using different carbohydrate active enzymes.

Carbon nanomaterial	RhaB1 binding (mg mg ⁻¹)	AgB binding (mg mg ⁻¹)
GO	4,88 ± 0,17	1,65 ± 0,04
GOC	5,90 ± 0,11	1,22 ± 0,14
rGO	1,98 ± 0,11	1,00 ± 0,03
rGOC	1,99 ± 0,23	0,70 ± 0,08

Although π - π stacking and hydrophobic effects are considered the predominant mechanisms of protein binding with graphene-based materials, and both phenomena should be more dominant after the reduction of graphene oxide, the reduced versions of GO and GOC did not improve the enzyme binding capacity of the untreated nanomaterials. Previous studies reporting the influence of graphene oxide reduction on protein binding capacity show controversial results [60,62,63,64]. As recently described by Qi and collaborators [64], changes on graphene-based nanomaterials' surface properties affect as well their aggregation properties, which may become a crucial factor influencing their protein adsorption capacity. The obtained result also showed that the maximum loading capacity of GO and GOC was significantly higher for the α -rhamnosidase RhaB1. A similar result was observed when using the reduced versions. Different enzymes could exhibit different enzyme loadings and stabilities when bound to graphene oxide

because of the differences in the charge status of their surface functional groups [65].

The obtained results using distinct unicellular models and biomolecules display significant changes in the toxicological potential of GO and GOC: the former had a higher ability to induce oxidative stress in human alveolar carcinoma epithelial cells A549, and the yeast *Saccharomyces cerevisiae*, while provoking a higher luminescence inhibition capacity on the bacteria *Vibrio fischeri* too. Also, both products behaved differently in their enzyme binding capacity. The lateral dimension, surface structure, functional groups, purity and protein corona, strongly influence the toxicity of graphene oxide in biological systems [66]. Since GO and GOC are distinct in terms of their apparent particle size distribution, elemental composition and in the presence of oxygen functional groups, identifying the most relevant factors determining the differences observed regarding their toxicological potential is difficult. Nevertheless, the present work contributes to have a better understanding on the biological impact and biotechnological potential of commercial grade graphene oxide.

Conclusions

The results obtained in the present study show the potential of different commercial graphene oxide nanomaterials to interact with distinct unicellular systems and biomolecules, pointing out the variability that can be found in terms of toxicological potential and binding affinity depending on the target organism or protein, and the selected nanomaterial. GO showed a higher

capacity than GOC to induce oxidative stress in both *S. cerevisiae* and human cells. In the same line, GO showed a significantly higher *V. fischeri* luminescence inhibition too. Also, differences in the binding capacity of both nanomaterials were observed, being their maximum loading capacity different as well, in function of the enzyme tested. Therefore, the presented results clearly indicate the usefulness of this type of studies in order to determine the actual toxicological and biochemical potential for specific commercial graphene oxide products.

Materials and Reagents

Most of the chemicals and reagents were purchased from Sigma-Aldrich (Merck KGaA, Darmstadt, Germany) and Acros Organics (Thermo Fisher Scientific Inc., Madrid, Spain). The graphene derivatives were obtained from different suppliers as well; graphene oxide nanocolloids (GOC; ref: 795534; old lot: MKBT5205V; new lot: MKCD9594) were purchased from Sigma-Aldrich, and monolayer graphene oxide (GO; C309/GORB014/D1) was purchased from Graphenea (San Sebastian, Spain). The α -l-rhamnosidase RhaB1 from *Lactobacillus plantarum* and the AbG β -d-glucosidase from *Agrobacterium* sp. (strain ATCC 21400) were obtained from Megazyme Ltd. (Biocon S.L., Barcelona, Spain).

ATR-FTIR Analysis

IR spectra were recorded on dry solid samples in the 4000–400 cm^{-1} region by a JASCO FT-IR 4200 spectrophotometer equipped with a Single Reflection

ATR PRO ONE device. Each of the graphics is the result of overlapping 128 scans with a 4 cm^{-1} resolution.

ICP-MS

Samples (0.1 g) were subjected to a digestion process with 7 mL of HNO₃ Suprapur (Merck KGaA, Darmstadt, Germany) (65% v/v) and 1 mL of H₂O₂ (30% v/v), while being subjected to the following thermal treatment: a temperature gradient from room temperature up to 80 °C in 4 min, followed by a second temperature gradient, from 80 to 120 °C in 4 min, and by a third temperature gradient, from 120 to 190 °C in 5 min. Then, temperature was kept constant at 190 °C for 30 min, and finally samples were cooled down for 1 h. The analysis of the digested samples was done with an Agilent 8900 ICP-QQQ instrument.

XPS Analysis

X-ray photoelectron spectroscopy (XPS) was done by the SGIker unit at the University of the Basque Country (UPV/EHU) using a SPECS system equipped with a Phoibos 150 on powders deposited into glass slides.

AFM and TEM Analysis

AFM and TEM analyses were performed at the Microscopy Unit from the University of Valladolid. Samples were deposited on Lacey Carbon Type-A, 300 mesh, copper grids, and visualized and photographed using a JEOL JEM-1011 HR TEM coupled with a Gatan Erlangshen ES1000W camera. For AMF analysis, samples were deposited on a mica surface from aqueous solutions

by drop casting. Images were recorded in AC mode (tapping mode) with a CYPHER ES instrument from Asylum Research (Oxford Instruments, Abingdon, UK), using silicon cantilevers AC160TS-R3 with aluminum reflex coating (Olympus) and tip radius <10 nm. The analysis was done using a set point of 500, 72 mV, a drive amplitude of 791.16, a drive frequency of 268.639, and integral gain of 268.639. Data acquisition and control was done with IGOR Pro 6.2 (Asylum Research, Oxford Instruments, Abingdon, UK). Images analysis was done with ARgyle (Argyle Software Ltd., Bath, UK).

Assays in A549 Cells

The human alveolar carcinoma epithelial cell line A549 (ATCC, CCL-185) was utilized for toxicity evaluation. Cells were grown in DMEM medium (Dulbecco's Modified Eagle Medium) supplemented with 10% fetal calf serum (FCS), 1% penicillin/streptomycin and grown in a humidified incubator at 37 °C in the presence of 5% CO₂.

Neutral Red Assay

A549 cells were seeded in 96 well plates at 3×10^4 cells per well and treated with 40, 80, and 160 mg L⁻¹ of the materials diluted in DMEM 1% FCS. After 24 h of exposure, cells were washed and incubated with 100 µL of the neutral red solution which was prepared as follows: neutral red stock (4 mg L⁻¹) was diluted 1/100 in treatment media, and incubated in the dark for 24 h at 37 °C before use. At that time, the solution was centrifuged to remove debris from

neutral red powder. After 2.5 h incubation, neutral red solution was discarded, cells were washed once with DPBS (Dulbecco's phosphate-buffered saline), and subsequently fixed with formaldehyde 4%. Cells were washed again with DPBS and a dye release solution (50% ethanol 96°, 49% distilled H₂O, and 1% acetic acid) was added to each well. After 10 min of gentle shaking, this solution was transferred to a new opaque 96-well plate, and fluorescence was measured with a microplate reader (BioTek Synergy HT, excitation wavelength, 530/25; emission wavelength 645/40). Results were expressed as percentage of control (absorbance of cells in absence of materials). Each assay included three independent replicates.

MTT Assay

A549 cells were seeded in 96 well plates at 5×10^3 cells per well and treated with 40, 80, and 160 mg L⁻¹ of the materials diluted in DMEM 1% FCS. Cells incubated with medium alone were used as controls. Plates were then incubated for 24 h and, after exposure, cell culture medium with materials was discarded, wells were washed with DPBS, and a solution of MTT (3-(4,5-dimethylthiazol-2-yl)-2,5-diphenyltetrazolium bromide) (0.5 mg L⁻¹) was added to each well and incubated for 3 h, followed by adding 100 μ L DMSO to dissolve the MTT crystals. After 15 min of gentle shaking, the absorbance was measured with a microplate reader (BioTek Synergy HT, OD 590 nm). Results were expressed as percentage of control (absorbance of cells in absence of materials). Each assay included three independent replicates.

ROS Determination in Human Cells

The quantitative measurement of intracellular reactive oxygen species (ROS) was investigated using 2,7-dichlorofluorescein diacetate (DCFH-DA). A549 cells were seeded in a 96 micro-well plate at 3×10^4 cells per well and labelled with $50 \mu\text{M}$ DCFH-DA in Hanks' Balanced Salt Solution (HBSS) for 30 min. After the incubation, cells were washed once with HBSS, and different concentrations of the materials diluted in HBSS were added to each well. Fluorescence was measured with a microplate reader (BioTek Synergy HT, excitation wavelength, 530/25; emission wavelength 645/40) after 1 h of incubation.

Apoptosis Assay

Flow cytometry was used for the quantitative assessment of apoptosis. A549 cells were seeded in 24 well plates at 10×10^4 cells per well and treated with 40, 80, and 160 mg L^{-1} of the materials diluted in DMEM 1%FCS. Cells incubated with medium alone were used as negative controls while cells treated with $50 \mu\text{M}$ cisplatin served as positive control for the staining. After 24 h of incubation, cells in suspension were harvested and collected together with the monolayers detached using trypsin-EDTA solution (Invitrogen), for each sample. After centrifugation, cells were resuspended in buffer and stained using a dead cell apoptosis kit with Annexin V-FITC and propidium iodide (Molecular Probes) according with manufacturer's protocol. Samples were filtered through $70\text{-}\mu\text{m}$ nylon meshes (Miltenyi Biotec) and acquired on a BD FACSVerser analyzer controlled by FACSuite software (BD Biosciences, Franklin Lakes, United States). Analysis was performed on the Cytobank

platform (<https://community.cytobank.org>). Single stained controls, using Triton-X-100 permeabilized (0.2% in PBS, 10 min) and untreated cells, respectively were generated for compensation purposes and gating thresholding. Results are depicted as color density plots and histograms.

Assays in *Saccharomyces Cerevisiae*

The *S. cerevisiae* BY4741 strain was grown and maintained in standard liquid YPD medium (1% yeast extract, 1% yeast bacto-peptone, 2% glucose). Cell cultures in liquid media were done on a rotary shaker at 185 rpm at 30 °C.

Colony Forming Units Determination

Yeast cells in exponential growth phase ($OD_{600} = 1$) were exposed to GO and GOC at 160 and 800 mg L⁻¹ in 1 mL cultures performed in 24-well plates. Samples were obtained after 2 and 24 h of cells exposure. To determine yeast colony forming units after the two exposure times, cells were inoculated on solid YPD medium (6% agar) and incubated at 30 °C.

ROS Determination in *S. cerevisiae*

Intracellular levels of reactive oxygen species were determined using the reagent CM-H2DCFDA following a protocol similar to that reported by James et al. (2015)⁶⁷. *S. cerevisiae* cells growing in exponential phase were pelleted, washed, and incubated with CM-H2DCFDA (7 μM) in DPBS for 60 min at 30 °C and 185 rpm. Afterwards, yeast cells were washed again, resuspended in YPD and subsequently exposed to the graphene oxide nanomaterials (160 mg L⁻¹) for 2 h. Then, yeast cells were washed two times with DPBS, incubated 2

min in a solution containing AcLi 2M, and subsequently washed and incubated again for 2 min in a solution containing SDS (0.01%) and chloroform (0.4%). Finally, cells were pelleted and the supernatant was transferred to a black opaque 96-micro-well plate, where the fluorescence was measured (excitation = 485; emission = 528) using a microplate reader (Synergy-HT, BioTek).

Vibrio Fischeri Luminescence Inhibition Assay

V. fischeri NRRL B-11177 cells were inoculated in 5 mL of Marine Broth 2216 and grown at 15 °C for 48 h. The bacterial suspension was pelleted, resuspended in 5 mL of NaCl 2% (w/v) at 15 °C and maintained at 10 °C for 30 min. The exposure experiment was started by pipetting 10 µL of the bacterial suspension in black opaque microplate wells containing 90 µL of GO and GOC (160 and 800 mg L⁻¹) in a water suspension containing NaCl 2% (w/v). The 96-well plate was incubated in a Thermomixer at 800 rpm and 15 °C, and *V. fischeri* luminescence was measured for 30 min using a microplate reader (Synergy-HT, BioTek). The luminescence inhibition (using as reference the negative control condition) was calculated using the values obtained at 10 (M10) and 30 (M30) min using the following formula, adapted from Jarque et al. (2016) ⁶⁸, where CF is a correction factor (the Mt/peak ratio in negative controls) reflecting natural attenuation of bacterial luminescence after 30 min of incubation in non-exposed conditions:

$$INH\% = 100 - \frac{St}{CF \times peak} \times 100$$

Preparation of rGO and rGOC

The mild reductant mercaptoethylamine-HCl was used to reduce commercial GO and GOC nanoparticles. Water suspensions of GO and GOC (1000 mg L⁻¹) containing 50 mM of the reducing agent concentrated were incubated overnight at 4 °C. Afterwards, rGO and rGOC were pelleted, using a Thermo ST 16R Sorvall centrifuge (5000 rpm; acceleration: 9, deceleration: 9), and subsequently washed with a sodium phosphate buffer (12.5 mM; pH 6.5) solution, three times. Finally, the reduced nanomaterials water suspensions were kept at a final concentration of 1000 mg L⁻¹ in sodium phosphate buffer (12.5 mM; pH 6.5), and stored at 4 °C.

Author Contributions

J.A.T.-R. conceived and designed the work. J.A.T.-R., B.D., C.R., J.G.-T., and L.E.S. performed the experiments. J.A.T.-R., B.D., C.R., J.G.-T., L.E.S., and G.N. analyzed and interpreted the data. J.A.T.-R. and C.R. drafted the manuscript. J.A.T.-R., C.R., and G.N. critically revised the manuscript for intellectual content. All authors have read and agreed to the submission of the manuscript. All authors have read and agreed to the published version of the manuscript.

Abbreviations

GO Monolayer graphene oxide

GOC Graphene oxide nanocolloids

ROS Reactive oxygen species

AFM Atomic force microscopy

TEM Transmission electron microscopy

FTIR Fourier-transform infrared spectroscopy

ICP-MS Inductively coupled plasma mass spectrometry

ppm parts-per-million

ATP Adenosine triphosphate

SD Standard deviation

PI Propidium iodide

MWCNs Multiwalled carbon nanotubes

O-SWCNTs Oxidized single-walled carbon nanotubes

rGO Reduced monolayer graphene oxide

rGOC Reduced graphene oxide nanocolloids

DMSO Dimethyl sulfoxide

Funding

This work was supported by the European Union's H2020 research and innovation programme under the Marie Skłodowska-Curie grant agreements N° 691095, N° 721642 and N° 734873; Junta de Castilla y Leon-FEDER under grants N° BU079U16, BU291P18 and BU022G18, and Ministerio de Economía y Competitividad CTQ2016-75023-C2-1-P and CTQ2015-70371-REDT

MetDrugs Network (Spain). We thank Anca Filimon for her invaluable assistance and SITEX 45, particularly to Dumitru Ulieru, for the support.

References

1. Bayat, Z.; Hassanshahian, M.; Cappello, S. Immobilization of microbes for bioremediation of crude oil polluted environments: A mini review. *Open Microbiol. J.* **2015**, *9*, 48–54.
2. Gurung, N.; Ray, S.; Bose, S.; Rai, V. A broader view: Microbial enzymes and their relevance in industries, medicine, and beyond. *Biomed. Res. Int.* **2013**, *2013*, 329121.
3. Robotjazi, S.M.; Shojaosadati, S.A.; Khalilzadeh, R.; Farahani, E.V.; Balochi, N. Immobilization of magnetic modified *Flavobacterium* ATCC 27551 using magnetic field and evaluation of the enzyme stability of immobilized bacteria. *Bioresour. Technol.* **2012**, *104*, 6–11.
4. Antón-Millán, N.; García-Tojal, J.; Marty-Roda, M.; Garroni, S.; Cuesta-López, S.; Tamayo-Ramos, J.A. Influence of three commercial graphene derivatives on the catalytic properties of a *Lactobacillus plantarum* α -l-rhamnosidase when used as immobilization matrices. *ACS Appl. Mater. Interfaces* **2018**, *10*, 18170–18182.
5. Tamayo-Ramos, J.A.; Rumbo, C.; Caso, F.; Rinaldi, A.; Garroni, S.; Notargiacomo, A.; Romero-Santacreu, L.; Cuesta-López, S. Analysis of polycaprolactone microfibers as biofilm carriers for biotechnologically relevant bacteria. *ACS Appl. Mater. Interfaces* **2018**, *10*, 32773–32781.
6. Li, Y.-G.; Gao, H.-S.; Li, W.-L.; Xing, J.-M.; Liu, H.-Z. In situ magnetic separation and immobilization of dibenzothiophene-desulfurizing bacteria. *Bioresour. Technol.* **2009**, *100*, 5092–5096.

7. Kurečić, M.; Rijavec, T.; Hribernik, S.; Lapanje, A.; Kleinschek, K.S.; Maver, U. Novel electrospun fibers with incorporated commensal bacteria for potential preventive treatment of the diabetic foot. *Nanomedicine* **2018**, *13*, 1583–1594.
8. Zhang, J.; Zhao, W.; Zhang, H.; Wang, Z.; Fan, C.; Zang, L. Recent achievements in enhancing anaerobic digestion with carbon-based functional materials. *Bioresour. Technol.* **2018**, *266*, 555–567.
9. Jesionowski, T.; Zdarta, J.; Krajewska, B. Enzyme immobilization by adsorption: A review. *Adsorption* **2014**, *20*, 801–821.
10. Putzbach, W.; Ronkainen, N.J. Immobilization techniques in the fabrication of nanomaterial-based electrochemical biosensors: A review. *Sensors* **2013**, *13*, 4811–4840.
11. Yang, S.H.; Lee, T.; Seo, E.; Ko, E.H.; Choi, I.S.; Kim, B.-S. Interfacing living yeast cells with graphene oxide nanosheaths. *Macromol. Biosci.* **2012**, *12*, 61–66.
12. Bilal, M.; Zhao, Y.; Rasheed, T.; Iqbal, H.M.N. Magnetic nanoparticles as versatile carriers for enzymes immobilization: A review. *Int. J. Biol. Macromol.* **2018**, *120*, 2530–2544.
13. Lin, L.-H.; Shih, J.-S. Immobilized fullerene C60-enzyme-based electrochemical glucose sensor. *J. Chin. Chem. Soc.* **2011**, *58*, 228–235.
14. Pagán, M.; Suazo, D.; Del Toro, N.; Griebenow, K. A comparative study of different protein immobilization methods for the construction of an efficient nano-structured lactate oxidase-SWCNT-biosensor. *Biosens. Bioelectron.* **2015**, *64*, 138–146.
15. Mubarak, N.M.; Wong, J.R.; Tan, K.W.; Sahu, J.N.; Abdullah, E.C.; Jayakumar, N.S.; Ganesan, P. Immobilization of cellulase enzyme on functionalized multiwall carbon nanotubes. *J. Mol. Catal. B Enzym.* **2014**, *107*, 124–131.

16. Fraga-García, P.; Kubbutat, P.; Brammen, M.; Schwaminger, S.; Berensmeier, S. Bare iron oxide nanoparticles for magnetic harvesting of microalgae: From interaction behavior to process realization. *Nanomaterials* **2018**, *8*, 292.
17. Ranmadugala, D.; Ebrahiminezhad, A.; Manley-Harris, M.; Ghasemi, Y.; Berenjian, A. Magnetic immobilization of bacteria using iron oxide nanoparticles. *Biotechnol. Lett.* **2018**, *40*, 237–248.
18. Banerjee, P.; Barman, S.R.; Swarnakar, S.; Mukhopadhyay, A.; Das, P. Treatment of textile effluent using bacteria-immobilized graphene oxide nanocomposites: Evaluation of effluent detoxification using *Bellamyia bengalensis*. *Clean Technol. Environ. Policy* **2018**, *20*, 2287–2298.
19. Durán, N.; Martinez, D.S.T.; Silveira, C.P.; Durán, M.; De Moraes, A.C.M.; Simões, M.B.; Alves, O.L.; Fávaro, W.J. Graphene oxide: A carrier for pharmaceuticals and a scaffold for cell interactions. *Curr. Top. Med. Chem.* **2015**, *15*, 309–327.
20. Poulin, P.; Jalili, R.; Neri, W.; Nallet, F.; Divoux, T.; Colin, A.; Aboutalebi, S.H.; Wallace, G.; Zakri, C. Superflexibility of graphene oxide. *Proc. Natl. Acad. Sci. USA* **2016**, *113*, 11088–11093.
21. Liao, C.; Li, Y.; Tjong, S. Graphene nanomaterials: Synthesis, biocompatibility, and cytotoxicity. *Int. J. Mol. Sci.* **2018**, *19*, 3564.
22. Lammel, T.; Boisseaux, P.; Fernández-Cruz, M.-L.; Navas, J.M. Internalization and cytotoxicity of graphene oxide and carboxyl graphene nanoplatelets in the human hepatocellular carcinoma cell line Hep G2. *Part. Fibre Toxicol.* **2013**, *10*, 27.
23. Wang, K.; Ruan, J.; Song, H.; Zhang, J.; Wo, Y.; Guo, S.; Cui, D. Biocompatibility of graphene oxide. *Nanoscale Res. Lett.* **2011**, *6*, 8.
24. Ge, L.; Chen, A.; Pei, J.; Zhao, L.; Fang, X.; Ding, G.; Wang, Z.; Xiao, W.; Tang, F. Enhancing the thermostability of α -l-rhamnosidase from *Aspergillus terreus* and the

- enzymatic conversion of rutin to isoquercitrin by adding sorbitol. *BMC Biotechnol.* **2017**, *17*, 21.
25. Li, R.; Guiney, L.M.; Chang, C.H.; Mansukhani, N.D.; Ji, Z.; Wang, X.; Liao, Y.-P.; Jiang, W.; Sun, B.; Hersam, M.C.; et al. Surface oxidation of graphene oxide determines membrane damage, lipid peroxidation, and cytotoxicity in macrophages in a pulmonary toxicity model. *ACS Nano* **2018**, *12*, 1390–1402.
 26. Pelin, M.; Fusco, L.; Martín, C.; Sosa, S.; Frontiñán-Rubio, J.; González-Domínguez, J.M.; Durán-Prado, M.; Vázquez, E.; Prato, M.; Tubaro, A. Graphene and graphene oxide induce ROS production in human HaCaT skin keratinocytes: The role of xanthine oxidase and NADH dehydrogenase. *Nanoscale* **2018**, *10*, 11820–11830.
 27. Malina, T.; Maršálová, E.; Holá, K.; Tuček, J.; Scheibe, M.; Zbořil, R.; Maršálek, B. Toxicity of graphene oxide against algae and cyanobacteria: Nanoblade-morphology-induced mechanical injury and self-protection mechanism. *Carbon N. Y.* **2019**, *155*, 386–396.
 28. Zhang, M.; Yu, Q.; Liang, C.; Liu, Z.; Zhang, B.; Li, M. Graphene oxide induces plasma membrane damage, reactive oxygen species accumulation and fatty acid profiles change in *Pichia pastoris*. *Ecotoxicol. Environ. Saf.* **2016**, *132*, 372–378.
 29. Arrais, A.; Diana, E.; Boccaleri, E. A study on the carbon soot derived from the wood combustion and on the relative alkali-extractable fraction. *J. Mater. Sci.* **2006**, *41*, 6035–6045.
 30. Wong, C.H.A.; Sofer, Z.; Kubešová, M.; Kučera, J.; Matějková, S.; Pumera, M. Synthetic routes contaminate graphene materials with a whole spectrum of unanticipated metallic elements. *Proc. Natl. Acad. Sci. USA* **2014**, *111*, 13774–13779.
 31. Eigler, S.; Dotzer, C.; Hof, F.; Bauer, W.; Hirsch, A. Sulfur species in graphene oxide. *Chem. A Eur. J.* **2013**, *19*, 9490–9496.

32. Seabra, A.B.; Paula, A.J.; De Lima, R.; Alves, O.L.; Durán, N. Nanotoxicity of graphene and graphene oxide. *Chem. Res. Toxicol.* **2014**, *27*, 159–168.
33. Gies, V.; Zou, S. Systematic toxicity investigation of graphene oxide: Evaluation of assay selection, cell type, exposure period and flake size. *Toxicol. Res. (Camb.)* **2018**, *7*, 93–101.
34. Chang, Y.; Yang, S.-T.; Liu, J.-H.; Dong, E.; Wang, Y.; Cao, A.; Liu, Y.; Wang, H. In vitro toxicity evaluation of graphene oxide on A549 cells. *Toxicol. Lett.* **2011**, *200*, 201–210.
35. Reshma, S.C.; Syama, S.; Mohanan, P.V. Nano-biointeractions of PEGylated and bare reduced graphene oxide on lung alveolar epithelial cells: A comparative in vitro study. *Colloids Surf. B Biointerfaces* **2016**, *140*, 104–116.
36. Mittal, S.; Kumar, V.; Dhiman, N.; Chauhan, L.K.S.; Pasricha, R.; Pandey, A.K. Physico-chemical properties based differential toxicity of graphene oxide/reduced graphene oxide in human lung cells mediated through oxidative stress. *Sci. Rep.* **2016**, *6*, 39548.
37. Hu, W.; Peng, C.; Luo, W.; Lv, M.; Li, X.; Li, D.; Huang, Q.; Fan, C. Graphene-based antibacterial paper. *ACS Nano* **2010**, *4*, 4317–4323.
38. Chng, E.L.K.; Pumera, M. The toxicity of graphene oxides: Dependence on the oxidative methods used. *Chem. A Eur. J.* **2013**, *19*, 8227–8235.
39. Das, S.; Singh, S.; Singh, V.; Joung, D.; Dowding, J.M.; Reid, D.; Anderson, J.; Zhai, L.; Khondaker, S.I.; Self, W.T.; et al. Oxygenated functional group density on graphene oxide: Its effect on cell toxicity. *Part. Part. Syst. Charact.* **2013**, *30*, 148–157.
40. Wu, W.; Yan, L.; Wu, Q.; Li, Y.; Li, Q.; Chen, S.; Yang, Y.; Gu, Z.; Xu, H.; Yin, Z.Q. Evaluation of the toxicity of graphene oxide exposure to the eye. *Nanotoxicology* **2016**, *10*, 1329–1340.

41. Mendonça, M.C.P.; Soares, E.S.; De Jesus, M.B.; Ceragioli, H.J.; Batista, Â.G.; Nyúl-Tóth, Á.; Molnár, J.; Wilhelm, I.; Maróstica, M.R.; Krizbai, I.; et al. PEGylation of reduced graphene oxide induces toxicity in cells of the blood–brain barrier: An in vitro and in vivo study. *Mol. Pharm.* **2016**, *13*, 3913–3924.
42. Pustovit, V.N.; Shahbazyan, T.V. Fluorescence quenching near small metal nanoparticles. *J. Chem. Phys.* **2012**, *136*, 204701.
43. Kasry, A.; Ardakani, A.A.; Tulevski, G.S.; Menges, B.; Copel, M.; Vyklicky, L. Highly efficient fluorescence quenching with graphene. *J. Phys. Chem. C* **2012**, *116*, 2858–2862.
44. Wu, X.; Xing, Y.; Zeng, K.; Huber, K.; Zhao, J.X. Study of fluorescence quenching ability of graphene oxide with a layer of rigid and tunable silica spacer. *Langmuir* **2018**, *34*, 603–611.
45. Ou, L.; Lin, S.; Song, B.; Liu, J.; Lai, R.; Shao, L. The mechanisms of graphene-based materials-induced programmed cell death: A review of apoptosis, autophagy, and programmed necrosis. *Int. J. Nanomed.* **2017**, *12*, 6633–6646.
46. Zhang, Y.; Ali, S.F.; Dervishi, E.; Xu, Y.; Li, Z.; Casciano, D.; Biris, A.S. Cytotoxicity effects of graphene and single-wall carbon nanotubes in neural pheochromocytoma-derived PC12 cells. *ACS Nano* **2010**, *4*, 3181–3186.
47. Markovic, Z.M.; Ristic, B.Z.; Arsikin, K.M.; Klisic, D.G.; Harhaji-Trajkovic, L.M.; Todorovic-Markovic, B.M.; Kepic, D.P.; Kravic-Stevovic, T.K.; Jovanovic, S.P.; Milenkovic, M.M.; et al. Graphene quantum dots as autophagy-inducing photodynamic agents. *Biomaterials* **2012**, *33*, 7084–7092.
48. Tabish, T.A.; Pranjol, M.Z.I.; Jabeen, F.; Abdullah, T.; Latif, A.; Khalid, A.; Ali, M.; Hayat, H.; Winyard, P.G.; Whatmore, J.L.; et al. Investigation into the toxic effects of graphene nanopores on lung cancer cells and biological tissues. *Appl. Mater. Today* **2018**, *12*, 389–401.

49. Adil, S.; Khan, M.; Khan, M.; Al-Marri, A.; Al-Warthan, A.; Alkhathlan, H.; Siddiqui, M.; Nayak, V.; Kamal, A. Apoptosis inducing ability of silver decorated highly reduced graphene oxide nanocomposites in A549 lung cancer. *Int. J. Nanomed.* **2016**, *11*, 873.
50. Mbeh, D.A.; Akhavan, O.; Javanbakht, T.; Mahmoudi, M.; Yahia, L. Cytotoxicity of protein corona-graphene oxide nanoribbons on human epithelial cells. *Appl. Surf. Sci.* **2014**, *320*, 596–601.
51. Yuan, X.; Liu, Z.; Guo, Z.; Ji, Y.; Jin, M.; Wang, X. Cellular distribution and cytotoxicity of graphene quantum dots with different functional groups. *Nanoscale Res. Lett.* **2014**, *9*, 108.
52. Zhu, S.; Luo, F.; Zhu, B.; Wang, G.-X. Toxicological effects of graphene oxide on *Saccharomyces cerevisiae*. *Toxicol. Res. (Camb.)* **2017**, *6*, 535–543.
53. Zhu, S.; Zhu, B.; Huang, A.; Hu, Y.; Wang, G.; Ling, F. Toxicological effects of multi-walled carbon nanotubes on *Saccharomyces cerevisiae*: The uptake kinetics and mechanisms and the toxic responses. *J. Hazard. Mater.* **2016**, *318*, 650–662.
54. Zhu, S.; Luo, F.; Li, J.; Zhu, B.; Wang, G.-X. Biocompatibility assessment of single-walled carbon nanotubes using *Saccharomyces cerevisiae* as a model organism. *J. Nanobiotechnol.* **2018**, *16*, 44.
55. Oliveira, R.; Johansson, B. Quantitative DNA damage and repair measurement with the yeast comet assay. *Methods Mol. Biol.* **2012**, *920*, 101–109.
56. Mortimer, M.; Kasemets, K.; Heinlaan, M.; Kurvet, I.; Kahru, A. High throughput kinetic *Vibrio fischeri* bioluminescence inhibition assay for study of toxic effects of nanoparticles. *Toxicol. Vitr.* **2008**, *22*, 1412–1417.
57. Patel, S.K.S.; Choi, S.H.; Kang, Y.C.; Lee, J.-K. Eco-friendly composite of Fe₃O₄-reduced graphene oxide particles for efficient enzyme immobilization. *ACS Appl. Mater. Interfaces* **2017**, *9*, 2213–2222.

58. Contreras Rodríguez, A.R.; Saiz-Poseu, J.; García-Pardo, J.; García, B.; Lorenzo, J.; Ojea-Jiménez, I.; Komilis, D.; Sedó, J.; Busqué, F.; Sánchez, A.; et al. Biocompatible polydopamine-like particles for the removal of heavy metals at extremely low concentrations. *RSC Adv.* **2016**, *6*, 40058–40066.
59. Ríos, F.; Fernández-Arteaga, A.; Fernández-Serrano, M.; Jurado, E.; Lechuga, M. Silica micro-and nanoparticles reduce the toxicity of surfactant solutions. *J. Hazard. Mater.* **2018**, *353*, 436–443.
60. Zhang, Y.; Zhang, J.; Huang, X.; Zhou, X.; Wu, H.; Guo, S. Assembly of graphene oxide-enzyme conjugates through hydrophobic interaction. *Small* **2012**, *8*, 154–159.
61. Barbero, F.; Russo, L.; Vitali, M.; Piella, J.; Salvo, I.; Borrajo, M.L.; Busquets-Fité, M.; Grandori, R.; Bastús, N.G.; Casals, E.; et al. Formation of the protein corona: The interface between nanoparticles and the immune system. *Semin. Immunol.* **2017**, *34*, 52–60.
62. Chong, Y.; Ge, C.; Yang, Z.; Garate, J.A.; Gu, Z.; Weber, J.K.; Liu, J.; Zhou, R. Reduced cytotoxicity of graphene nanosheets mediated by blood-protein coating. *ACS Nano* **2015**, *9*, 5713–5724.
63. Wei, X.-Q.; Hao, L.-Y.; Shao, X.-R.; Zhang, Q.; Jia, X.-Q.; Zhang, Z.-R.; Lin, Y.-F.; Peng, Q. Insight into the interaction of graphene oxide with serum proteins and the impact of the degree of reduction and concentration. *ACS Appl. Mater. Interfaces* **2015**, *7*, 13367–13374.
64. Qi, Y.; Chen, W.; Liu, F.; Liu, J.; Zhang, T.; Chen, W. Aggregation morphology is a key factor determining protein adsorption on graphene oxide and reduced graphene oxide nanomaterials. *Environ. Sci. Nano* **2019**, *6*, 1303–1309.
65. Zhang, Y.; Wu, C.; Guo, S.; Zhang, J. Interactions of graphene and graphene oxide with proteins and peptides. *Nanotechnol. Rev.* **2013**, *2*, 27–45.

66. Ou, L.; Song, B.; Liang, H.; Liu, J.; Feng, X.; Deng, B.; Sun, T.; Shao, L. Toxicity of graphene-family nanoparticles: A general review of the origins and mechanisms. *Part. Fibre Toxicol.* **2016**, *13*, 57.
67. James, J.; Fiji, N.; Roy, D.; Andrew MG, D.; Shihabudeen, M.S.; Chattopadhyay, D.; Thirumurugan, K. A rapid method to assess reactive oxygen species in yeast using H₂DCF-DA. *Anal. Methods* **2015**, *7*, 8572–8575.
68. Jarque, S.; Masner, P.; Klánová, J.; Prokeš, R.; Bláha, L. Bioluminescent *Vibrio fischeri* assays in the assessment of seasonal and spatial patterns in toxicity of contaminated river sediments. *Front. Microbiol.* **2016**, *7*, 1738.

Chapter 3

Transition Metal Dichalcogenides (TMDs)

Fate assessment of commercial 2D MoS₂ aqueous dispersions at physicochemical and toxicological level

Brixhilda Domí¹, Kapil Bhorkar^{2,3}, Carlos Rumbo¹, Labrini Sygellou², Spyros N. Yannopoulos², Roberto Quesada⁴, Juan Antonio Tamayo-Ramos^{*1}

¹ International Research Centre in Critical Raw Materials-ICCRAM, Universidad de Burgos, Plaza Misael Banuelos s/n, 09001 Burgos, Spain

² Foundation for Research and Technology Hellas – Institute of Chemical Engineering Sciences (FORTH/ICE-HT), P.O. Box 1414, GR-26504, Rio-Patras, Greece

³ Univ Rennes, CNRS, ISCR - UMR 6226, F-35000 Rennes, France

⁴ Departamento de Química, Facultad de Ciencias, Universidad de Burgos, 09001, Burgos, Spain

*Contact email: ja.tamayoramos@gmail.com

KEYWORDS: molybdenum disulfide, nanoparticles, fate, physicochemical composition, unicellular organisms, toxicity, oxidative stress, cell viability

ABSTRACT: The physicochemical properties and the toxicological potential of commercially available MoS₂ nanoparticles with different lateral size and degradation stage were studied in the present research work. To achieve this, the structure and stoichiometry of fresh and old aqueous suspensions of micro-MoS₂ and nano-MoS₂ was analyzed by Raman, while X-ray photoelectron spectroscopy (XPS) allowed to identify more quantitatively the nature of the formed oxidized species. A, the toxicological impact of the nanomaterials under analysis was studied using adenocarcinomic human alveolar basal epithelial cells (A549 cells) and the unicellular fungus *Saccharomyces cerevisiae* as biological models. Cell viability assays and reactive oxygen species (ROS) determinations demonstrated different toxicity levels depending on the cellular model used and in function of the degradation state of the selected commercial nanoproductions. Both MoS₂ nanoparticle types induced sublethal damage on the A549 cells though the increase of intracellular ROS levels, while comparable concentrations reduced the viability of yeast cells. In addition, the old MoS₂ nanoparticles suspensions exhibited a higher toxicity for both human and yeast cells than the fresh ones. Our findings demonstrate that the fate assessment of nanomaterials is a critical aspect to increase the understanding on their characteristics and on their potential impact on biological systems along their life cycle.

Introduction

Two-dimensional (2D) layered materials include a wide range of compounds such as graphene-based nanomaterials, transition metal dichalcogenides (TMDs), hexagonal boron nitride (h-BN), layered metal oxides and other compounds[1]. Due to their atomic or nanoscale thickness and large lateral size[2], 2D layered materials are suitable for biological and biomedical applications such as drug delivery, tissue engineering, bioimaging and biosensing[3]. Layered transition metal dichalcogenide nanomaterials such as molybdenum disulphide (MoS_2), represent an emerging class of 2D materials[4]. The bulk crystal is organized by covalently bonded monolayers stacked vertically with weak van der Waals forces, which enable the possibility to easily exfoliate it into monolayer nanosheets, like graphite and hexagonal boron nitride. One of the main industrial application of layered MoS_2 is solid lubrication, and the potential of 2D MoS_2 films as solid lubricants for micro- and nanoscale mechanical systems is being explored too.[5] The large surface area of the layered nanosheets facilitates their biological interaction with cell membranes[6], and the distinctive physicochemical characteristics of MoS_2 have attracted considerable interest for the development of functional nano-agents for biosensing[7], drug delivery[8], cancer therapy[9], in conjunction with other biomedical applications such as tissue regeneration [10] and antibacterial effects[11]. However, it has been reported that MoS_2 nanomaterials can induce cell membrane damage in different unicellular systems [12].

Given the above context, assessing the toxicity of MoS₂ biological systems is an essential matter. Specific parameters such as lateral dimensions, number of layers, surface area, purity, shape, and size can substantially influence the interaction between MoS₂ and biological systems[13]. For that reason, the same compound can show different antibacterial and cytotoxic mechanisms depending on different physicochemical parameters. Overall, understanding how MoS₂ nanoparticles interact with cellular models and their components is important to identify their safety and biocompatibility. However, while a great progress has been achieved in understanding how safe are 2D nanosheets such as graphene and its derivatives, there is still limited knowledge about the toxicological potential of others derived from different layered materials, like those from the TMD family. Recently, toxicological studies of 2D MoS₂ have been undertaken, with particular attention to mammalian cell lines. For instance, the interaction between MoS₂ and human cell lines has been studied using tumoral cells, such as adenocarcinomic human alveolar basal epithelial cells A549, gastric adenocarcinoma epithelial cells AGS and breast cancer epithelial cells MCF, and normal like epithelial kidney cells HEK293f and keratinocytes cells HaCaT cell lines [14–17]. The aim of these studies was to investigate different parameters such as cytotoxicity, cellular uptake and inflammatory responses using several cell lines that could represent the human potential exposure routes. Others have investigated the interaction between 2D MoS₂ with microbial systems, such as Gram-positive and Gram-negative bacteria, to determine the potential antibacterial activity of the nanomaterial and to identify potential toxicity pathways[18]. The availability of studies

analyzing the toxicological effect of MoS₂ flakes on fungal species is even more scarce. To date, only two studies using bulk MoS₂ and chitosan functionalized MoS₂ (CS-MoS₂) nanosheets have investigated the toxicological properties of the TMDs using the yeast *Saccharomyces cerevisiae* as a fungal model [19,20]. Therefore, to obtain a more comprehensive understanding on the toxicological potential of 2D MoS₂ additional studies are needed with their focus put on physicochemical aspects and fate of the nanomaterial, paying attention to additional biological models and biomolecules to those already assessed. While the availability of research works comparing the toxicity of pristine and transformed nanoproducts is very low, assessing the stability and degradation of TMDs is an essential aspect to increase the understanding on the impact of these materials and their transformation products in biological systems. MoS₂ nanosheets have been shown to be thermodynamically and kinetically unstable to oxidation under ambient conditions in aqueous media, resulting in measurable morphological changes and in the release of soluble molybdenum and sulfur species, generating protons able to destabilize the remaining sheets [21,22].

In the present study, we investigate the biological effects of commercially available mono- and bilayer MoS₂ flakes of different lateral sizes with distinct integrity stages, using different cell models, such as adenocarcinomic human alveolar basal epithelial cells (A549)[23] and the yeast *S. cerevisiae* [24]. Raman spectroscopy and X-ray photoelectron spectroscopy (XPS) were used to determine the extent of oxidation and to identify the relevant species derived

from MoS₂ nanosheets in water suspensions. Hence, we analyzed to what extent the nanomaterials oxidation influence the toxicological responses of the laboratory models used. The obtained results provide information about the time-dependent oxidation degree of MoS₂ nanoparticles, which is critical to understand and regulate issues related to their environmental fate, and their impact on different biological models.

Results and discussion

Selection and Characterization of Commercial Molybdenum Disulfide

In the present work, commercial water suspensions (1 mg/mL) and powders of MoS₂ platelets prepared using lithium-based intercalation method and supplied by ACS material® were selected: Monolayer Molybdenum Disulfide (micro-MoS₂) and Nano Size Monolayer Molybdenum Disulfide (nano-MoS₂). The characterization information provided by the supplier indicates a lateral size of 0.2-5 µm and a thickness of 1 nm for the micro-MoS₂ powder, and a diameter of 20-500 nm and the thickness of 1 nm for the nano-MoS₂ material. To further understand the morphologic features of both MoS₂ samples, AFM (Figure 1) and TEM (Figure 2) analyses were performed by drop-casting the samples on a mica surface and carbon-coated copper grids, respectively. Even if drop-casting and drying nanoparticle monodispersions can induce aggregated forms, for instance, due to surface dewetting, preventing the accurate visualization and quantification of particle size distribution, the combination of AFM and TEM allowed to observe a population of both nanoparticle types as well as morphological features. As can be seen in Figure 1, AFM images of the

two MoS₂ products showed the presence of possible aggregates with different shape and a significant population of particles with a lateral size distribution in the nanoscale range, with a round shape. Height profile curves displayed gave insights into the thickness of the observed nanoforms. TEM images confirmed that the both the micro- and nano-MoS₂ particles have a 2D platelet-like shape as previously described for this type of nanomaterials (Figure 2) [25]. No clear differences amongst both products could be observed in terms of size, aggregation state or morphological characteristics.

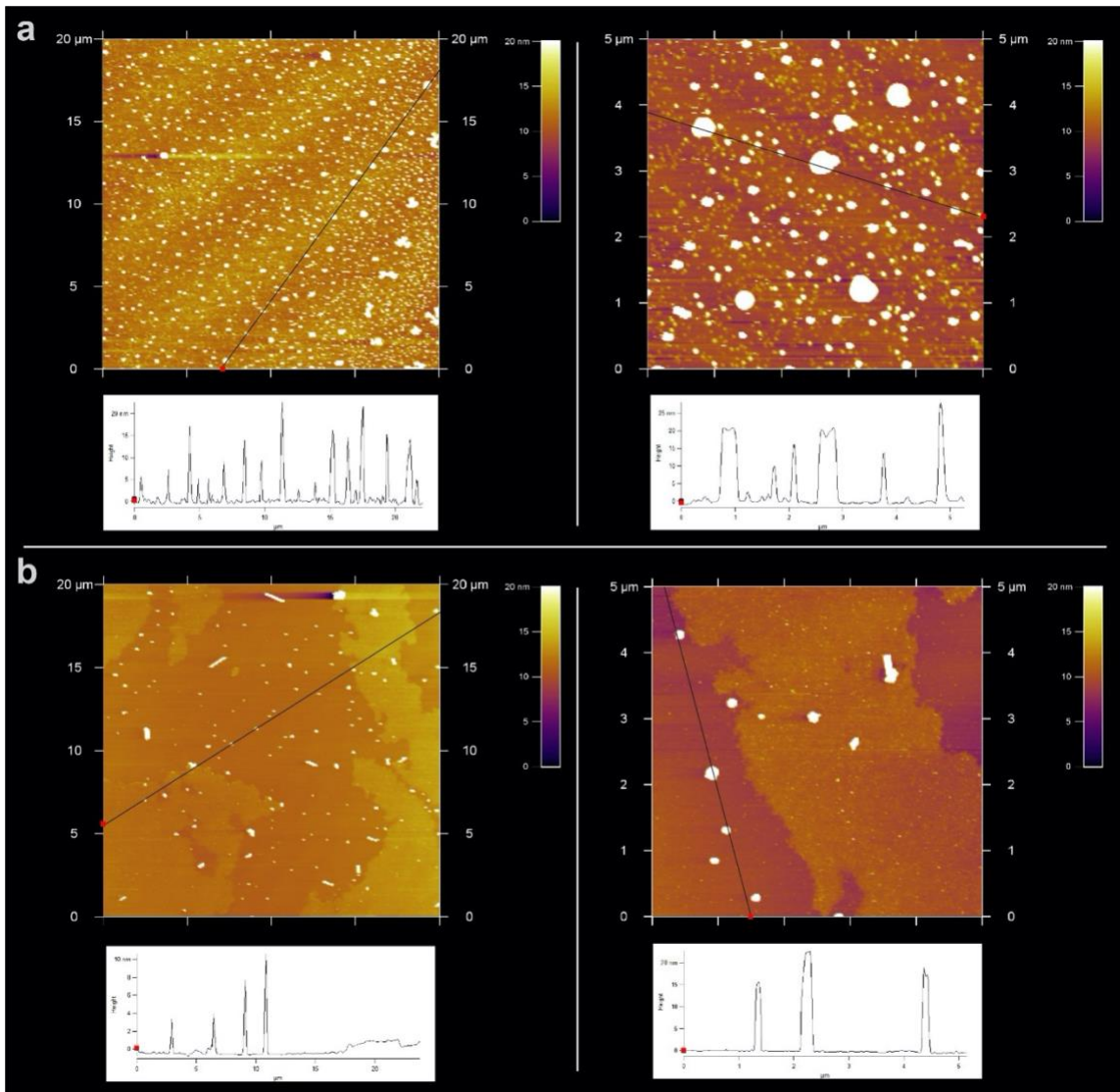


Figure 1: AFM images and corresponding height profiles of micro-MoS₂ (a) and nano-MoS₂ (b). Molybdenum disulfide dispersions with a concentration of 20 mg L⁻¹ were deposited by drop-casting on a mica surface.

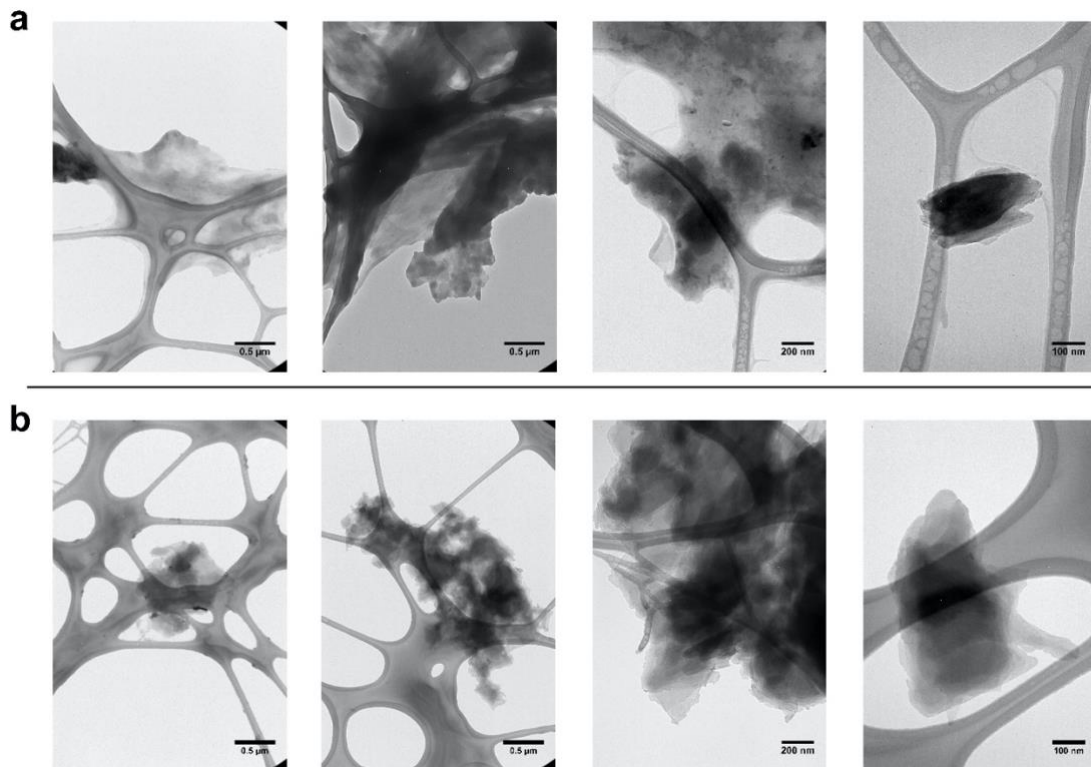


Figure 2: TEM images of micro-MoS₂ (a) and nano-MoS₂ (b). Molybdenum disulfide dispersions with a concentration of 20 mg L⁻¹ were deposited by drop-casting on carbon-coated copper grids.

To explore the structure and stoichiometry of micro- and nano-MoS₂ samples at different integrity states, Raman spectra of recently purchased (fresh) and 10 months old (old) water suspensions were collected and analyzed. Since the probed area (1-2 μm in diameter) is quite small to provide reliable information with a single measurement, various points of drop-casted films on Si were analyzed. The measurements showed a very homogeneous behavior of the spectra at various points. Representative Raman spectra of the fresh and old micro- and nano-MoS₂ suspensions are shown in Figure 3. The first order Raman spectrum of MoS₂ is characterized by peaks with symmetries A_{1g} and

E_{2g}^1 . These peaks are observed in all the spectra displayed, at near 405 cm^{-1} and 385 cm^{-1} , respectively. A strong band near 520 cm^{-1} in all spectra originates from the Si substrate. The Raman spectra of the pristine (dry) powders are also presented, revealing that the particles are free of oxides or other contaminants. The samples stored in water present considerable changes in Raman spectra, since the fraction of MoS_2 decreases systematically due to oxidation. The difference in the A_{1g} and E_{2g}^1 modes amounts to $\Delta\omega \approx 22.8\text{ cm}^{-1}$ and $\approx 23.0\text{ cm}^{-1}$ for the nano- and micro-sized MoS_2 , respectively. These values indicate a thickness of the particles of about 2-3 monolayers [26]. For better visualization, the spectra of nano- MoS_2 was enhanced by factors of 2 and 10 for the fresh and old samples, respectively. The Raman data indicates that nano- MoS_2 is more vulnerable to oxidation during water storage, in comparison to micro- MoS_2 . The frequency difference of the A_{1g} and E_{2g}^1 Raman bands becomes smaller in soaked samples, as $\Delta\omega \approx 20\text{-}21\text{ cm}^{-1}$ indicates the prevalence of flakes with mono- or bi-layer thickness for both the micro- and nano- MoS_2 samples. For comparison, the spectrum of the MoO_3 crystal is also shown in Figure 3. The most intense Raman band of MoO_3 is located at 820 cm^{-1} , while a weak broad band appears near this energy in the spectra of the oxidized samples. Additional Raman bands appear in the spectra of the oxidized samples at ~ 150 and $\sim 219\text{ cm}^{-1}$. Raman spectra of oxides [27] show the existence of bands near these wavenumbers which correspond to MoO_x species ($2 < x < 3$). A broader composite band with components at ~ 458 and $\sim 472\text{ cm}^{-1}$ appears for particles dispersed in water.

This band is strongly enhanced in case of resonance Raman scattering of MoS₂, typically recorded with 632.8 nm near bandgap excitation (~1.96 eV). The appearance of this band in the current spectra and its intensification upon increasing the soaking time indicates the continuous change of the particle composition. The particle structure changes gradually by oxidation; this causes bandgap widening, as the oxidized species come into resonance with the excitation source. The creation of mixed oxysulfide MoS_xO_y species could in principle be responsible for this effect.

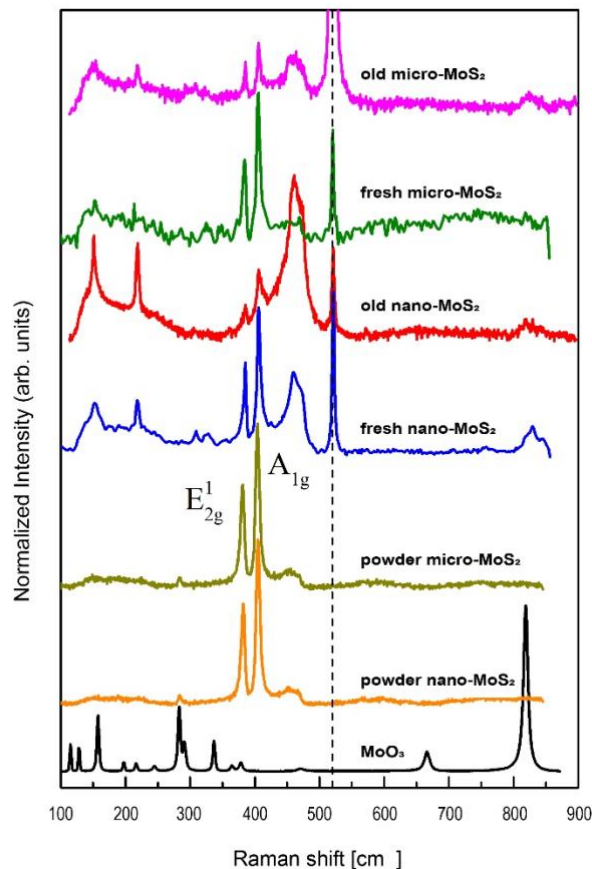


Figure 3: Raman spectra of the micro- and nanosized MoS₂ soaked in water (fresh and 10-months-old). The spectra of the dry powders and the spectrum of MoO₃ are also shown for comparison.

In addition to Raman, XPS was employed to identify more quantitatively the nature of the oxidized species. The same samples used for Raman scattering were studied by XPS. This technique probes a much larger area (~0.5 mm²) in comparison to Raman scattering, hence providing a consistent picture of the whole sample area. Figure 4 displays detailed XPS scans for the Mo3d peaks, in the samples under study. The Mo3d peak is deconvoluted into two doublets with a spin orbit splitting of 3.3 eV. The binding energy of Mo3d_{5/2} at 233.1±0.1

eV is assigned to MoO_3 [28] while that at 229.0 ± 0.1 eV has been associated to MoS_2 . [29] In the same energy region, the S2s band is present. This band consists of two components assigned to 2H- MoS_2 and to bonds of sulfur oxide. The obtained results show a progressive oxidation of the MoS_2 platelets in the water dispersion as a function of time, being more accelerated in the nano- MoS_2 sample.

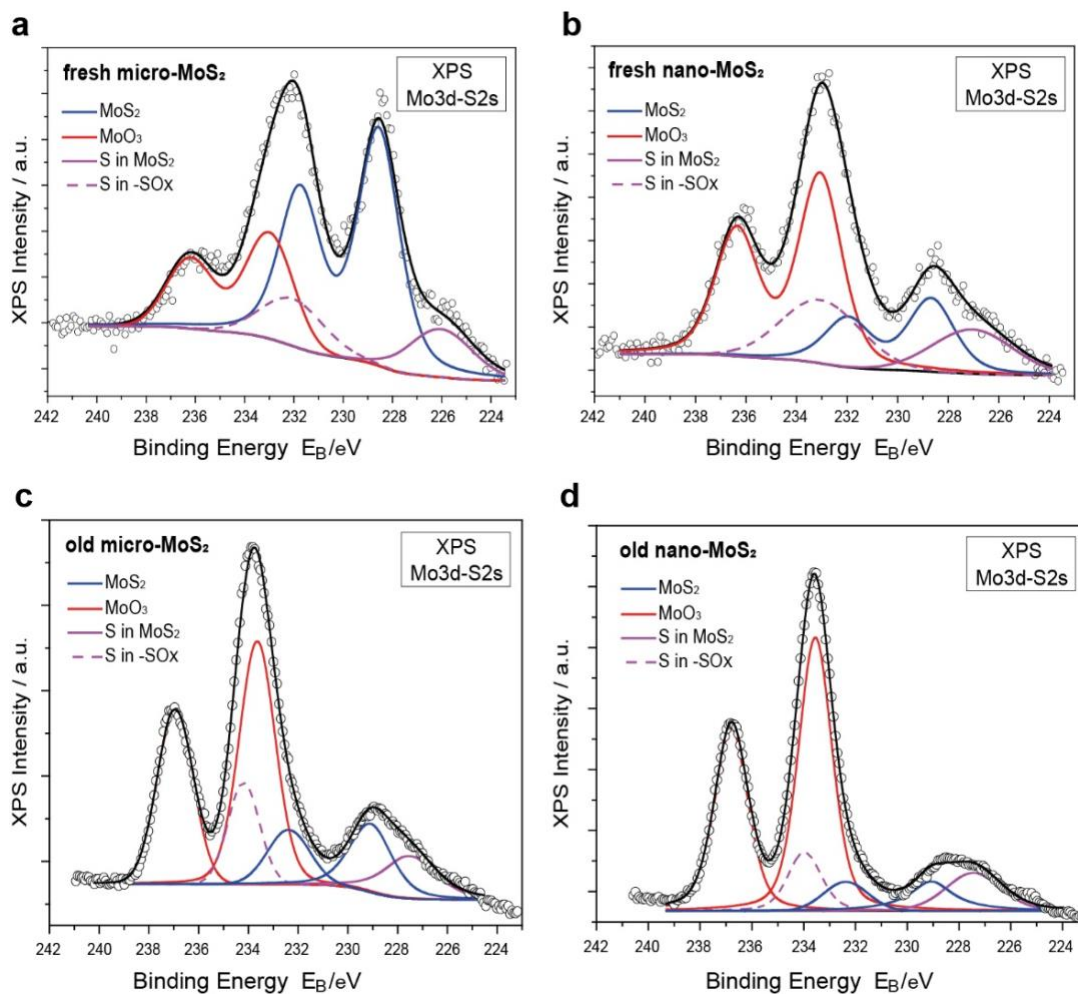


Figure 4: Deconvoluted Mo3d XP spectra of (a) fresh micro- MoS_2 , (b) fresh nano- MoS_2 , (c) old micro- MoS_2 , and (d) old nano- MoS_2 .

To gain insight into the nature of the MoS₂ nanosheets oxidation process, the obtained S2p bands were analyzed into their components. Figure 5 displays representative XPS scans for the S2p peaks for the micro- and nanosized MoS₂ old samples. The S2p band is deconvoluted into 4 doublets with spin orbit splitting 1.2 eV. The binding energies of the S2p_{3/2} peaks and their assignment is as follows: (1) 162.0±0.1eV; S atom at the basal plane of MoS₂; (2) 163.5±0.1eV; unsaturated sulphur atoms; (3) 167.2±0.1eV; sulphates; (4) 168.4±0.1eV, thionates, [S_n(SO₃)₂]²⁻ [29,30], and or sulphonyl groups (-SO₂-groups) [31].

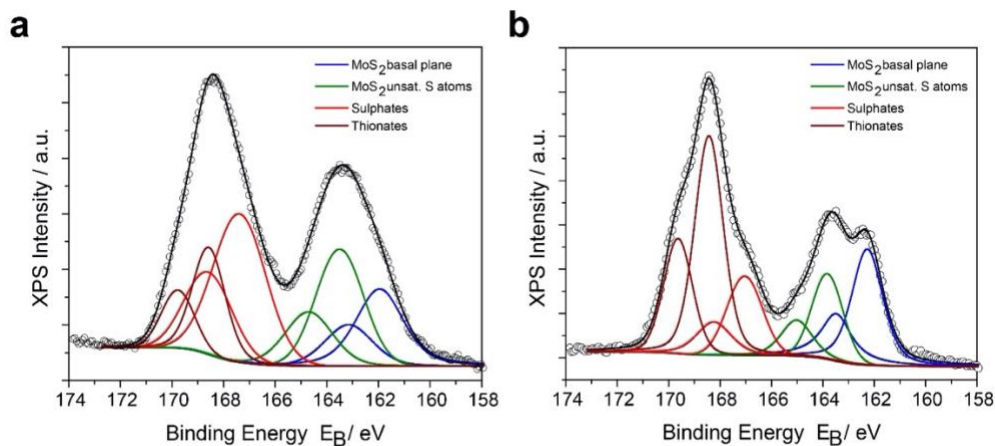


Figure 5: Deconvoluted S2p XP spectra of micro-MoS₂ (a) and nano-MoS₂ (b) samples obtained from old water suspensions.

Toxicology assessment using adenocarcinoma A549 human cells

The biological response towards the selected commercial MoS₂ nanoparticles (recently purchased (fresh) and 10 months old (old) water suspensions) was firstly assessed using the human lung (carcinoma) cell line A549, which

represents alveolar type II cells, a potential target of nanomaterials after inhalation.[32] The cells were exposed to different concentrations of fresh and old micro- and nano-MoS₂ suspensions, up to 160 mg L⁻¹, for a period of 24 hours. The Neutral Red assay was chosen to determine the cells viability in the described exposure conditions, as it is one of the most used cytotoxicity tests, including those that evaluate nanomaterials toxicity.[33] The method is based on the capability of viable cells to incorporate and bind the supravital dye Neutral Red inside the lysosomes, being amongst the most sensitive cytotoxicity tests.[34] As displayed in Figure 6, cells exposed to both types of fresh and old MoS₂ nanosheets (160 mg L⁻¹) showed to have the same viability as the negative control. The same result was observed for the lower concentrations tested of the different nanoparticles suspensions, indicating that the viability of A549 cells is not negatively affected in the presence of micro-MoS₂ and nano-MoS₂, nor by their transformation and degradation products, at the studied conditions. In addition, no significant viability differences were observed between cells exposed to micro- and nano-MoS₂ particles.

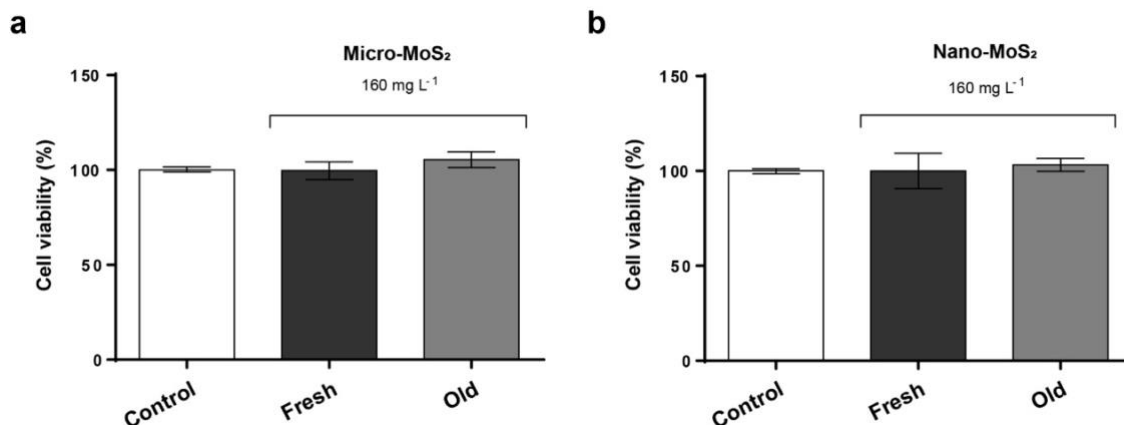


Figure 6: Viability of A549 cells (Neutral Red assay) exposed to 160 mg L⁻¹ of fresh and old micro-MoS₂ (a) and nano-MoS₂ (b) for 24 hours. Results are expressed as % of control (non-exposed cells). Data represent the mean (\pm standard deviation, SD) of three independent replicates. Differences were established using a One-way ANOVA followed by Dunnett *post hoc* test to compare every mean with the control.

The observed results are comparable to those reported for MoS₂ nanosheets obtained using methylithium (Me-Li) as intercalating agent [35], where similar concentrations showed to elicit low cytotoxicity on A549 cells as well. In contrast, MoS₂ exfoliated with other intercalating reagents, such as n-butylithium (n-Bu-Li) and tert-butylithium (t-Bu-Li), had a stronger cytotoxic impact in the cells at the same concentration range. The potential toxicological effects of MoS₂ nanosheets against other human *in vitro* models has been investigated, like the cancer cell line TPH1 and the non-tumorigenic lung epithelial cell BEAS 2B, where no cytotoxicity was observed at concentrations up to 50 mg L⁻¹ [36]. Interestingly, aggregated MoS₂ showed higher toxicological potential than that caused by 2D-MoS₂. More recent literature also

reports the impact of MoS₂ nanoparticles present in aqueous dispersions and coatings, against other human cell line types [16].

Although no previous reports compare the potential toxicity of commercial pristine MoS₂ nanosheets with that of their transformation products, a recent study revealed the potential toxicity of two polyvinylpyrrolidone-modified 2H-phase MoS₂ nanosheets oxidation products, such as MoO₃ and MoO₄²⁻, in exposed HUVECs and SMMC-7721 cells [37]. The nanomaterial oxidation products showed ability to reduce the cell vitality in concentrations higher than 200 mg mL⁻¹. Interestingly, a study comparing the toxicity elicited by exfoliated TMDs and graphene derivatives, also indicated that MoS₂ toxicity up 200 mg L⁻¹ is low, being lower as well than that induced by graphene oxide and derivatives [38].

Nanomaterials present at sublethal concentrations can still alter cell viability by inducing high levels of ROS [39], which frequently trigger programmed cell death (apoptosis) [40]. Hence, to obtain additional insights on the potential adverse biological effects of MoS₂ nanosheets on human cells we further investigated the oxidative stress levels of A549 cells exposed to the selected nanoparticles suspensions (fresh micro-MoS₂ and nano-MoS₂) and to their transformation products (old micro-MoS₂ and nano-MoS₂), using the DCFH-DA assay [41]. As done previously in the viability assay, the ROS generation was determined after 1 hour exposure to concentrations up to 160 mg L⁻¹ of fresh and old micro- and nano-MoS₂. In these conditions, no significant increase of oxidative stress levels were observed in exposed A549 cells. Recent studies

investigating the possible cytotoxic effect of dispersible MoS₂ nanosheets on human dermal fibroblasts and hepatoma cells have reported increased oxidative stress in exposed cells. MoS₂ induced a dosage-dependent ROS production in human dermal fibroblasts, which showed an increase of ~50% and ~75% of ROS levels with respect to the control condition in cells exposed 100 and 200 mg L⁻¹ respectively [42]. The ROS induction by MoS₂ nanosheets on human hepatoma cells HepG2 was even more striking, with significantly higher oxidative stress levels being observed even in the presence of 2 mg L⁻¹ [43].

In relation to the ROS levels observed in A549 cells exposed to the old nanoparticles suspensions, higher levels of oxidative stress were observed (Figure 7 b). Cells exposed to old micro- and nano-MoS₂ showed 3.6 and 3.1 times higher ROS levels respectively, than the non-exposed cells. The significant oxidative levels induced by the old samples suggest a mixture toxicity effect derived from the MoS₂ nanosheets transformation products. For instance, MoO₃ is considered an irritant product, with reported animal carcinogenicity[44]. MoO₃ nanoplatelets were shown to induce ROS in iMCF-7 cells because of elevated ROS levels [45], but limited information is available on the toxicity of MoO₃ and other MoS₂ transformation products, such as molybdenum oxysulfide (MoO_xS_y) on different human cell lines.

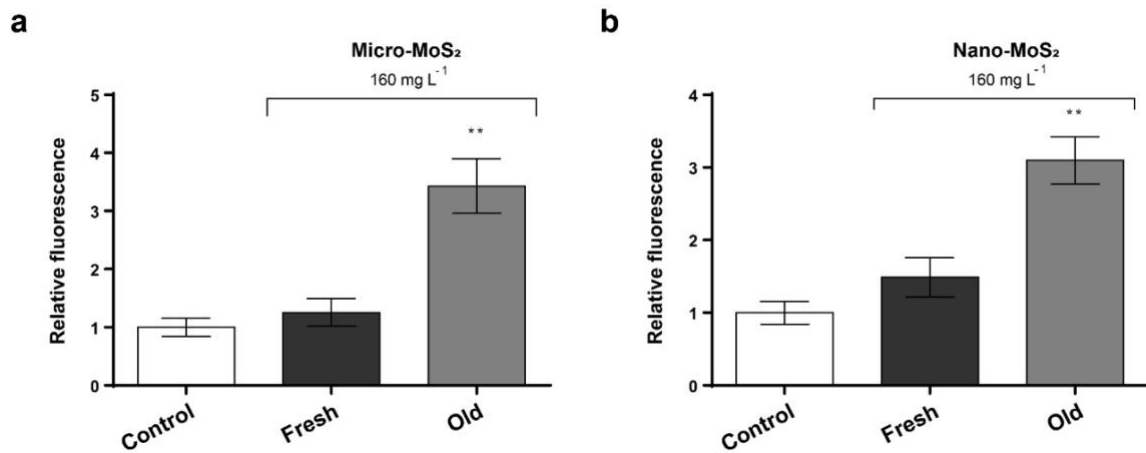


Figure 7: ROS production of A549 cells exposed to 160 mg L⁻¹ of fresh and old micro-MoS₂ (a) and nano-MoS₂ (b) for 1 hour. The reported values are expressed in arbitrary units and correspond to the averages of two biological replicates per culture condition. Data represent the mean of 2 replicates (\pm standard deviation, SD). Differences were established using a One-way ANOVA followed by Dunnett post hoc test to compare every mean with the control and considered significant at $P \leq 0.05$. ** $P \leq 0.01$.

Toxicology assessment using *Saccharomyces cerevisiae*

The toxicity of MoS₂ nanosheets has been mostly studied in distinct human cell lines, while the impact of these nanomaterials and other 2D TMDs in other unicellular organisms is less known.

For instance, in case of *S. cerevisiae*, another eukaryotic model commonly used in toxicology studies, only few reports have described the effect of MoS₂ forms on yeast cells, such as bulk MoS₂ and chitosan functionalized MoS₂ [19,20]. Here, as previously described for the A549 cells, the impact of different concentrations of fresh and old MoS₂ nanosheets suspensions on the yeast

strain BY4741 was analyzed. A colony forming units (CFUs) determination of *S. cerevisiae* cells exposed to 160 and 800 mg L⁻¹ of the different MoS₂ nanoforms for 2 and 24 h was performed (see Materials and methods) [46]. As displayed in Figure 8, their impact on the viability of yeast cells was dependent on the product type, concentration and exposure time.

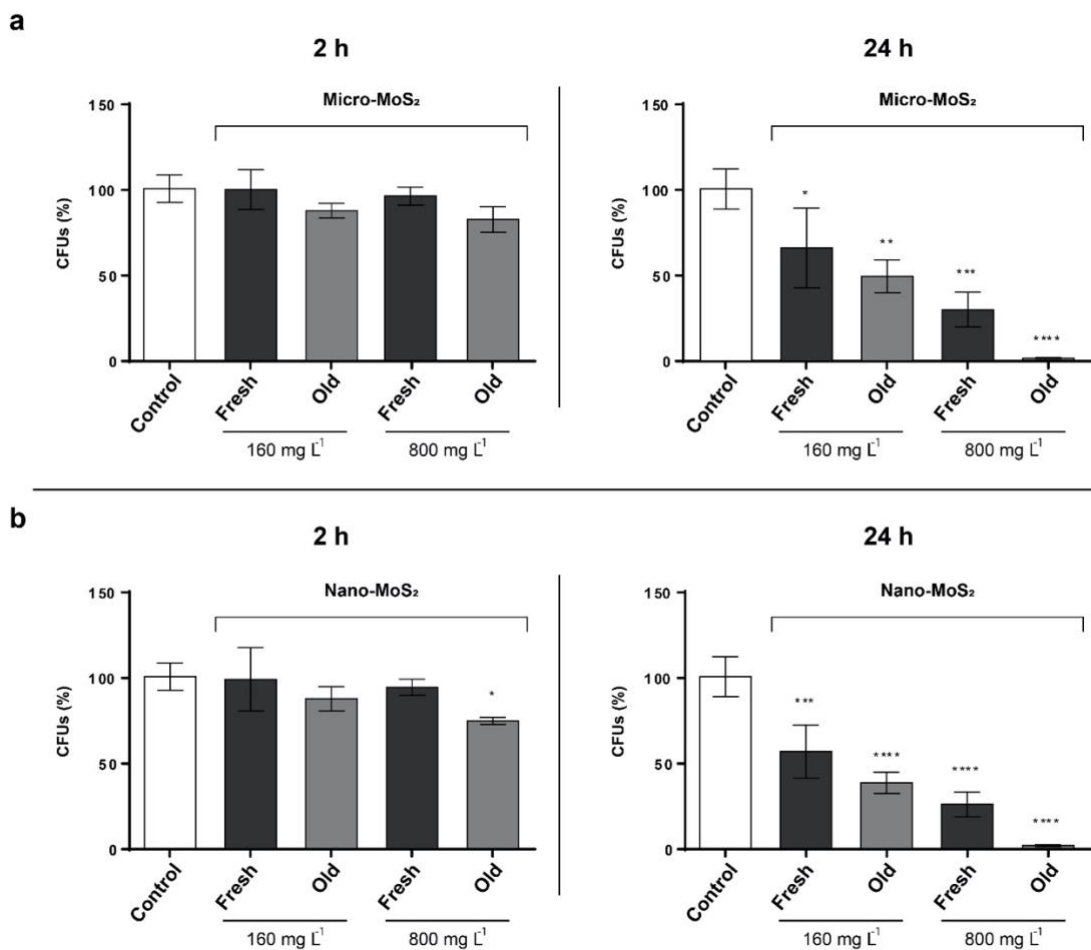


Figure 8: Colony forming units (CFUs) determination of *S. cerevisiae* cells exposed to 160 and 800 mg L⁻¹ of fresh and old micro-MoS₂ (a) and nano-MoS₂ (b), for 2 and 24 hours. The reported values are the averages of three biological

replicates per culture condition. Differences were established using a One-way ANOVA followed by Dunnett post hoc test to compare every mean with the control, and considered significant at $P \leq 0.05$. * $P \leq 0.05$, *** $P \leq 0.001$, **** $P \leq 0.0001$.

After a short exposure time (2 h), no significant viability changes were observed in the different conditions tested, except for that of yeast cells exposed to the high concentration of old nano-MoS₂, where an average decrease on CFUs of 20% was observed. However, a clear decrease on yeast viability was observed in exposures of 24 h, being more drastic when cells were exposed to the old suspensions of both nanoparticle types. The toxicity provoked by micro-MoS₂ and nano-MoS₂ was comparable. In the presence of 160 mg L⁻¹, the fresh nanoparticles suspensions induced a decrease on yeast viability of ~40%, while the presence of 800 mg L⁻¹ reduced the CFUs around 70%. In case of the old nanoparticles suspensions, 160 mg L⁻¹ reduced the yeast cells viability 50 to 60%, while in the presence of the higher concentration only 1% of the exposed cells survived.

As previously mentioned, the higher toxicity levels induced by the old samples, this time in *S. cerevisiae* cells, suggest a possible mixture toxicity effect produced by the MoS₂ nanosheets transformation products. The fact that 160 mg L⁻¹ of both fresh and old nanoparticles were able to reduce the viability of *S. cerevisiae* indicates that these products are more toxic for yeast cells than for the A549 cell line. Previous studies have demonstrated the antimicrobial properties of MoO₃ [47,48], while the antifungal properties of SO₂ are well

known [49], which could explain the higher toxicity observed. Yu Y. *et al* investigated the exposure of yeast cells to bulk MoS₂, concluding that concentrations higher than 1 mg L⁻¹ could produce a negative effect on the cell membrane integrity and inducing ROS accumulation, possibly due to the discrete crystal planes and surface defects of the material [20]. Many studies have demonstrated that fungal cells toxicity of nanomaterials, including MoS₂ and its transformation products, often involve oxidative stress and ROS [48,50–54]. Therefore, to find out whether the selected MoS₂ nanoparticles could also increase the intracellular reactive oxygen species level in yeast cells, we exposed the BY4741 strain to 160 and 800 mg L⁻¹ of the fresh and old samples for 2 hours (see Materials and methods). As shown in the Figure 8, no significant differences in ROS levels were observed between the control condition and the conditions where yeast cells were exposed to 160 mg L⁻¹ of the different nanomaterials suspensions. However, 800 mg L⁻¹ of both types of fresh nanomaterials increased ROS significantly, while the same concentration of the old suspensions increased the oxidative stress levels at a minor, non-significant level. This result indicates that the fresh nanoparticles have a higher capacity to induce oxidative stress in yeast cells. Also, that the toxicity mechanisms induced by the old nanoparticles suspensions are not necessarily associated to the presence of ROS, at least at an early exposure stage. Nevertheless, ROS measurements on *S. cerevisiae* cells exposed to the old nanomaterials suspensions (160 mg L⁻¹) for 24 hours showed that oxidative stress levels were three times higher in the test conditions than in the control

condition, indicating that the transformation products of the MoS₂ nanosheets are also able to induce significant ROS levels in yeast cells.

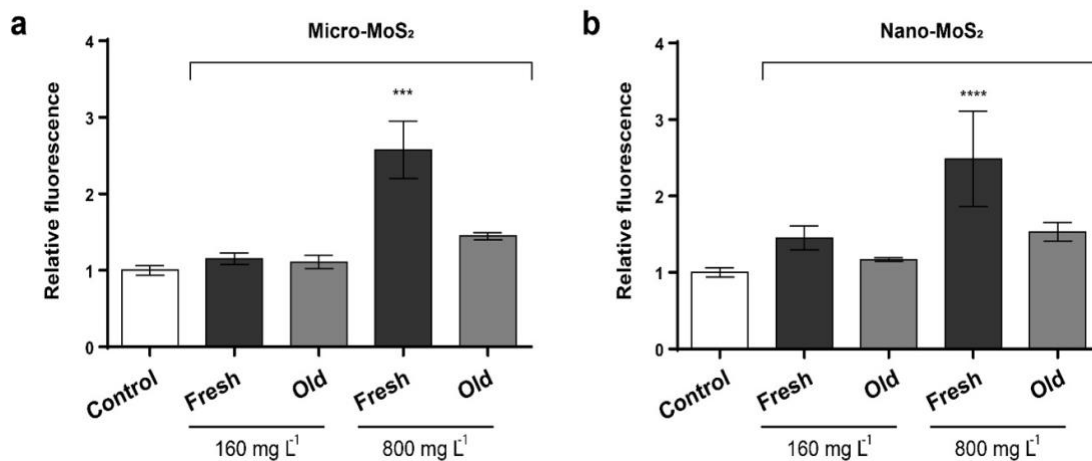


Figure 9: Oxidative stress (ROS) determination of *S. cerevisiae* cells exposed to 160 and 800 mg L⁻¹ of fresh and old micro-MoS₂ (a) and nano-MoS₂ (b) during 2 hours. The reported values are expressed in arbitrary units and correspond to the averages of two biological replicates per culture condition. Differences were established using a One-way ANOVA followed by Dunnett post hoc test to compare every mean with the control, and considered significant at $P \leq 0.05$. *** $P \leq 0.001$, **** $P \leq 0.0001$.

The use of N-doped MoS₂ nanostructures and MoO₃ as antifungal agents have been recently explored [48,54]. The results obtained in the present study also indicate that MoS₂ nanomaterials have antifungal properties, producing an enhanced effect once they are degraded and transformed in a mix of MoO_x, oxysulfide, and MoS_xO_y species. The use of chemicals as nanoparticles in fungicidal applications is a good alternative to the use of bulk forms, due to

their higher dispersibility and larger surface to volume ratio, and to the use of ionic forms, thanks to their lower leachability.

Conclusion

The results obtained in the present study provide novel insights into the fate of MoS₂ nanoparticles in aqueous suspensions and their toxicological impact on different biological systems at distinct material life cycle stages. The morphological analysis of commercial micro-MoS₂ and nano-MoS₂ determined a lateral size in the nanoscale range for both products, while the analysis of their structure and chemical composition through Raman and XPS revealed high similarity between both pristine nanomaterials, but remarkable differences in the chemical composition of fresh and old water suspensions. Nano-MoS₂ nanoparticles stored as aqueous suspensions were degraded faster, but in both cases 10 months old suspensions were highly enriched in a mixture of defected MoS_x species, and oxysulfides MoS_xO_y. The differences in composition of fresh and old MoS₂ aqueous suspensions affected their toxicological impact, which was evaluated using human A549 cells and the yeast *S. cerevisiae*. Different toxicity levels for both model organisms were observed when using comparable exposure conditions. While the selected nanoparticles provoked a sublethal damage on the A549 cells though the increase of intracellular ROS levels, equal concentrations reduced the viability of yeast cells. Additionally, the old MoS₂ nanoparticles suspensions showed higher toxicity for both human and yeast cells than the fresh ones. The presented results highlight the relevance of analyzing the fate of nanomaterials

at physicochemical and toxicological level to increase the understanding on their characteristics and their potential impact on biological systems along their life cycle.

Materials and Methods

Materials and reagents

Most chemicals and reagents were purchased from Sigma-Aldrich (Merck KGaA, Darmstadt, Germany) and Acros Organics (Thermo Fisher Scientific Inc., Madrid, Spain). Monolayer Molybdenum Disulfide (micro-MoS₂) and Nano Size Monolayer Molybdenum Disulfide (nano-MoS₂) were purchased at ACS material®. The 10 months old (old) water suspensions were obtained by storing purchased bottles for 10 months at 4°C.

AFM and TEM

For AFM analysis, samples were dropped on a mica surface from aqueous solutions by drop-casting. Images were recorded in AC mode (tapping mode) with a CYPHER ES instrument from Asylum Research (Oxford Instruments), using silicon cantilevers AC160TS-R3 with aluminum reflex coating (Olympus) and tip radius <10 nm. The analysis was completed using a set point of 500, 72mV, a drive amplitude of 791.16 and a drive frequency of 268.639. IGOR Pro 6.2 (Asylum Research) was used for data acquisition and control. ARgyle software was utilized for all the images analysis. For TEM analysis samples were placed on Lacey Carbon Type-A, 300 mesh, copper grids, and visualized and photographed using a JEOL JEM-1011 HR TEM coupled with a Gatan

Erlangshen ES1000W camera at the Microscopy Unit from the University of Valladolid.

Raman Analysis

Raman spectra were recorded at ambient conditions from the same drop-casted samples using the 441.6 nm radiation as an excitation source emerging from a He-Cd laser (Kimon). The laser light was focused by a 50× objective creating a focusing area of 1-2 μm . The scattered light was collected by the same objective and analyzed using by the LabRam HR800 (Jobin-Yvon) spectrometer operating at a spectral resolution of $\sim 2.0 \text{ cm}^{-1}$. A very low light fluence (275 μW) on the maple was used to avoid heat induced effects (oxidation and decomposition). The Raman mode of Si single crystal at 520 cm^{-1} was used to calibrate the wavenumber scale of the spectra.

XPS

The surface analysis study was performed in a UHV chamber ($P < 10^{-9}$ mbar) equipped with a SPECS LHS-10 hemispherical electron analyzer and a dual anode X-ray gun. The XPS measurements were carried out at room temperature using the unmonochromatized AlK α radiation under conditions optimized for maximum signal (constant ΔE mode with pass energy of 97 eV giving a full width at half maximum, FWHM, of 1.7 eV for the Ag3d $_{5/2}$ peak). The XPS core level spectra were analyzed using a fitting routine, which allows the decomposition of each spectrum into individual mixed Gaussian-Lorentzian components after a Shirley background subtraction. The samples were

prepared by drop-casting aliquots of the MoS₂ water dispersions onto 1×1 cm² Si wafers. Errors in the quantitative data are in the range of ~10%, (peak areas) while the accuracy for binding energy (BEs) assignments is ~0.1 eV.

A549 Cell culture

The human alveolar carcinoma epithelial cell line A549 (ATCC, CCL-185) was utilized for toxicological evaluation. Cells were grown in DMEM medium (Dulbecco's Modified Eagle Medium) supplemented with 10% foetal calf serum (FCS), 1% penicillin, 1% streptomycin and grown in a humidified incubator at 37 °C (5% CO₂). In all assays performed, cells were trypsinized after 24 h of incubation, at 90% confluency. Around 3×10⁴ cells (suspended in 200 µl of growth media) in each well of a 96 well micro-plate were allowed to adhere and grow for 24 hours.

Dispersions of micro and nano MoS₂ for A549 cells toxicity assays

The solutions for the Neutral Red assay were prepared using the commercial stocks (1 g L⁻¹) in treatment medium (DMEM 1% FCS) and sterile water to prepare final stocks of 160 mg L⁻¹. Afterwards, to prepare the solutions for the ROS assay, the commercial stocks were diluted in HBSS (Hank's Balanced Salt Solution) 10x and sterile water. After an initial sonication of the mother stock samples, the suspended (micro- and nanoscale) MoS₂ samples were vortexed for few seconds to homogenize the final solution for the toxicity assays.

A549 cells Neutral Red assay

After 24 hours incubation, cell culture medium was discarded and cells were washed DPBS (Dulbecco's phosphate-buffered saline). The central wells of the 96 well micro-plate were incubated with treatment medium with the final concentration of 20, 40, 80 and 160 mg L⁻¹. Cells were then incubated for 24 hours at 37°C, under 5% CO₂. Successively to the 24 hours exposure to the nanomaterials, cells were washed and incubated with 100 µL of the Neutral Red solution for 2,5 hours at 37°C in the dark. The Neutral Red solution was prepared as follows: 1:100 dilution of the Neutral Red stock (3-amino-7-dimethylamino-2-methyl-phenazine hydrochloride) was prepared in treatment medium (DMEM 1% FCS), previously incubated for 24 h at 37°C and centrifuged at 3000 rpm for 10 minutes to precipitate crystals formations. After incubation, Neutral Red Solution and nanoparticles were discarded and each well washed with DPBS. Afterwards, 100 µL of a fixation solution (formaldehyde 4%) was added to each well for 2 minutes, and cells were washed again. Each well was treated with 150 µL of solubilization solution (50% ethanol 96%, 49% H₂O, 1% acetic acid) at room temperature for 10 minutes with shaking and covered from light. To measure the fluorescence, 100 µL of each extract from cells was transferred into a black opaque 96 micro-well plate. The micro-plate reader spectrophotometer (Synergy-HT, BioTek) was used to read fluorescence at excitation 525/30 nm and emission at 640/645 nm.

A549 cells ROS assay

The quantitative measurement of intracellular reactive oxygen species (ROS) was investigated using 2,7-dichlorofluorescein diacetate (DCFH-DA). The DCFH-DA inactively pass the cell's membrane and reacts with the intracellularly ROS. The last product of this reaction is the highly fluorescent compound dichlorofluorescein (DCF). Twenty-four hours after seeding, A549 cells were transferred in a 96 micro-well plate, washed twice with HBSS and incubated with 200 μL of DCFH-DA (50 M) for 30 minutes at 37 °C. After the exposure time, cells were washed with HBSS and incubated with 200 μL of nanoparticles solutions at 20, 40, 80 and 160 mg L^{-1} . The ROS production is measurable due to the oxidation reaction of DCFH to dichlorofluorescein (DCF) intracellularly. Fluorescence intensity was measured after 1 h incubation, at 485 nm excitation and 520 nm emission using a microplate reader (Synergy-HT, BioTek). The experiment was repeated three times.

Yeast Culture

S. cerevisiae B4741 was maintained in liquid and agar media of YPD medium (1% yeast extract, 1% yeast bacto-peptone, 2% glucose). In exposure experiments, cells were firstly grown on a rotary shaker at 185 rpm at 30 °C until the final $\text{OD}_{600 \text{ nm}}$ was equal to 1 (exponential phase).

Yeast Colony Forming Units (CFUs) determination

A 24 multi-well plate was used for the incubation of yeast ($\text{OD}_{600 \text{ nm}} = 1$) in the presence of micro-MoS₂ and nano-MoS₂. The concentration ranges tested for

all the samples were 160 and 800 mg L⁻¹, for 2 and 24 hours. To define cells viability after each exposure time, aliquots were diluted 10⁴ times, in case of 2 hours exposure, and 10⁵ times, in case of 24 hours exposure, and 100 µL of the diluted suspensions was plated on solid YPD medium (6% agar). Plates were incubated at 30°C for 48 hours and CFUs were determined.

Yeast ROS assay

For the evaluation of ROS, a 24 multi well plate was used. Cells with a final OD₆₀₀ nm equal to 1 (exponential phase) were centrifuged (for 3 minutes at 4000 rpm), washed and suspended in 12.5 mL of DPBS (OD₆₀₀ nm= 16). Successively, the commercial stock with dry CM-H₂DCFDA (General Oxidative Stress Indicator) was suspended in 20 µL of DMSO (Dimethyl Sulfoxide) and the final concentration of the reagent is equal to 4,33 mM. Subsequently, cells were incubated with 20 µL of CM-H₂DCFDA in the dark for 60 minutes at 30 °C and 185 rpm. Cells were then centrifuged, washed with DPBS and suspended in 5 mL YPD 5x liquid medium. Then, cells were incubated with the nanomaterial suspensions (final volume 1 mL) for 2 hours at 30 °C and 185 rpm in the orbital shaker. The concentrations tested were 160 and 800 mg L⁻¹. After the 2 hours incubation, 500 µL of each sample were centrifuged and washed two times with DPBS. Next, each sample was suspended in 200 µL of AcLi (lithium acetate) 2M and incubated for 2 minutes with moderate agitation in the thermomixer at 400 rpm. Thus, cells were centrifuged and the pellet was suspended in 200 µL OF 0.01 % SDS (sodium dodecyl sulfate) + chloroform (150 µL in 40 mL) and incubated for 2 minutes. Afterwards, 150 µL of each

sample was transferred on a black opaque 96 micro-well plate and the fluorescence was measured at 485 nm excitation and 528 nm emission using a microplate reader (Synergy-HT, BioTek).

Statistics

Statistical analysis data are presented as means \pm SD. Differences between the negative control and the treatment with MoS₂ samples were established using a Student's t test. The one-way analysis of variance (ANOVA) was used for multiple comparisons, followed by Dunnet post hoc test. Statistical tests were carried out using Prism 6.0 (GraphPad Prism, GraphPad Software, Inc.). Statistical significance is considered with a *P* values of less than 0.05. Each experiment was repeated three times in triplicate.

Conflict of Interest

The authors declare that they have no conflict of interests.

AUTHOR INFORMATION

Corresponding Author

Juan Antonio Tamayo-Ramos

International Research Centre in Critical Raw Materials-ICCRAM, Universidad de Burgos, Plaza Misael Banuelos s/n, 09001 Burgos, Spain

E-mail: ja.tamayoramos@gmail.com

Funding Sources

This work was supported by the European Union's H2020 research and innovation programme under the Marie Skłodowska-Curie grant agreement N^o 721642.

ACKNOWLEDGMENTS

We would like to thank Sonia Martel for her invaluable support.

REFERENCES

- [1] Fojtů M, Teo W Z and Pumera M 2017 Environmental impact and potential health risks of 2D nanomaterials *Environ. Sci. Nano* 4
- [2] Zhang H 2015 Ultrathin Two-Dimensional Nanomaterials *ACS Nano* 9 9451–69
- [3] Liu T and Liu Z 2018 2D MoS₂ Nanostructures for Biomedical Applications *Adv. Healthc. Mater.*
- [4] Ganatra R and Zhang Q 2014 Few-Layer MoS₂: A Promising Layered Semiconductor *ACS Nano* 8 4074–99
- [5] Vazirisereshk M R, Martini A, Strubbe D A and Baykara M Z 2019 Solid lubrication with MoS₂: A review *Lubricants* 7
- [6] Jian J, Chang H and Xu T 2019 Structure and properties of single-layer MoS₂ for nano-photoelectric devices *Materials (Basel)*. 12 1–10

- [7] Barua S, Dutta H S, Gogoi S, Devi R and Khan R 2017 Nanostructured MoS₂ -Based Advanced Biosensors: A Review *ACS Appl. Nano Mater.* 1 2–25
- [8] Zeng G, Chen T, Huang L, Liu M, Jiang R, Wan Q, Dai Y, Wen Y, Zhang X and Wei Y 2018 Surface modification and drug delivery applications of MoS₂ nanosheets with polymers through the combination of mussel inspired chemistry and SET-LRP *J. Taiwan Inst. Chem. Eng.* 82 205–13
- [9] Yin F, Anderson T, Panwar N, Zhang K, Tjin S C, Ng B K, Yoon H S, Qu J and Yong K-T 2018 Functionalized MoS₂ Nanosheets as Multi-Gene Delivery Vehicles for In Vivo Pancreatic Cancer Therapy *Nanotheranostics* 2 371–86
- [10] Wu S, Wang J, Jin L, Li Y and Wang Z 2018 Effects of Polyacrylonitrile/MoS₂ Composite Nanofibers on the Growth Behavior of Bone Marrow Mesenchymal Stem Cells *ACS Appl. Nano Mater.* acsanm.7b00188
- [11] Yang X, Li J, Liang T, Ma C, Zhang Y, Chen H, Hanagata N, Su H and Xu M 2014 Antibacterial activity of two-dimensional MoS₂ sheets *Nanoscale* 6 10126–33
- [12] Chng E L K, Sofer Z and Pumera M 2014 MoS₂ exhibits stronger toxicity with increased exfoliation *Nanoscale*
- [13] Fojtů M, Teo W Z and Pumera M 2017 Environmental impact and potential health risks of 2D nanomaterials *Environ. Sci. Nano* 4 1617–33

- [14] Appel J H, Li D O, Podlevsky J D, Debnath A, Green A A, Wang Q H and Chae J 2016 Low Cytotoxicity and Genotoxicity of Two-Dimensional MoS₂ and WS₂ *ACS Biomater. Sci. Eng.* 2 361–7
- [15] Moore C, Movia D, Smith R J, Hanlon D, Lebre F, Lavelle E C, Byrne H J, Coleman J N, Volkov Y and McIntyre J 2017 Industrial grade 2D molybdenum disulphide (MoS₂): An in vitro exploration of the impact on cellular uptake, cytotoxicity, and inflammation *2D Mater.* 4
- [16] Kaur J, Valadan M, Nebbioso A, Vergara A, Montone A M I, Benedetti R, Rossi M, Giardina P, Cutarelli A, Altucci L, Altucci C, Corrado F, Singh M and Dell'Aversana C 2018 Biological interactions of biocompatible and water-dispersed MoS₂ nanosheets with bacteria and human cells *Sci. Rep.*
- [17] Kenry and Lim C T 2017 Biocompatibility and Nanotoxicity of Layered Two-Dimensional Nanomaterials *ChemNanoMat* 3 5–16
- [18] Alimohammadi F, Sharifian M, Attanayake N H, Thenuwara A C, Gogotsi Y, Anasori B and Strongin D R 2018 Antimicrobial Properties of 2D MnO₂ and MoS₂ Nanomaterials Vertically Aligned on Graphene Materials and Ti₃C₂ MXene *Langmuir* 34 7192–200
- [19] Yang Q, Zhang L, Ben A, Wu N, Yi Y, Jiang L, Huang H and Yu Y 2018 Effects of dispersible MoS₂ nanosheets and Nano-silver coexistence on the metabolome of yeast *Chemosphere* 198 216–25

- [20] Yu Y, Yang Q, Wu N, Tang H, Yi Y, Wang G, Ge Y, Zong J, Madzak C, Zhao Y, Jiang L and Huang H 2017 Effect of Bulk MoS₂ on the Metabolic Profile of Yeast *J. Nanosci. Nanotechnol.* 18 3901–7
- [21] Wang Z, Von Dem Bussche A, Qiu Y, Valentin T M, Gion K, Kane A B and Hurt R H 2016 Chemical Dissolution Pathways of MoS₂ Nanosheets in Biological and Environmental Media *Environ. Sci. Technol.* 50 7208–17
- [22] Zhang X, Jia F, Yang B and Song S 2017 Oxidation of Molybdenum Disulfide Sheet in Water under in Situ Atomic Force Microscopy Observation *J. Phys. Chem. C* 121 9938–43
- [23] Fröhlich E and Salar-Behzadi S 2014 Toxicological assessment of inhaled nanoparticles: Role of in vivo, ex vivo, in vitro, and in Silico Studies *Int. J. Mol. Sci.* 15 4795–822
- [24] Braconi D, Bernardini G and Santucci A 2016 *Saccharomyces cerevisiae* as a model in ecotoxicological studies: A post-genomics perspective *J. Proteomics* 137 19–34
- [25] Hu K H, Hu X G, Wang J, Xu Y F and Han C L 2012 Tribological properties of MoS₂ with different morphologies in high-density polyethylene *Tribol. Lett.* 47 79–90
- [26] Lee C, Yan H, Brus L E, Heinz T F, Hone J and Ryu S 2010 Anomalous lattice vibrations of single- and few-layer MoS₂ *ACS Nano* 4 2695–700

- [27] Kumari L, Ma Y R, Tsai C C, Lin Y W, Wu S Y, Cheng K W and Liou Y 2007 X-ray diffraction and Raman scattering studies on large-area array and nanobranched structure of 1D MoO₂ nanorods *Nanotechnology* 18
- [28] Ahmed B, Shahid M, Nagaraju D H, Anjum D H, Hedhili M N and Alshareef H N 2015 Surface Passivation of MoO₃ Nanorods by Atomic Layer Deposition toward High Rate Durable Li Ion Battery Anodes *ACS Appl. Mater. Interfaces* 7 13154–63
- [29] Kondekar N P, Boebinger M G, Woods E V. and McDowell M T 2017 In Situ XPS Investigation of Transformations at Crystallographically Oriented MoS₂ Interfaces *ACS Appl. Mater. Interfaces* 9 32394–404
- [30] Liang X, Hart C, Pang Q, Garsuch A, Weiss T and Nazar L F 2015 A highly efficient polysulfide mediator for lithium-sulfur batteries *Nat. Commun.* 6 1–8
- [31] Marletta G and Iacona F 1996 Chemical selectivity and energy transfer mechanisms in the radiation-induced modification of polyethersulphone *Nucl. Instruments Methods Phys. Res. Sect. B Beam Interact. with Mater. Atoms* 116 246–52
- [32] Lanone S, Rogerieux F, Geys J, Dupont A, Maillot-Marechal E, Boczkowski J, Lacroix G and Hoet P 2009 Comparative toxicity of 24 manufactured nanoparticles in human alveolar epithelial and macrophage cell lines *Part. Fibre Toxicol.* 6 1–12

- [33] Costa C, Brandão F, Bessa M J, Costa S, Valdiglesias V, Kiliç G, Fernández-Bertólez N, Quaresma P, Pereira E, Pásaro E, Laffon B and Teixeira J P 2016 In vitro cytotoxicity of superparamagnetic iron oxide nanoparticles on neuronal and glial cells. Evaluation of nanoparticle interference with viability tests *J. Appl. Toxicol.* 36 361–72
- [34] Repetto G, del Peso A and Zurita J L 2008 Neutral red uptake assay for the estimation of cell viability/cytotoxicity. *Nat. Protoc.* 3 1125–31
- [35] Chng E L K, Sofer Z and Pumera M 2014 MoS₂ exhibits stronger toxicity with increased exfoliation *Nanoscale* 6 14412–8
- [36] Wang X, Mansukhani N D, Guiney L M, Ji Z, Chang C H, Wang M, Liao Y P, Song T Bin, Sun B, Li R, Xia T, Hersam M C and Nel A E 2015 Differences in the Toxicological Potential of 2D versus Aggregated Molybdenum Disulfide in the Lung *Small* 11 5079–87
- [37] Mei L, Zhang X, Yin W, Dong X, Guo Z, Fu W, Su C, Gu Z and Zhao Y 2019 Translocation, biotransformation-related degradation, and toxicity assessment of polyvinylpyrrolidone-modified 2H-phase nano-MoS₂ *Nanoscale* 11 4767–80
- [38] Teo W Z, Chng E L K, Sofer Z and Pumera M 2014 Cytotoxicity of Exfoliated Transition-Metal Dichalcogenides (MoS₂, WS₂, and WSe₂) is Lower Than That of Graphene and its Analogues *Chem. - A Eur. J.* 20 9627–32

- [39] Pujalté I, Passagne I, Brouillaud B, Tréguer M, Durand E, Ohayon-Courtès C and L'Azou B 2011 Cytotoxicity and oxidative stress induced by different metallic nanoparticles on human kidney cells *Part. Fibre Toxicol.* 8 10
- [40] Khanna P, Ong C, Bay B and Baeg G 2015 Nanotoxicity: An Interplay of Oxidative Stress, Inflammation and Cell Death *Nanomaterials* 5 1163–80
- [41] Aranda A, Sequedo L, Tolosa L, Quintas G, Burello E, Castell J V. and Gombau L 2013 Dichloro-dihydro-fluorescein diacetate (DCFH-DA) assay: A quantitative method for oxidative stress assessment of nanoparticle-treated cells *Toxicol. Vitr.* 27 954–63
- [42] Yu Y, Wu N, Yi Y, Li Y, Zhang L, Yang Q, Miao W, Ding X, Jiang L and Huang H 2017 Dispersible MoS₂ Nanosheets Activated TGF- β /Smad Pathway and Perturbed the Metabolome of Human Dermal Fibroblasts *ACS Biomater. Sci. Eng.* 3 3261–72
- [43] Liu S, Shen Z, Wu B, Yu Y, Hou H, Zhang X X and Ren H Q 2017 Cytotoxicity and Efflux Pump Inhibition Induced by Molybdenum Disulfide and Boron Nitride Nanomaterials with Sheetlike Structure *Environ. Sci. Technol.* 51 10834–42
- [44] National Toxicology P 1997 NTP Toxicology and Carcinogenesis Studies of Nitromethane (CAS No. 75-52-5) in F344/N Rats and B6C3F1 Mice (Inhalation Studies) *Natl Toxicol Progr. Tech Rep Ser* 461 1–289

- [45] Anh Tran T, Krishnamoorthy K, Song Y W, Cho S K and Kim S J 2014 Toxicity of nano molybdenum trioxide toward invasive breast cancer cells *ACS Appl. Mater. Interfaces* 6 2980–6
- [46] Kwolek-Mirek M and Zadrag-Tecza R 2014 Comparison of methods used for assessing the viability and vitality of yeast cells *FEMS Yeast Res.* 14 1068–79
- [47] Shafaei S, Van Opdenbosch D, Fey T, Koch M, Kraus T, Guggenbichler J P and Zollfrank C 2016 Enhancement of the antimicrobial properties of orthorhombic molybdenum trioxide by thermal induced fracturing of the hydrates *Mater. Sci. Eng. C* 58 1064–70
- [48] Chaves-Lopez C, Nguyen H N, Oliveira R C, Nadres E T, Paparella A and Rodrigues D F 2018 A morphological, enzymatic and metabolic approach to elucidate apoptotic-like cell death in fungi exposed to h- and α -molybdenum trioxide nanoparticles *Nanoscale* 10 20702–16
- [49] KING A D, PONTING J D, SANSHUCK D W, JACKSON R and MIHARA K 1981 Factors Affecting Death of Yeast by Sulfur Dioxide *J. Food Prot.* 44 92–7
- [50] Sousa C A, Soares H M V M and Soares E V. 2018 Nickel Oxide (NiO) Nanoparticles Induce Loss of Cell Viability in Yeast Mediated by Oxidative Stress *Chem. Res. Toxicol.* 31 658–65
- [51] Domi B, Rumbo C, García-Tojal J, Elena Sima L, Negroiu G and Tamayo-Ramos J A 2019 Interaction Analysis of Commercial Graphene Oxide

Nanoparticles with Unicellular Systems and Biomolecules *Int. J. Mol. Sci.* 21
205

[52] Suarez-Diez M, Porras S, Laguna-Teno F, Schaap P J and Tamayo-Ramos J A 2020 Toxicological response of the model fungus *Saccharomyces cerevisiae* to different concentrations of commercial graphene nanoplatelets *Sci. Rep.* 10 1–12

[53] Yu Y, Yang Q, Wu N, Tang H, Yi Y, Wang G, Ge Y, Zong J, Madzak C, Zhao Y, Jiang L and Huang H 2018 Effect of Bulk MoS₂ on the Metabolic Profile of Yeast *J. Nanosci. Nanotechnol.* 18 3901–7

[54] Basu P, Chakraborty J, Ganguli N, Mukherjee K, Acharya K, Satpati B, Khamrui S, Mandal S, Banerjee D, Goswami D, Nambissan P M G and Chatterjee K 2019 Defect-Engineered MoS₂ Nanostructures for Reactive Oxygen Species Generation in the Dark: Antipollutant and Antifungal Performances *ACS Appl. Mater. Interfaces* 11 48179–91

Toxicological assessment of commercial 2D WS₂ aqueous suspensions using different eukaryotic models

Brixhilda Domi¹, Kapil Bhorkar^{2,3}, Carlos Rumbo¹, Labrini Sygellou,² Sonia Martel Martin¹, Roberto Quesada⁴, Spyros N. Yannopoulos², Juan Antonio Tamayo-Ramos*¹

¹ International Research Centre in Critical Raw Materials-ICCRAM, Universidad de Burgos, Plaza Misael Banuelos s/n, 09001 Burgos, Spain

² Foundation for Research and Technology Hellas – Institute of Chemical Engineering Sciences (FORTH/ICE-HT), P.O. Box 1414, GR-26504, Rio-Patras, Greece

³ Univ Rennes, CNRS, ISCR - UMR 6226, F-35000 Rennes, France

⁴ Departamento de Química, Facultad de Ciencias, Universidad de Burgos, 09001, Burgos, Spain

* Corresponding author:

Juan Antonio Tamayo-Ramos: jatramos@ubu.es Phone: +34 947 49 20 05

HIGHLIGHTS

Commercial 2D WS₂ aqueous suspensions with different lateral size were characterized

The suspensions were composed by a combination of 1T'-WS₂, 2H-WS₂, WO₃ and SO₂

Both commercial samples showed no reduction on cellular vitality in A549 cells

Both commercial samples reduced the cellular vitality of *Saccharomyces cerevisiae*

Submitted to *Chemosphere*, 30 Sep 2020

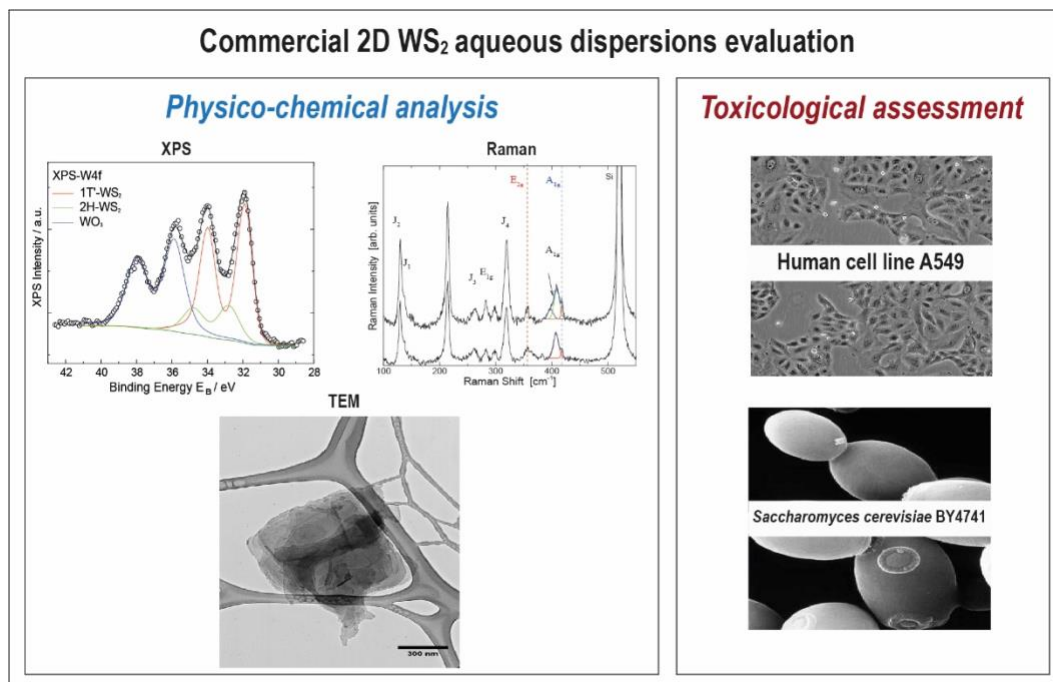
Abstract

Commercially available aqueous dispersions of 2D WS₂ nanomaterials with distinct lateral size were subjected to physico-chemical and toxicological evaluations using different eukaryotic biological models. The structure and stoichiometry of monolayer tungsten disulfide (WS₂-ACS-M) and nano size monolayer tungsten disulfide (WS₂-ACS-N) was analyzed by Raman spectroscopy, whereas a more quantitative approach to study the nature of formed oxidized species was undertaken employing X-ray photoelectron spectroscopy. Adenocarcinomic human alveolar basal epithelial cells (A549 cells) and the ecotoxicology model *Saccharomyces cerevisiae* were selected as unicellular eukaryotic systems to assess the cytotoxicity of the nanomaterials. Cell viability and reactive oxygen species (ROS) determinations demonstrated different toxicity levels depending on the cellular model used. While both 2D WS₂ suspensions showed very low toxicity towards the A549 cells, a comparable concentration (160 mg L⁻¹) reduced the viability of yeast cells. The toxicity of a nano size 2D WS₂ commercialized in dry form from the same provider was also assessed, showing ability to reduce yeast cells viability as well.

Keywords

2D WS₂; structure; stoichiometry; eukaryotic cells; cell viability; oxidative stress

Graphical abstract



Introduction

Tungsten disulfide (WS₂) nanomaterials are standing out within the transition metal dichalcogenides (TMDs) family due to their unique physico-chemical properties and to the more favourable commercial availability of W, when compared to other transition metals with similar properties (Eftekhari, 2017). WS₂ has shown potential for applications in different industrial settings for the production of transistors, sensors or photocatalytic and electronic devices (Choi et al., 2017). Since WS₂ exhibits both low friction coefficient and high strength, it also represents an excellent dry lubricant (Ratoi et al., 2013). Furthermore, as a result of the low friction coefficient, tungsten disulfide is used in clinical dentistry for orthodontic implants (Katz et al., 2006). In addition, WS₂ is currently being used in manufacturing, marine, agriculture, and automotive applications (Eftekhari, 2017). As a consequence of the increased use of WS₂, there is also the

necessity to study the potential toxicological effects of this material, due to the increasing degree of environmental and human exposure. The structures of exfoliated TMD materials are very different to those exhibited by conventional bulk structures (Jeevanandam et al., 2018), and even though all TMDs exhibit similar layered 2D morphology, their biocompatibility can be significantly altered depending on several parameters such size, shape or the method used to prepare the 2D TMD nanosheets (Lv et al., 2015). The toxicity of WS₂ nanomaterials is yet understudied, only a limited number of toxicological studies are available using distinct eukaryotic and prokaryotic models (Appel et al., 2016; Liu et al., 2017; Yuan et al., 2018, 2020). For instance, Appel *et al* studied the potential toxicological effects of WS₂ nanoparticles prepared by several methods such as mechanical exfoliation and chemical vapor deposition (CVD) toward human epithelial kidney cells (HEK293f) (Appel et al., 2016), while other authors focused on the evaluation of the impact of commercial 2D WS₂ powders on the viability of other human cell lines, such as NL-20, HEPG2 and macrophages (Corazzari et al., 2014; Pardo et al., 2014). The potential synergistic toxic effects on different human cell lines (RAW264.7 and A549) of WS₂ nanosheets and organic pollutants have been reported recently as well, showing their capability to damage the plasma membrane and cytoskeleton, resulting in increased membrane permeability and enhanced organic pollutant uptake (Yuan et al., 2020). Moreover, molecular dynamics simulations suggest the ability of WS₂ nanosheets to disturb the secondary structure of efflux pumps, hampering xenobiotics elimination (Yuan et al., 2020). The biological responses of Gram-negative *Escherichia*

coli and Gram-positive *Staphylococcus aureus* to WS₂ nanosheets have been reported as well, indicating a time and concentration dependent antibacterial activity for both bacterial strains (Liu et al., 2017). The potential toxic effects of chemically exfoliated WS₂ nanosheets (Ce-WS₂) and annealed exfoliated WS₂ nanosheets (Ae-WS₂, 2H phase) were investigated toward the single-celled green algae *Chlorella vulgaris*, where differences in the toxicity of both nanomaterials towards the microorganism were observed, possibly due to differences in the physico-chemical parameters of the two materials (Yuan et al., 2018). Notably, while recently we have observed that MoS₂ nanomaterials exert a negative impact on the viability of the yeast *Saccharomyces cerevisiae* (Domi et al., 2020), no reports are available yet about the effect of WS₂ nanomaterials on yeast or other fungal species. Thus, in the present work, we explored the *in vitro* cytotoxicity of commercial 2D WS₂ materials in two different eukaryotic models: human alveolar carcinoma epithelial cells A549 to mimic the potential hazard *via* inhalation exposure (Lanone et al., 2009; Visalli et al., 2015) and the yeast *S. cerevisiae*, as a well-established model in ecotoxicology, to investigate their potential impact in fungi (Braconi et al., 2016; Mell and Burgess, 2002; Michels, 2003).

Materials and Methods

2.1 Materials and reagents

Chemicals employed were purchased from Sigma-Aldrich (Merck KGaA, Darmstadt, Germany) and Acros Organics (Thermo Fisher Scientific Inc., Madrid, Spain). Monolayer tungsten disulfide water dispersion (WS₂-ACS-M), and nano size monolayer tungsten disulfide water dispersion (WS₂-

ACS-N) and dry powder (WS_2 -ACS-N-PW) forms were purchased at ACS material®.

2.2 Atomic Force Microscopy (AFM) and Transmission Electron Microscopy (TEM) Analysis

AFM images were recorded in tapping mode with an Alpha300R-Alpha300A AFM Witec instrument, using Arrow NC cantilevers with a tip radius <10 nm and a force constant of 42 N/m. All the WS_2 samples were placed on a mica surface from aqueous solutions by drop casting. TEM analysis was performed at the microscopy unit from the University of Valladolid, using a JEOL JEM-1011 high-resolution (HR) TEM coupled with a Gatan Erlangshen ES1000W camera. Samples were deposited on Lacey Carbon Type-A, 300 mesh, copper grids.

2.3 Raman Spectroscopy

Raman spectra were excited by the 441.6 nm radiation emerging from a He-Cd laser (Kimon). The laser light was focused by a 50x objective creating a focusing area of 2-3 μm . The scattered light was collected by the same objective and analyzed using by the LabRam HR800 (Jobin-Yvon) spectrometer operating at a spectral resolution of ~ 2.0 cm. A very low light fluence (275 μW) on the sample was used to avoid heat induced effects (oxidation and decomposition). The Raman mode of Si single crystal at 520 cm^{-1} was used to calibrate the wavenumber scale of the spectra.

2.4 X-ray Photoelectron Spectroscopy

The surface analysis measurements were performed in a UHV chamber ($P \sim 5 \times 10^{-10}$ mbar) equipped with a SPECS Phoibos 100-1D-DLD

hemispherical electron analyzer and a non-monochromatized dual-anode Mg/Al x-ray source for XPS. The spectra were recorded with AlK α at 1486.6 eV photon energy using analyzer pass energy of 10 eV which results to full width at half maximum (FWHM) of 0.85 eV for Ag3d5/2 line. The analyzed area was a rectangle with dimensions 7x15 mm². Spectra were accumulated and processed using SpecsLab Prodigy (Specs GmbH, Berlin) software. The XPS peaks were deconvoluted with mixed Gaussian – Lorentzian functions after a Shirley background subtraction. The WS₂-ACS-M and WS₂-ACS-N samples were prepared by drop casting the dispersion on Si wafers, whereas powder of the WS₂-ALK-N was pressed on Indium foil.

2.5 A549 Cell culture

The human alveolar carcinoma epithelial cell line A549 (ATCC, CCL-185) were grown in DMEM medium (Dulbecco's Modified Eagle Medium) supplemented with 10% foetal calf serum (FCS) and 1% penicillin/streptomycin (Sigma-Aldrich). Cells were grown in a humidified incubator at 37 °C and 5% CO₂.

2.6 A549 cells Neutral Red assay

Around 3×10⁴ cells were incubated in culture media with 5% CO₂ for 24 h at 37 °C. Then, A549 cells were seeded in 96 well plates and exposed to 20, 40, 80 and 160 mg L⁻¹ of the nanomaterials diluted in DMEM 1% FCS. After 24 hours of exposure, cells were washed and incubated with 100 μ L of the Neutral Red solution which was prepared as follows: neutral red stock (4 mg L⁻¹) was diluted 1:100 in treatment media then incubated for 24 h at

37°C protected from light. After 2.5 hours incubation, cells were washed once with DPBS and fixed with formaldehyde 4%. Then, cells were washed again with DPBS and a solution of extraction (50% ethanol 96°, 49% distilled H₂O and 1% acetic acid) was added to all wells. After 10 minutes of moderate shaking, this solution was transferred to a new opaque 96-well plate, and fluorescence was measured with a microplate reader (BioTek Synergy HT, excitation wavelength, 530/25; emission wavelength 645/40). Results were expressed as percentage of control (absorbance of cells in absence of materials). Each assay included two independent replicates.

2.7 A549 cells ROS determination

2,7-dichlorofluorescein diacetate (DCFH-DA) was used to perform quantitative measurements of oxidative stress production via intracellular reactive oxygen species (ROS). Around 3×10^4 cells per well were seeded in a 96 micro-well plate and labelled for 30 min with 50 µM DCFH-DA in Hanks' Balanced Salt Solution (HBSS). After the incubation, cells were washed once with HBSS and several (20, 40, 80 and 160 mg L⁻¹) concentrations of the nanomaterials (diluted in HBSS) were added to each well. Fluorescence was measured with a microplate reader (BioTek Synergy HT, excitation wavelength, 530/25; emission wavelength 645/40) after 1 hour of incubation.

2.8 Yeast culture

The yeast *S. cerevisiae* BY4741 strain was utilized to perform toxicological assays and was grown in standard liquid YPD medium (1% yeast extract,

1% yeast bacto-peptone, 2% glucose). Cells were cultured in liquid media on a rotary shaker at 185 rpm at 30 °C.

2.9 Yeast Colony forming units (CFUs) determination

Yeast cells in exponential growth phase ($OD_{600} = 1$) were incubated with different 2D WS₂ samples at 160 and 800 mg L⁻¹ in 1 mL cultures in 24 well plates. The cultures were sampled at two different exposure times (2 and 24 hours), and colony forming units determination was done by inoculating adequate dilutions in solid YPD medium plates, which were incubated at 30 °C for 48 hours.

2.10 Yeast ROS assay

The reagent CM-H₂DCFDA (Invitrogen, General Oxidative Stress Indicator) was utilized to determine ROS in yeast following a protocol similar to that reported by James *et al.*²⁴ *S. cerevisiae* cells growing in exponential phase were pelleted, washed and incubated with CM-H₂DCFDA (7 μM) in DPBS for 60 minutes at 30 °C and 185 rpm. Consequently, yeast cells were washed, suspended in YPD medium and thus exposed to the three WS₂ samples (160 and 800 mg L⁻¹) for 2 and 24 hours. Next, cells were washed two times with DPBS, incubated 2 minutes in a solution containing lithium acetate 2M, washed again and incubated for 2 minutes in a solution containing SDS (sodium dodecyl sulfate) (0.01 %) and chloroform (0.4 %). Finally, cells were pelleted and the supernatant was transferred to a black opaque 96 micro-well plate, where the fluorescence was measured (excitation= 485; emission= 528) using a microplate reader (Synergy-HT, BioTek).

2.11 Statistical analysis

Statistical analysis data are shown as means \pm SD. Differences between the negative control and exposure conditions were established using one-way analysis of variance (ANOVA) for multiple comparisons, followed by Dunnet *post hoc* test. Statistical tests were carried out using Prism 6.0 (GraphPad Prism, GraphPad Software, Inc.). *P* values of less than 0.05 were considered to indicate statistical significance.

Results and Discussion

3.1 Selection and Characterization of Commercial 2D Tungsten Disulfide

Initially, we selected two commercial 2D WS₂ aqueous suspensions from ACS material[®], namely monolayer tungsten disulfide (WS₂-ACS-M) and nano size monolayer tungsten disulfide (WS₂-ACS-N), with a distinct lateral size according to the supplier (0.1-4 μ m and 20-500 nm respectively). To confirm their morphologic characteristics TEM analysis was performed by drop casting the samples on a carbon-coated copper grid. Both nanomaterials (Figure 1a and 1b) showed to have a platelet-like morphology as expected considering the supplier information. However, no clear differences between the two products could be observed in terms of size, aggregation state or morphological characteristics.

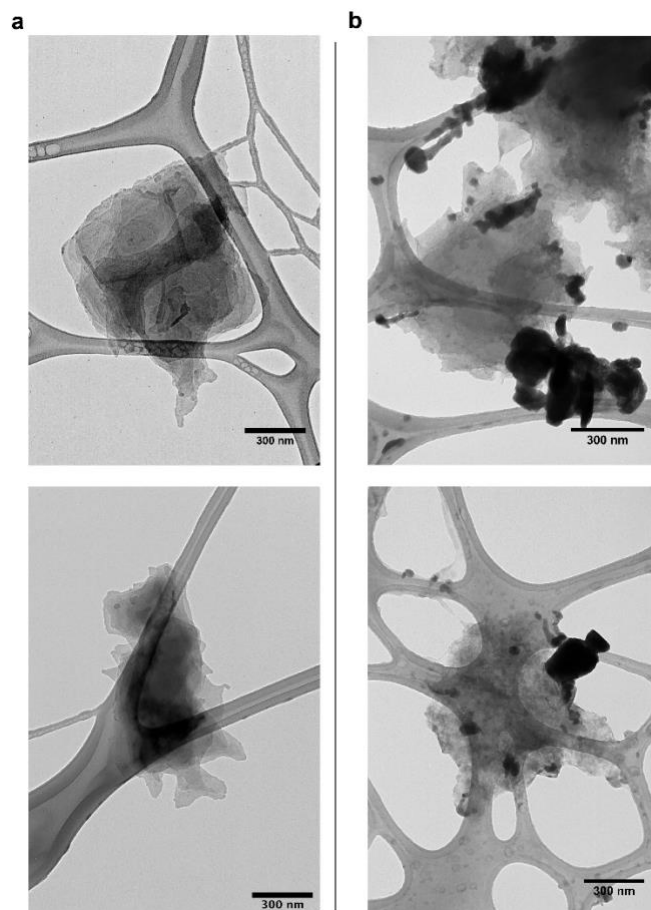


Figure 1: TEM images of WS₂-ACS-M (a) and WS₂-ACS-N (b). Tungsten disulfide dispersions with a concentration of 20 mg L⁻¹ were deposited by drop casting on carbon-coated copper grids.

To analyze the structure and stoichiometry of the materials, X-ray photoelectron spectra (XPS) and Raman spectra of the samples were collected and analyzed. In relation to the XPS analysis, Figures 2a and 2b show the W4f spectra of WS₂-ACS-M and WS₂-ACS-N, respectively. The spectra consist of three doublets with a spin orbit splitting W4f_{7/2}-W4f_{5/2} of ~2.0 eV. The binding energies (BE) of the W4f_{7/2} components obtained by the fitting analysis are located at 31.9, 32.8 and 35.9 eV, which are assigned to the phases 1T'-WS₂, 2H-WS₂, and the WO₃ oxide, respectively (Liu et al., 2018). Deconvoluted XP spectra of the S2p peak are shown in Figures

2c and 2d. The XP spectra of both materials are analyzed into three doublets with a spin orbit splitting $S2p_{3/2}-S2p_{1/2}$ of ~ 1.2 eV. The binding energies of $S2p_{3/2}$ components located at ~ 161.6 , ~ 162.5 and ~ 168.0 eV, are assigned to $1T'$ - WS_2 , $2H$ - WS_2 (Liu et al., 2018), and to sulphonyl groups ($-SO_2-$ groups) (Marletta and Iacona, 1996), respectively. The relative fraction of the various components, corresponding to the W and S species identified by the fitting analysis are shown in Table 1.

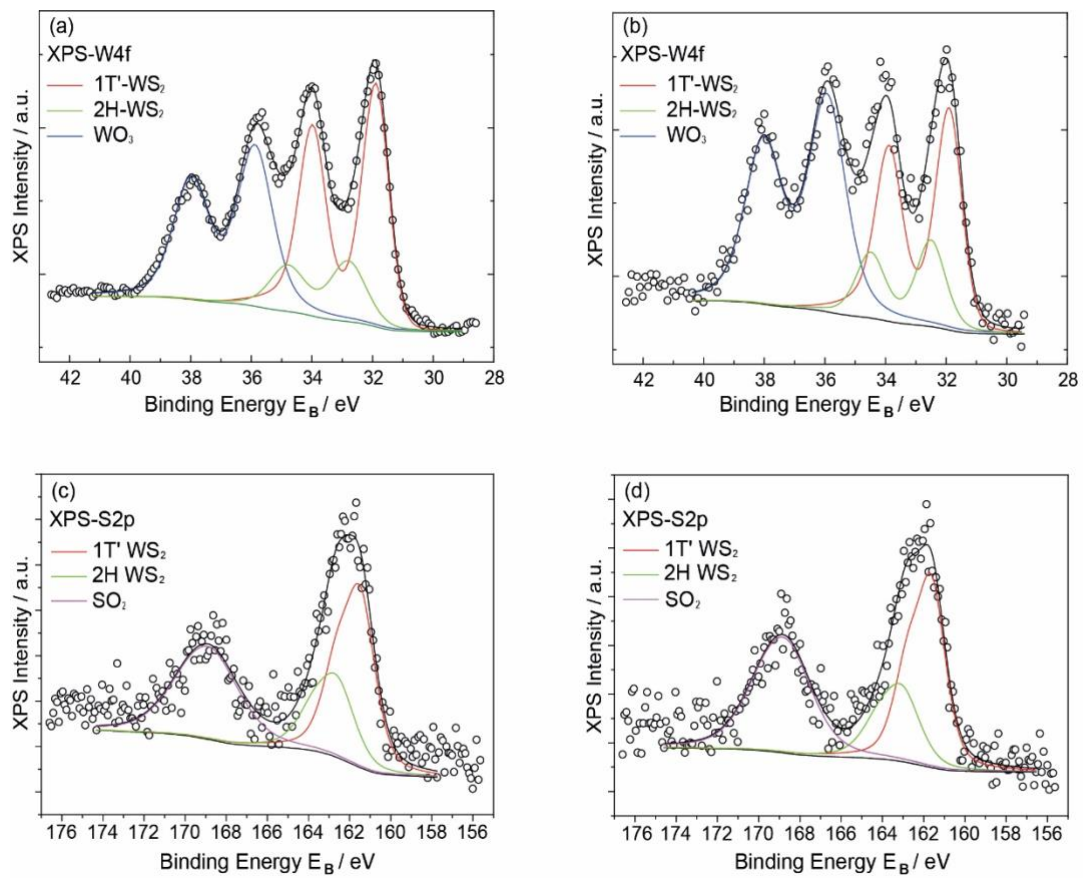


Figure 2: De-convoluted W4f spectra of (a) WS_2 -ACS-M, and (b) WS_2 -ACS-N, and deconvoluted S2p XPS spectra of (c) WS_2 -ACS-M, and (d) WS_2 -ACS-N samples.

% concentration of WS ₂ phases and WO ₃			
	1T'-WS ₂	2H-WS ₂	WO ₃
WS ₂ -ACS-M	47.7 ± 0.7	13.9 ± 0.7	38.3 ± 0.7
WS ₂ -ACS-N	38.7 ± 0.8	14.5 ± 0.8	46.8 ± 0.8
% concentration of WS ₂ phases and SO ₂			
	1T'-WS ₂	2H-WS ₂	SO ₂
WS ₂ -ACS-M	42.8 ± 0.7	21.8 ± 0.7	35.5 ± 0.7
WS ₂ -ACS-N	41.8 ± 0.8	19.6 ± 0.8	38.6 ± 0.8

Table 1: Relative fraction of the 2D WS₂ aqueous dispersions components, corresponding to the W and S species identified.

Raman spectra for the 2D WS₂ samples are shown in Figure 3. The vertical dashed lines represent the energies of the in-plane E_{2g}^1 and out-of-plane A_{1g} symmetries of the 2H-WS₂ phase located at 356 and 417.5 cm⁻¹, respectively (Berkdemir et al., 2013). The spectrum of WS₂-ACS-M and WS₂-ACS-N exhibit the mentioned bands, albeit as weak features. A strong band near 408 cm⁻¹ overwhelms the intensity of the A_{1g} mode; hence, a fitting analysis was performed to identify the correct energy of the A_{1g} band. Typical examples of the fitting for the spectra of both the WS₂-ACS-M and WS₂-ACS-N samples are shown in Figure 3. The peak energies and their differences of the E_{2g}^1 and A_{1g} bands suggest the existence of monolayer WS₂ for both samples. In line with XPS analysis, the weak intensity of the 2H-WS₂, indicates a rather small relative fraction of this phase, in comparison to other phases present in WS₂-ACS-M and WS₂-ACS-N. Indeed, a number of additional strong bands emerge in the Raman spectra of the selected 2D WS₂ samples. As the current excitation (441.6 nm) is far

from resonance conditions (514.5 nm), the additional Raman bands cannot be assigned to resonance bands. Based on the XPS analysis, which revealed the presence of the $1T'$ - WS_2 phase and WO_3 oxide, we attempt a Raman band assignment based on these two phases. A number of vibrational bands have been observed in the Raman spectrum of the $1T'$ - WS_2 phase (Tan et al., 2017). These bands are labeled as J_1 (139 cm^{-1}) J_2 (133 cm^{-1}) J_3 (265 cm^{-1}) and J_4 (321 cm^{-1}). All these bands are observed also in the current spectra, albeit with a red-shift of 2 to 3 cm^{-1} . For both WS_2 -ACS-M and WS_2 -ACS-N samples, the metallic phase ($1T'$) was found to be the dominant one in relation to the semiconducting phase (2H).

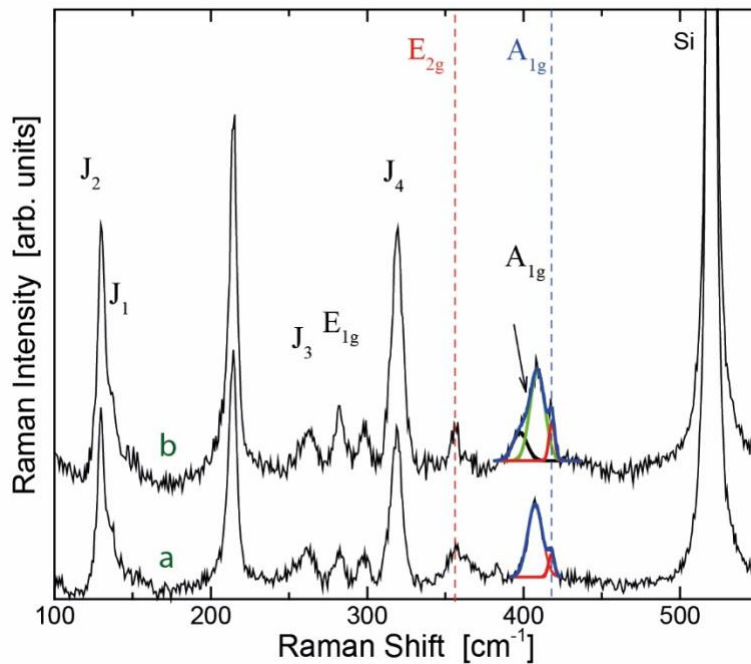


Figure 3: Raman spectra of WS_2 -ACS-M (a) and WS_2 -ACS-N (b) samples.

3.2 Toxicology assessment using adenocarcinoma A549 human cells

To assess the potential toxicity of the selected commercial 2D WS₂ products, human lung carcinoma A549 cells were exposed to different concentrations of WS₂-ACS-M and WS₂-ACS-N (20, 40, 80 and 160 mg L⁻¹) for a period of 24 hours. To study the percentage of the surviving cells after the incubation with the nanomaterials, the Neutral Red assay was chosen as a very common cytotoxicity test for the evaluation of the potential toxicity of nanoparticles (Repetto et al., 2008). The assay allows the relative quantification of living cells in a culture, due to the capability of vital cells to absorb the Neutral Red dye, following the accumulation into the cellular lysosomes. The results obtained after a 24 h exposure to both 2D WS₂ nanomaterial types are displayed in Figure 4.

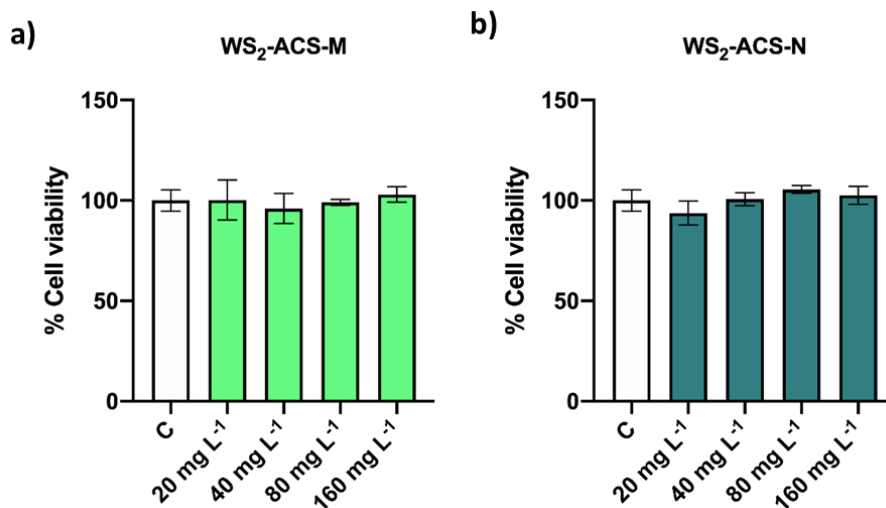


Figure 4: Viability of A549 cells (Neutral Red assay) exposed to different concentrations of WS₂-ACS-M (a) and WS₂-ACS-N (b) for 24 hours. Results are expressed as % of control (non-exposed cells). Data represent the mean (\pm standard deviation, SD) of two independent experiments.

Differences were established using a One-way ANOVA followed by Dunnett *post hoc* test to compare every mean with the control.

As it can be observed, the viability of the A549 cells was not reduced in the presence of the different concentrations tested. Few studies have assessed the toxicological effects of different WS₂ nanomaterials toward lung epithelial cells, reporting in some cases opposite results. While the work of Teo *et al.* indicated low cytotoxicity of exfoliated WS₂ nanosheets using thiazolyl blue tetrazolium bromide (MTT) and water-soluble tetrazolium salt (WST-8) assays in concentrations up to 400 mg L⁻¹, Liu *et al.* observed an evident negative impact of WS₂ nanoparticles on A549 cells with concentrations of 50 mg L⁻¹ or higher, employing the CCK-8 assay. However, in concordance with the results obtained in the present work, most of the studies testing the toxicity of different TMD nanoforms, including WS₂, indicate a low degree of cytotoxicity towards respiratory models and other human cell lines (Appel *et al.*, 2016; Corazzari *et al.*, 2014; Pardo *et al.*, 2014; Teo *et al.*, 2014).

Although the WS₂ nanoparticles did not induce significant cell death, we aimed to study the possible generation of intracellular ROS triggered by these materials. ROS generation can result in cell damage, inflammation and several diseases and pathologies (Holmström and Finkel, 2014). Henceforth, as done previously in the Neutral Red viability assay, we determined the ROS generation after the cell's exposure during 1 hour to different concentrations from 20 to 160 mg L⁻¹ of the 2D WS₂ samples (Figure 5).

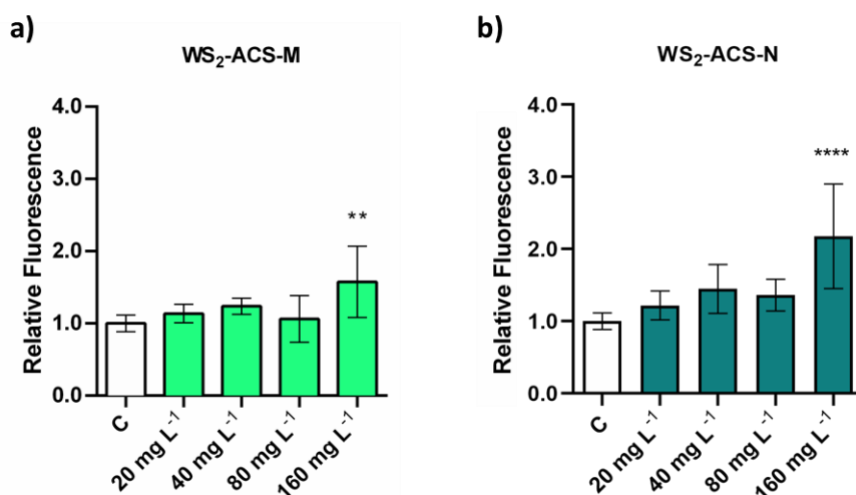


Figure 5: ROS production of A549 cells treated with different concentrations of WS₂-ACS-M (a) and WS₂-ACS-N (b). The reported values are expressed as the relative fluorescence value to the control (untreated cells) which was assigned a value of 1. Data represent the mean of 2 independent experiments (\pm standard deviation, SD). Differences were established using a One-way ANOVA followed by Dunnett *post hoc* test to compare every mean with the control and considered significant at $P \leq 0.05$. ** $P \leq 0.01$, **** $P \leq 0.0001$.

The ROS levels observed in the different conditions tested remained at relatively low level in comparison with the non-treated cells condition. This result is similar to that observed as well in exposed A549 cells by Corazzari *et al.*, where the presence of WS₂ fullerene-like spherical engineered nanomaterials did not induce oxidative stress at different concentrations (Corazzari *et al.*, 2014). The exposure of other human unicellular models, such as human kidney cells (HEK293f), nontumorigenic human bronchial epithelial cells (NL-20) and human liver carcinoma cells (HepG2) to different WS₂ nanoforms has produced similar results to those observed in the

present work, where low cytotoxicity levels were observed (Appel et al., 2016) (Pardo et al., 2014).

3.3 Toxicology assessment using *S. cerevisiae*

The yeast *S. cerevisiae* is a well-consolidated and widely used model organism utilized for the evaluation of cellular response to stress and ecotoxicology studies (Braconi et al., 2016; Ivask et al., 2014; Sousa et al., 2018). So far, no nanosafety studies are available on the cytotoxicity of WS₂ nanoforms on *S. cerevisiae*, while recently, 2D MoS₂ have been reported to exert a significant toxicological impact on yeast cells, at least when the nanoparticles concentration range is from 160 to 800 mg L⁻¹ (Domi et al., 2020). Thus, we decided to investigate the possible toxicological potential of commercial 2D WS₂ flakes toward yeast, using the same concentration range. One of the most used assays in toxicological analyses when using microorganisms as model organisms is the determination of the number of colony forming units (CFUs) (Kwolek-Mirek and Zadrag-Tecza, 2014). Normally, cell viability is defined as a percentage of living cells in a whole population after the exposure to a certain substance in a specific time of incubation. *S. cerevisiae* cells were exposed to WS₂-ACS-M and WS₂-ACS-N at the concentrations of 160 and 800 mg L⁻¹ for 2 and 24 h. As displayed in Figure 6, no significant differences in viability were observed in the selected exposure conditions after 2 hours of exposure in the two concentrations tested for both samples, compared to the control of non-treated cells. However, after 24 hours exposure, a significant decrease on the viability of yeast incubated with 2D WS₂ could be observed. Lower average CFUs were observed, being this more evident in the presence of

800 mg L⁻¹, where the average percentage of surviving cells after the exposure to WS₂-ACS-M and WS₂-ACS-N was around 50%.

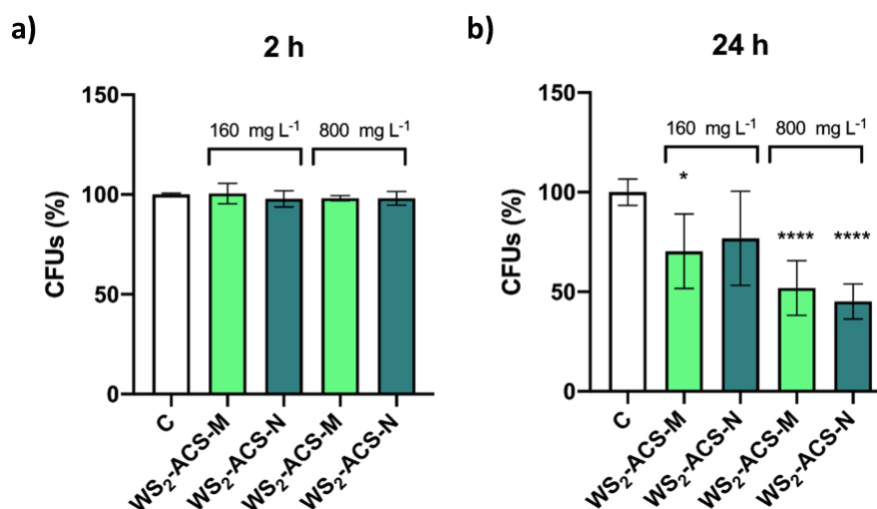


Figure 6: CFUs determination of *S. cerevisiae* cells exposed to 160 and 800 mg L⁻¹ of WS₂-ACS-M and WS₂-ACS-N during 2 (a) and 24 h (b). The reported values are the averages of two independent experiments. Differences were established using a One-way ANOVA followed by Dunnett *post hoc* test to compare every mean with the control, and considered significant at $P \leq 0.05$. * $P \leq 0.05$, **** $P \leq 0.0001$.

The molecular pathway of the programmed cell death is associated with the production of ROS in an extensive variety of organisms, including *S. cerevisiae* (Perrone et al., 2008). When the level of oxidative stress production overwhelms antioxidant defense systems, the cell redox homeostasis is altered, resulting in the oxidation of proteins, peroxidation of lipids, DNA alterations, leading to reduced cell viability (Perrone et al., 2008). It has been reported that a large variety of nanoparticles can induce ROS in yeast, such as 2D MoS₂ (Domi et al., 2020), graphene oxide (Domi et al., 2019), metalloid oxides (Sousa et al., 2019) and magnetic

nanomaterials (Peng et al., 2018). Consequently, to understand whether the decrease of yeast viability could be associated to higher levels of oxidative stress, we analyzed ROS levels in cells exposed to WS₂. Hence, yeast cells were exposed to 160 and 800 mg L⁻¹ of both commercial 2D WS₂ samples for 2 and 24 hours. As shown in Figure 7, oxidative stress levels in all exposure conditions were only slightly higher than those observed for the non-exposed cells, indicating a low capacity of the nanomaterials to induce the formation of intracellular ROS in yeast cells.

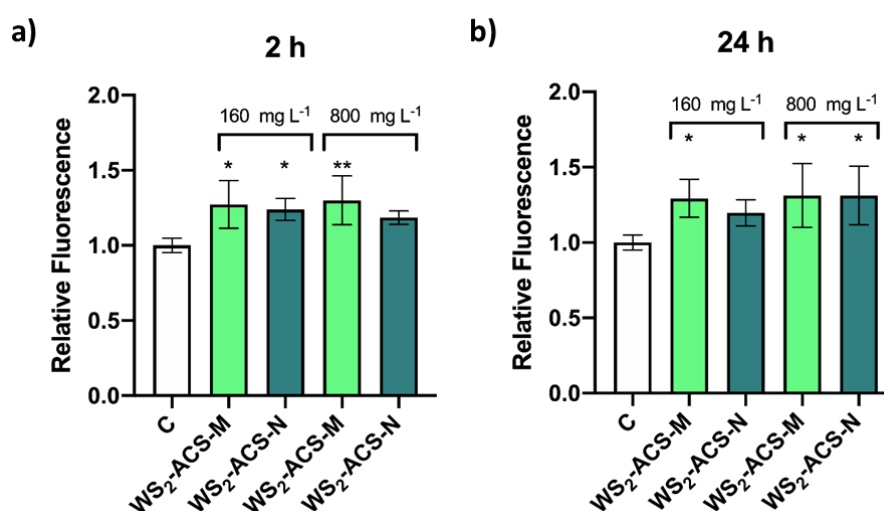


Figure 7: Oxidative stress (ROS) determination of *S. cerevisiae* cells exposed to 160 and 800 mg L⁻¹ of WS₂-ACS-M and WS₂-ACS-N during 2 hours (a) and 24 hours (b). The reported values are the averages of two independent experiments, and are expressed as the relative fluorescence value to the control (untreated cells) which was assigned a value of 1. Differences were established using a One-way ANOVA followed by Dunnett *post hoc* test to compare every mean with the control, and considered significant at $P \leq 0.05$. * $P \leq 0.05$, ** $P \leq 0.01$.

Interestingly, high concentrations (800 mg L⁻¹) of 2D nanomaterials, such as MoS₂ and graphene oxide, induced a clearer increase of ROS levels in yeast than those observed in the presence of 2D WS₂ (Domi et al., 2019, 2020). This difference is particularly remarkable in case of graphene oxide, where commercial products from different suppliers induced 20 to 30 times higher ROS levels compared to the non-treated cells condition.

In the present work, commercial aqueous suspensions of 2D WS₂ were selected due to their high nanoparticle dispersibility. Commercial 2D WS₂ dry powders, which are the most common commercialized form of the 2D nanomaterial, are obtained by drying 2D WS₂ aqueous suspensions that have been prepared through Li-intercalation and exfoliation in water. The copious gas evolution that occurs once water is added to Li_xWS₂ to induce 2D WS₂ exfoliation, enables the formation of highly dispersed, stable colloidal 2D WS₂ suspensions. However, when resuspending commercially available dry 2D WS₂ nanopowders in water to obtain aqueous suspensions, even when assisted by ultrasonication, the nanoparticle dispersion rate and the colloidal stability of the suspension obtained is lower (internal communication of the supplier). For this reason, we decided to test as well whether aqueous suspensions prepared in our laboratory using commercially available dry 2D WS₂ nanopowders reduced the viability of yeast too. Figure 8 displays *S. cerevisiae* CFUs determination (Figure 8a and 8b) and ROS assays (Figure 8c and 8d), showing that the same concentrations of dry 2D WS₂ nanopowders aqueous suspensions and exposure conditions are able to produce a similar negative impact on *S. cerevisiae* cells viability. The different components identified in the analyzed

commercial aqueous suspensions (1T'-WS₂, 2H-WS₂, WO₃, and sulphonyl groups), might have a role on their negative impact in yeast, which might be due to a mixture toxicity effect or through the action of one of the components identified. In particular, the antifungal properties of SO₂ are well known (KING et al., 1981).

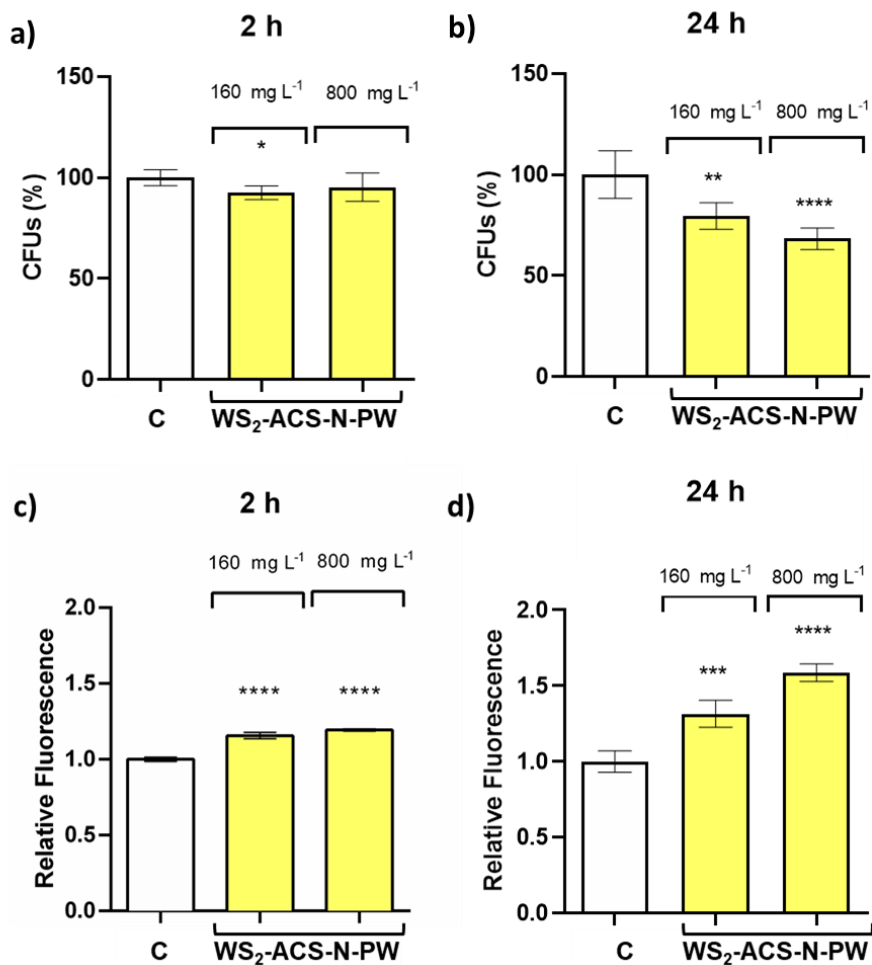


Figure 8: CFUs and ROS determination of *S. cerevisiae* cells exposed to 160 and 800 mg L⁻¹ of WS₂-ACS-N-PW, during 2 and 24 h. The reported values are the averages of two independent experiments per culture condition. Differences were established using a One-way ANOVA followed by Dunnett *post hoc* test to compare every mean with the control, and

considered significant at $P \leq 0.05$. * $P \leq 0.05$, ** $P \leq 0.01$, *** $P \leq 0.001$, **** $P \leq 0.0001$.

Conclusions

The results obtained in the present work reveal the physico-chemical properties and the potential toxicity of commercial 2D WS₂ aqueous suspensions when interacting with distinct eukaryotic organisms, showing differences in function of the biological system exposed. Analysing the stoichiometry and structure of the nanomaterials it has been revealed that the particles are primarily monolayers, and they are composed by a combination of 1T'-WS₂, 2H-WS₂, WO₃ and SO₂ species. Toxicity analyses on human cells showed that both aqueous 2D WS₂ suspensions have not the ability to impact on their viability, and a small capacity to induce oxidative stress. The viability of *S. cerevisiae* was reduced in the presence of the nanomaterials after long exposure times, although their ability to trigger ROS production in this organism was very low. Additionally, the obtained results indicated that the same concentrations of aqueous suspensions prepared with dry 2D WS₂ nanopowders, employing comparable exposure conditions, are able to produce a similar toxicity impact on *S. cerevisiae* cells.

Conflict of Interest

The authors declare that they have no conflict of interests.

Author contributions

Brixhilda Domi: Investigation, Formal analysis, Writing - Original Draft - Review & Editing.

Kapil Bhorkar: Investigation, Formal analysis, Writing - Review & Editing.

Carlos Rumbo: Investigation, Formal analysis, Review & Editing.

Labrini Sygellou: Investigation, Formal analysis, Review.

Sonia Martel Martin: Resources, Review & Editing.

Roberto Quesada: Supervision, Review & Editing.

Spyros N. Yannopoulos: Resources, Methodology, Supervision, Writing - Review & Editing.

Juan Antonio Tamayo-Ramos: Resources, Conceptualization, Methodology, Validation, Formal analysis, Investigation, Writing - Final Draft, Review & Editing, Supervision.

Corresponding Author

Juan Antonio Tamayo-Ramos

International Research Centre in Critical Raw Materials-ICCRAM,
Universidad de Burgos, Plaza Misael Banuelos s/n, 09001 Burgos, Spain

E-mail: jatramos@ubu.es; ja.tamayoramos@gmail.com

Funding Sources

This work was supported by the European Union's H2020 research and innovation programme under the Marie Skłodowska-Curie grant agreement N° 721642.

Acknowledgements

We would like to thank Rocío Barros for her invaluable support.

References

- Appel, J.H., Li, D.O., Podlevsky, J.D., Debnath, A., Green, A.A., Wang, Q.H., Chae, J., 2016. Low Cytotoxicity and Genotoxicity of Two-Dimensional MoS₂ and WS₂. *ACS Biomater. Sci. Eng.* 2, 361–367. <https://doi.org/10.1021/acsbiomaterials.5b00467>
- Berkdemir, A., Gutiérrez, H.R., Botello-Méndez, A.R., Perea-López, N., Elías, A.L., Chia, C.I., Wang, B., Crespi, V.H., López-Urías, F., Charlier, J.C., Terrones, H., Terrones, M., 2013. Identification of individual and few layers of WS₂ using Raman Spectroscopy. *Sci. Rep.* 3, 1–8. <https://doi.org/10.1038/srep01755>
- Braconi, D., Bernardini, G., Santucci, A., 2016. *Saccharomyces cerevisiae* as a model in ecotoxicological studies: A post-genomics perspective. *J. Proteomics* 137, 19–34. <https://doi.org/10.1016/j.jprot.2015.09.001>
- Choi, W., Choudhary, N., Han, G.H., Park, J., Akinwande, D., Lee, Y.H., 2017. Recent development of two-dimensional transition metal dichalcogenides and their applications. *Mater. Today*. <https://doi.org/10.1016/j.mattod.2016.10.002>
- Corazzari, I., Deorsola, F.A., Gulino, G., Aldieri, E., Bensaid, S., Turci, F., Fino, D., 2014. Hazard assessment of W and Mo sulphide nanomaterials for automotive use. *J. Nanoparticle Res.* <https://doi.org/10.1007/s11051-014-2401-7>
- Domi, B., Bhorkar, K., Rumbo, C., Sygellou, L., Yannopoulos, S.N., Quesada, R., Tamayo-Ramos, J.A., 2020. Fate assessment of commercial

2D MoS₂ aqueous dispersions at physicochemical and toxicological level. *Nanotechnology* 31, 445101. <https://doi.org/10.1088/1361-6528/aba6b3>

Domi, B., Rumbo, C., García-Tojal, J., Elena Sima, L., Negroiu, G., Tamayo-Ramos, J.A., 2019. Interaction Analysis of Commercial Graphene Oxide Nanoparticles with Unicellular Systems and Biomolecules. *Int. J. Mol. Sci.* 21, 205. <https://doi.org/10.3390/ijms21010205>

Eftekhari, A., 2017. Tungsten Dichalcogenides (WS₂, WSe₂, and WTe₂): Materials Chemistry and Applications. *J. Mater. Chem. A* 18299–18325. <https://doi.org/10.1039/C7TA04268J>

Holmström, K.M., Finkel, T., 2014. Cellular mechanisms and physiological consequences of redox-dependent signalling. *Nat. Rev. Mol. Cell Biol.* 15, 411–421. <https://doi.org/10.1038/nrm3801>

Ivask, A., Kurvet, I., Kasemets, K., Blinova, I., Aruoja, V., Suppi, S., Vija, H., Kakinen, A., Titma, T., Heinlaan, M., Visnapuu, M., Koller, D., Kisand, V., Kahru, A., 2014. Size-dependent toxicity of silver nanoparticles to bacteria, yeast, algae, crustaceans and mammalian cells in vitro. *PLoS One* 9. <https://doi.org/10.1371/journal.pone.0102108>

Jeevanandam, J., Barhoum, A., Chan, Y.S., Dufresne, A., Danquah, M.K., 2018. Review on nanoparticles and nanostructured materials: History, sources, toxicity and regulations. *Beilstein J. Nanotechnol.* <https://doi.org/10.3762/bjnano.9.98>

Katz, A., Redlich, M., Rapoport, L., Wagner, H.D., Tenne, R., 2006. Self-lubricating coatings containing fullerene-like WS₂ nanoparticles for

orthodontic wires and other possible medical applications. *Tribol. Lett.* 21, 135–139. <https://doi.org/10.1007/s11249-006-9029-4>

KING, A.D., PONTING, J.D., SANSHUCK, D.W., JACKSON, R., MIHARA, K., 1981. Factors Affecting Death of Yeast by Sulfur Dioxide. *J. Food Prot.* 44, 92–97. <https://doi.org/10.4315/0362-028x-44.2.92>

Kwolek-Mirek, M., Zadrag-Tecza, R., 2014. Comparison of methods used for assessing the viability and vitality of yeast cells. *FEMS Yeast Res.* 14, 1068–1079. <https://doi.org/10.1111/1567-1364.12202>

Lanone, S., Rogerieux, F., Geys, J., Dupont, A., Maillot-Marechal, E., Boczkowski, J., Lacroix, G., Hoet, P., 2009. Comparative toxicity of 24 manufactured nanoparticles in human alveolar epithelial and macrophage cell lines. *Part. Fibre Toxicol.* 6, 1–12. <https://doi.org/10.1186/1743-8977-6-14>

Liu, X., Duan, G., Li, W., Zhou, Z., Zhou, R., 2017. Membrane destruction-mediated antibacterial activity of tungsten disulfide (WS₂). *RSC Adv.* 7, 37873–37880. <https://doi.org/10.1039/c7ra06442j>

Liu, Z., Li, N., Su, C., Zhao, H., Xu, L., Yin, Z., Li, J., Du, Y., 2018. Colloidal synthesis of 1T' phase dominated WS₂ towards durable electrocatalysis. *Nano Energy* 50, 176–181. <https://doi.org/10.1016/j.nanoen.2018.05.019>

Lv, R., Robinson, J.A., Schaak, R.E., Sun, D., Sun, Y., Mallouk, T.E., Terrones, M., 2015. Transition metal dichalcogenides and beyond: Synthesis, properties, and applications of single- and few-layer nanosheets. *Acc. Chem. Res.* 48, 56–64. <https://doi.org/10.1021/ar5002846>

- Marletta, G., Iacona, F., 1996. Chemical selectivity and energy transfer mechanisms in the radiation-induced modification of polyethersulphone. *Nucl. Instruments Methods Phys. Res. Sect. B Beam Interact. with Mater. Atoms* 116, 246–252. [https://doi.org/10.1016/0168-583X\(96\)00041-9](https://doi.org/10.1016/0168-583X(96)00041-9)
- Mell, J.C., Burgess, S.M., 2002. Yeast as a Model Genetic Organism.
- Michels, C.A., 2003. *Saccharomyces cerevisiae* as a Genetic Model Organism. *Genet. Tech. Biol. Res.* 6, 1–22. <https://doi.org/10.1002/0470846623.ch1>
- Pardo, M., Shuster-Meiseles, T., Levin-Zaidman, S., Rudich, A., Rudich, Y., 2014. Low Cytotoxicity of Inorganic Nanotubes and Fullerene-Like Nanostructures in Human Bronchial Epithelial Cells: Relation to Inflammatory Gene Induction and Antioxidant Response. *Environ. Sci. Technol.* 48. <https://doi.org/10.1021/es500065z>
- Peng, Q., Huo, D., Li, H., Zhang, B., Li, Y., Liang, A., Wang, H., Yu, Q., Li, M., 2018. ROS-independent toxicity of Fe₃O₄ nanoparticles to yeast cells: Involvement of mitochondrial dysfunction. *Chem. Biol. Interact.* 287, 20–26. <https://doi.org/10.1016/j.cbi.2018.03.012>
- Perrone, G.G., Tan, S.X., Dawes, I.W., 2008. Reactive oxygen species and yeast apoptosis. *Biochim. Biophys. Acta - Mol. Cell Res.* 1783, 1354–1368. <https://doi.org/10.1016/j.bbamcr.2008.01.023>
- Ratoi, M., Niste, V.B., Walker, J., Zekonyte, J., 2013. Mechanism of action of WS₂ lubricant nanoadditives in high-pressure contacts. *Tribol. Lett.* 52, 81–91. <https://doi.org/10.1007/s11249-013-0195-x>

Repetto, G., del Peso, A., Zurita, J.L., 2008. Neutral red uptake assay for the estimation of cell viability/cytotoxicity. *Nat. Protoc.* 3, 1125–31. <https://doi.org/10.1038/nprot.2008.75>

Sousa, C.A., Soares, H.M.V.M., Soares, E. V., 2018. Nickel Oxide (NiO) Nanoparticles Induce Loss of Cell Viability in Yeast Mediated by Oxidative Stress. *Chem. Res. Toxicol.* 31, 658–665. <https://doi.org/10.1021/acs.chemrestox.8b00022>

Sousa, C.A., Soares, H.M.V.M., Soares, E. V, 2019. Metal(loid) oxide (Al₂O₃, Mn₃O₄, SiO₂ and SnO₂) nanoparticles cause cytotoxicity in yeast via intracellular generation of reactive oxygen species. *Appl. Microbiol. Biotechnol.* 103, 6257–6269. <https://doi.org/10.1007/s00253-019-09903-y>

Tan, S.J.R., Abdelwahab, I., Ding, Z., Zhao, X., Yang, T., Loke, G.Z.J., Lin, H., Verzhbitskiy, I., Poh, S.M., Xu, H., Nai, C.T., Zhou, W., Eda, G., Jia, B., Loh, K.P., 2017. Chemical Stabilization of 1T' Phase Transition Metal Dichalcogenides with Giant Optical Kerr Nonlinearity. *J. Am. Chem. Soc.* 139, 2504–2511. <https://doi.org/10.1021/jacs.6b13238>

Teo, W.Z., Chng, E.L.K., Sofer, Z., Pumera, M., 2014. Cytotoxicity of Exfoliated Transition-Metal Dichalcogenides (MoS₂, WS₂, and WSe₂) is Lower Than That of Graphene and its Analogues. *Chem. - A Eur. J.* 20, 9627–9632. <https://doi.org/10.1002/chem.201402680>

Visalli, G., Bertuccio, M.P., Iannazzo, D., Piperno, A., Pistone, A., Di Pietro, A., 2015. Toxicological assessment of multi-walled carbon nanotubes on A549 human lung epithelial cells. *Toxicol. Vitro.* 29, 352–362. <https://doi.org/10.1016/J.TIV.2014.12.004>

Yuan, P., Zhou, Q., Hu, X., 2020. WS2 Nanosheets at Noncytotoxic Concentrations Enhance the Cytotoxicity of Organic Pollutants by Disturbing the Plasma Membrane and Efflux Pumps. *Environ. Sci. Technol.* 54, 1698–1709. <https://doi.org/10.1021/acs.est.9b05537>

Yuan, P., Zhou, Q., Hu, X., 2018. The Phases of WS2 Nanosheets Influence Uptake, Oxidative Stress, Lipid Peroxidation, Membrane Damage, and Metabolism in Algae. *Environ. Sci. Technol.* 52, 13543–13552. <https://doi.org/10.1021/acs.est.8b04444>

Chapter 4

Boron nitride nanosheets

Low toxicity of commercial 2D boron nitride nanopowder and nanoplatelets towards eukaryotic cellular models

Brixhilda Domi¹, Kapil Bhorkar^{2,3}, Carlos Rumbo¹, Labrini Sygellou², Spyros N. Yannopoulos², Rocio Barros¹, Roberto Quesada,⁴ Juan Antonio Tamayo-Ramos¹

¹ International Research Centre in Critical Raw Materials-ICCRAM, Universidad de Burgos, Plaza Misael Banuelos s/n, 09001 Burgos, Spain

² Foundation for Research and Technology Hellas – Institute of Chemical Engineering Sciences (FORTH/ICE-HT), P.O. Box 1414, GR-26504, Rio-Patras, Greece

³ Univ Rennes, CNRS, ISCR - UMR 6226, F-35000 Rennes, France

⁴ Departamento de Química, Facultad de Ciencias, Universidad de Burgos, 09001, Burgos, Spain

* Corresponding author:

Juan Antonio Tamayo-Ramos: jatramos@ubu.es Phone: +34 947 49 20 05

HIGHLIGHTS

Commercial 2D boron nitride samples with different lateral size were characterized

Raman and XPS spectra revealed commonalities and differences amongst the samples

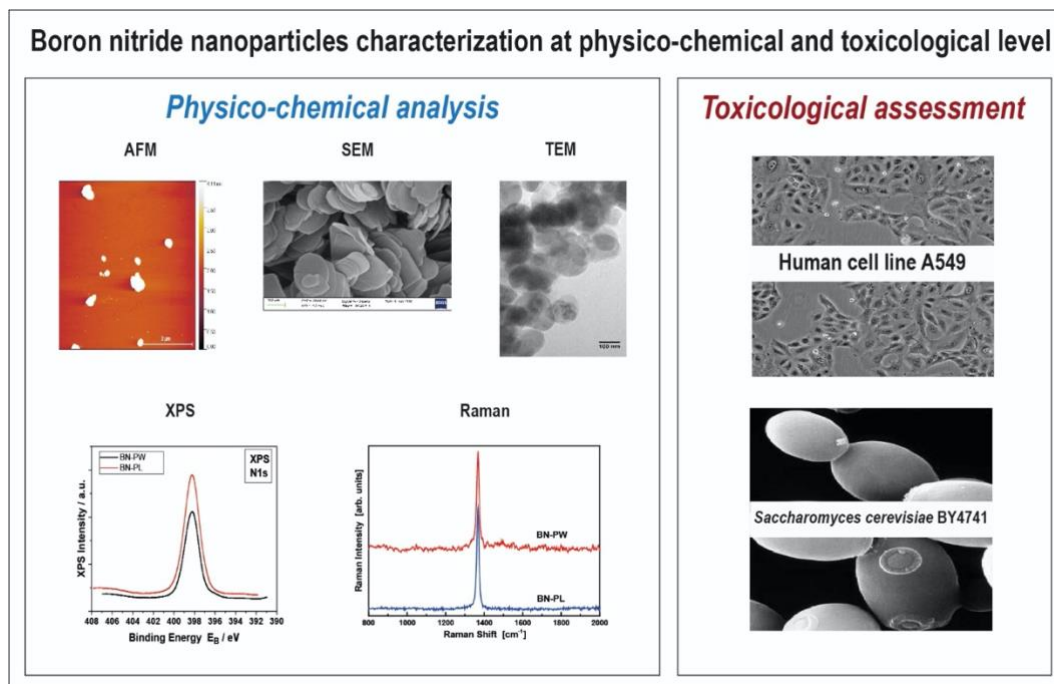
Both commercial samples showed no reduction on cellular vitality in A549 cells

Both samples had a very low impact on *Saccharomyces cerevisiae* vitality

ABSTRACT

Boron nitride (BN) nanomaterials have been increasingly explored for potential biological applications due to their two-dimensional layered structure similar to graphene. However, contradictory results have been reported in relation to their potential toxicological and environmental impact. Hence, in this work, we explore the physicochemical properties of two commercial 2D BN samples, namely BN-nanopowder (BN-PW) and BN-nanoplatelet (BN-PL), to identify possible alterations in the toxicological behavior in relation to the size and the shape of the particles selected and compare the biological responses of different cellular models. The possible toxicological effects of the selected 2D BN samples were investigated using adenocarcinomic human alveolar basal epithelial cells (A549 cells) and the unicellular fungus *Saccharomyces cerevisiae* as eukaryotic models for *in vitro* assays. In both cases, cellular viability assays and reactive oxygen species (ROS) determinations showed a very low cytotoxicity of the selected commercial products. Even at the highest concentration and exposure time, no major adverse effects on the percentage of living cells and oxidative stress production was observed in human cells and yeast. Our results, indicate no significant differences in the toxicological potential of BN-nanopowder and BN-nanoplatelets, representing safe products at the concentration and exposure tested for the prospective future applications in the biomedical and environmental field.

GRAPHICAL ABSTRACT



KEYWORDS

2D boron nitride; eukaryotic cellular model; nanotoxicity; cell viability; oxidative stress

INTRODUCTION

In recent years, the progress of nanotechnology has fuelled the design and manufacturing of novel engineered nanomaterials (ENM). In particular, different types of 2D nanomaterials have been investigated for a wide range of potential applications (Xu et al., 2013; Zhang, 2015). Amongst them, low dimensional boron nitride (BN) materials, have attracted the attention of the scientific community due to their promising properties, such as superb mechanical stiffness, high thermal conductivity, wide optical bandgap, strong ultraviolet emission, thermal stability and chemical inertness (Pakdel et al., 2012). BN consists of an equal number of boron and nitrogen atoms,

which are arranged differently depending on pressure and temperature conditions, giving rise to distinct crystalline forms (hexagonal, rhombohedral, diamond-like cubic and wurtzite).

The material is generally considered safe, being extensively used in the cosmetics industry, although not in its nanomaterial form (Czarniewska et al., 2019; Fiume et al., 2015). However, the potential toxicity of the nanomaterial forms is inadequately comprehended, with conflicting results reported in the scientific literature. Good biocompatibility has been reported for BN nanotubes, when exposed to HEK-293 human cells and freshwater planarians (Chen et al., 2009; Salvetti et al., 2015), while hollow BN nanospheres are able to induce apoptosis and inhibit the proliferation for both the androgen-sensitive LNCap and androgen-independent DU145 prostate cancer cells (Li et al., 2017).

As regards 2D BN nanomaterials, there is no clear consensus for their biocompatibility so far, but it seems to be dependent on cell type, dosage, and aspect ratio (Emanet et al., 2019). For instance, BN with sheet-like structure produced adverse effects on human hepatoma HepG2 cells, decreasing cellular viability, enhancing intracellular ROS production, inducing adverse effects in mitochondrial depolarization, and membrane integrity has been recently reported (Liu et al., 2017). Similarly, BN nanosheets changed from non-toxic to toxic towards SaOS2 cells when their diameters were reduced from the micro to nanometer range (Mateti et al., 2018). In a more recent study, *in vivo* and *in vitro* studies employing insect haemocytes, L929 mouse cells and human erythrocytes showed that hexagonal BN (h-BN) nanosheets functionalized with hydroxyl groups had

low cytotoxicity, although the behavior of the insect immunocompetent cells was found to be altered (Czarniewska et al., 2019).

The potential use of BN nanostructures as antimicrobial agents have recently attracted the interest of researchers as well, aiming to develop polymer based biomedical devices protected against bacterial proliferation. 2D BN nanoparticles incorporated in polyhydroxybutyrate chitosan matrixes behaved as antibacterial agents against multi drug resistant *Escherichia coli* and *Staphylococcus aureus* strains, while showing good biocompatibility towards immortalized human keratinocytes (HaCaT) cell lines (Mukheem et al., 2019). Similarly, BN flakes present in extruded low density polyethylene polymers displayed bactericidal effect when evaluated against *E. coli*, *S. aureus*, *Staphylococcus epidermidis*, and *Pseudomonas aeruginosa*, strains (Pandit et al., 2019). Experimental and theoretical approaches employing transmission electron microscopy and molecular dynamics simulations suggest that the hydrophobicity of BN nanosheets can play a relevant role in damaging both bacterial outer and inner membranes (Zhang et al., 2019).

The ability of BN nanosheets to exert antifungal effect is less known, although a recent work that investigated the activity of hBN nanoparticles against different bacterial species and *Candida* sp. M25 reported a low minimum inhibitory concentration and antibiofilm capacity towards the yeast strain (Kivanç et al., 2018). The present work aims to contribute to the understanding of the potential biocompatibility and antifungal properties of different BN nanoforms by assessing their physico-chemical properties and toxicological potential on adenocarcinomic human alveolar basal epithelial

cells (A549) as a potential inhalation target, and on the yeast *Saccharomyces cerevisiae*, as a well-established fungal model for toxicology studies.

MATERIALS AND METHODS

Materials and reagents

Chemicals employed were supplied by Sigma-Aldrich (Merck KGaA, Darmstadt, Germany) and Acros Organics (Thermo Fisher Scientific Inc., Madrid, Spain). BN nanopowders (BN-PW; ref 790532) and nanoplatelets (BN-PL; ref 900405) were purchased at Sigma-Aldrich®.

Atomic Force Microscopy and Transition Electron Microscopy

To perform and evaluate AFM analysis, all the BN samples were dropped on a mica surface from aqueous suspensions. Images were recorded in AC mode (tapping mode) with a CYPHER ES instrument from Asylum Research (Oxford Instruments), using silicon cantilevers AC160TS-R3 with aluminum reflex coating (Olympus) and tip radius <10 nm. The analysis was done using a set point of 500, 72mV, a drive amplitude of 791.16, a drive frequency of 268.639. Data acquisition and control was done with IGOR Pro 6.2 (Asylum Research). Images analysis was done with ARgyle software. AFM analysis was performed at the laboratory of instrumental techniques unit service from the University of Valladolid.

Raman Analysis

Raman spectra were excited by the 514.5 nm radiation emerging from an Ar ion laser. The laser light was focused by a 50x objective creating a

focusing area of 2-3 μm . The scattered light was collected by the same objective and analyzed using by the T-64000 (Jobin-Yvon) spectrometer operating at a spectral resolution of $\sim 2.0\text{ cm}^{-1}$. The Raman mode of Si single crystal at 520 cm^{-1} was used to calibrate the wavenumber scale of the spectra.

X-Ray photoelectron spectroscopy

The X-Ray photoelectron spectroscopy (XPS) measurements were performed in a UHV chamber ($P \sim 5 \times 10^{-10}$ mbar) equipped with a SPECS Phoibos 100-1D-DLD hemispherical electron analyzer and a non-monochromatized dual-anode Mg/Al x-ray source for XPS. The XP Spectra were recorded with MgKa at 1253.6 eV photon energy and an analyzer pass energy of 10 eV giving a Full Width at Half Maximum (FWHM) of 0.85 eV for Ag3d_{5/2} line. The analyzed area was a rectangle of 4x20mm². The atomic ratios were calculated from the intensity (peak area) of the XPS peaks weighted with the corresponding relative sensitivity factors (RSF), taking into account the energy analyzer transmission function. For spectra collection and treatment, the commercial software SpecsLab Prodigy (by Specs GmbH, Berlin) was used.

Electron Microscopies

High-resolution field-emission scanning electron microscope (FE-SEM) instrument (Zeiss, SUPRA 35VP) operating at 10 kV, and transmission electron microscope (TEM) analysis using a JEOL JEM-1011 high-resolution (HR) TEM coupled with a Gatan Erlangshen ES1000W camera, were employed to investigate the texture and morphology of the

commercially purchased BN nano-powders and nano-platelets were investigated. TEM analysis was performed at the advanced microscopy unit service from the University of Valladolid.

Assays in A549 Cells

For the toxicological evaluations using cell lines, the human alveolar carcinoma epithelial cell line A549 (ATCC, CCL-185) was utilized. Cells were grown in DMEM medium (Dulbecco's Modified Eagle Medium) supplemented with 10% fetal calf serum (FCS) and 1% penicillin/streptomycin in a humidified incubator at 37 °C in the presence of 5% CO₂.

A549 cells Neutral Red assay

Approximately 3×10^4 cells per well were seeded in 96 well plates and exposed to 20, 40, 80, and 160 mg L⁻¹ of the BN materials previously diluted in DMEM 1% FCS. After 24 hours of incubation with nanomaterials, cells were washed with DPBS (Dulbecco's Phosphate Buffered Saline) and incubated 2.5 h with 100 µL of the neutral red solution which was prepared as follows: neutral red stock (4 mg L⁻¹) was diluted 1:100 in treatment media, and incubated at 37 °C for 24 h before use covered from light. After the 2.5 h incubation, neutral red solution was discarded, cells were washed with DPBS and fixed with formaldehyde 4%. Subsequently, cells were washed again and a dye release solution (50% ethanol 96°, 49% distilled H₂O, and 1% acetic acid) was added to each well. After 10 min of moderate shaking, this solution was transferred to a new opaque 96-well plate, and

fluorescence was measured with a microplate reader (BioTek Synergy HT, excitation wavelength, 530/25; emission wavelength 645/40).

A549 cells ROS determination

To explore the production of intracellular reactive oxygen species (ROS) the 2,7-dichlorofluorescein diacetate (DCFH-DA) fluorescent dye was used. A549 cells were seeded in a 96 micro-well plate (around 3×10^4 cells per well) and labelled with 50 μM DCFH-DA in Hanks' Balanced Salt Solution (HBSS) for 30 min in the dark. Afterward, cells were washed once with HBSS, and different concentrations of the BN nanomaterials diluted in HBSS (from 20 to 40 mg L^{-1}) were added to each well. Fluorescence was measured with a microplate reader (BioTek Synergy HT, excitation wavelength, 530/25; emission wavelength 645/40) after 1 h of exposure.

Yeast culture

The *S. cerevisiae* BY4741 strain was grown and maintained in standard liquid and solid YPD medium (1% yeast extract, 1% yeast bacto-peptone, 2% glucose).

Yeast Colony forming units (CFUs) determination

S. cerevisiae cells were pre-grown on YPD medium until an O.D.600 nm = 1 was reached, and then they were exposed to 160 or 800 mg L^{-1} of either BN-PL or BN-PW in the same medium culture, or cultured non exposed (negative control), in 24-well plates (final volume of 1 mL). Subsequently, culture samples were obtained after 2 and 24 h of exposure to the nanomaterials. To determine CFUs after both exposure times, 100 μL of cells were diluted 10^4 times, in case of 2 hours exposure, and 10^5 times, in

case of 24 hours exposure, inoculated on solid YPD medium (6% agar) plates, and incubated at 30 °C, for 48 hours.

Yeast ROS assay

To investigate the intracellular levels of reactive oxygen species, the reagent CM-H₂DCFDA (General Oxidative Stress Indicator) was utilized, following a protocol similar to that reported by James *et al.* *S. cerevisiae* cells in the exponential phase were pelleted, washed with DPBS and incubated with CM-H₂DCFDA (7 μM) in DPBS at 30 °C and 185 rpm for 60 min. Subsequently, cells were washed, resuspended in YPD liquid medium and exposed to BN nanomaterials (160 and 800 mg L⁻¹) for 2 and 24 h. Then, cells were washed two times with DPBS, incubated 2 min in a solution containing AcLi (lithium acetate) 2M, and washed and incubated again for 2 min in a solution containing SDS (sodium dodecyl sulfate) (0.01%) and chloroform (0.4%). Finally, cells were pelleted and the supernatant was transferred to a black opaque 96-micro-well plate, where the fluorescence was measured using a microplate reader (Synergy-HT, BioTek) (excitation = 485; emission = 528).

Statistics

Statistical analysis data are presented as means ± SD. The one-way analysis of variance (ANOVA) was performed for multiple comparisons, followed by Dunnet *post hoc* test. Statistical tests were carried out using Prism 6.0 (GraphPad Prism, GraphPad Software, Inc.). *P* values ≤0.05 were considered to indicate statistical significance.

RESULTS AND DISCUSSION

Selection and Characterization of Commercial Boron Nitride

In the present study, commercial BN nanopowder (BN-PW) and nanoplatelets (BN-PL) supplied by Sigma-Aldrich® were selected. The characterization information provided by the supplier indicates an average particle size of <150 nm for BN-PW and a lateral size dimension of <1 micron for BN-PL. To confirm the provider descriptions, both products were subjected to AFM, SEM and TEM analyses, where a population of both types of nanoparticle as well as morphological features could be observed. As can be seen in Figure 1, AFM images of the two BN products showed the presence of possible aggregates with different shape and a significant population of particles with a lateral size distribution in the nanoscale range, with a round shape. Representative FE-SEM images (Figure 2) of the platelets and powders at two different magnifications revealed that the nanoparticles in both materials have comparable disk-like geometry, while TEM images (Figure 3) confirmed that BN-PW and BN-PL have a 2D platelet-like shape. The main difference among the two samples at morphological level was related to the diameter of the disk-like particles, which was observed to be of the order of 200-300 nm for BN-PL and 100-150 nm for BN-PW.

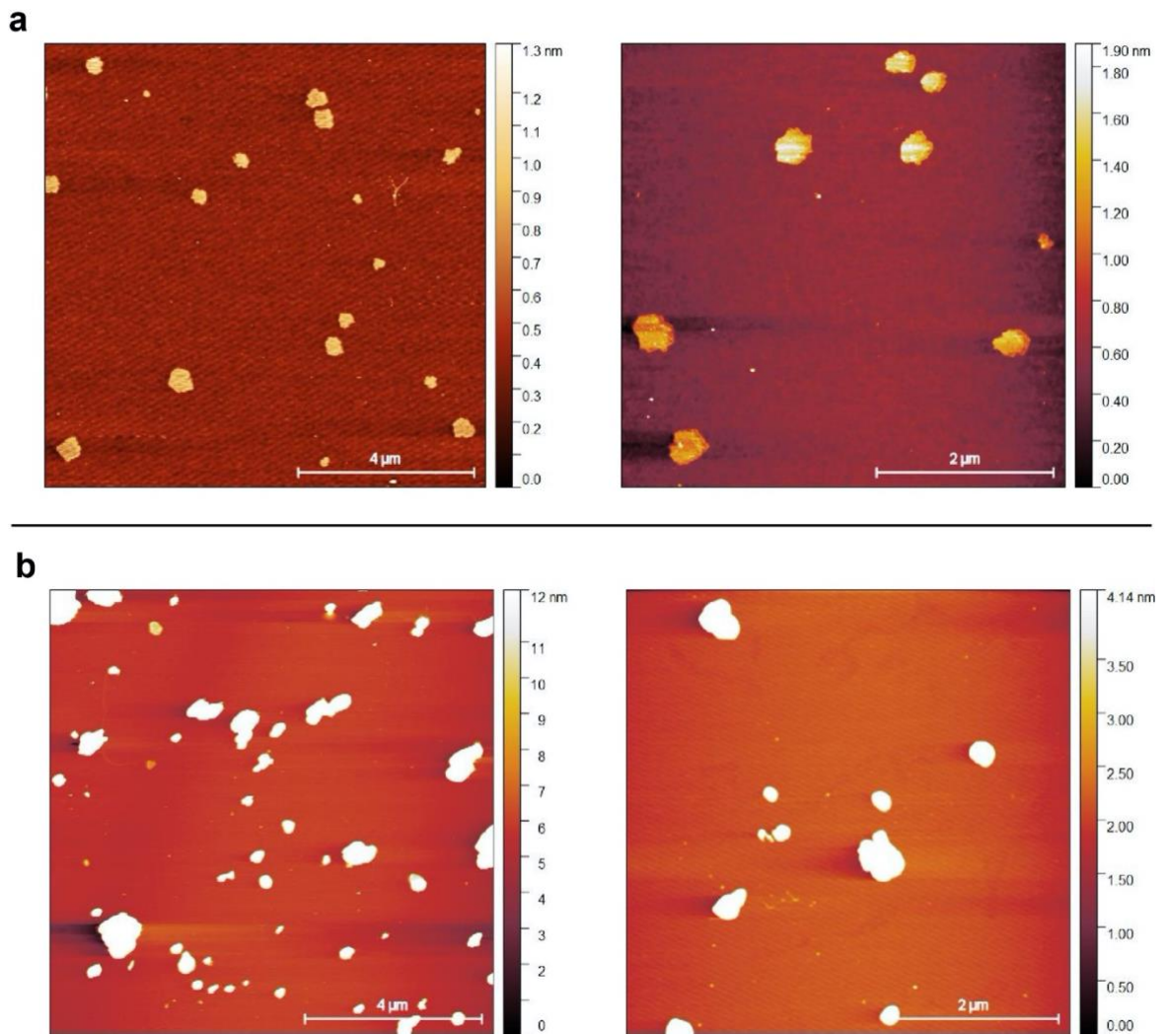


Figure 1: AFM images of BN-PW (a) and BN-PL (b). BN samples dispersions with a concentration of 20 mg L^{-1} were deposited by drop casting on a mica surface.

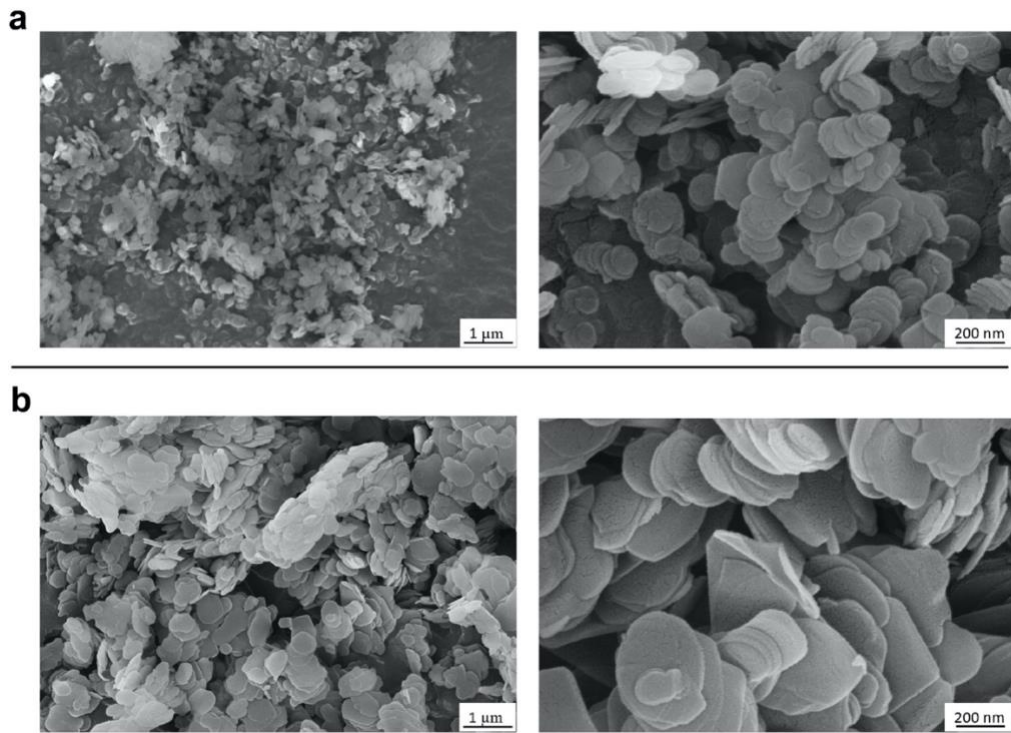


Figure 2: FE-SEM images of BN nanopowder (a) and BN nanoplatelets (b). Minute quantities of both samples were directly dropped on carbon tape.

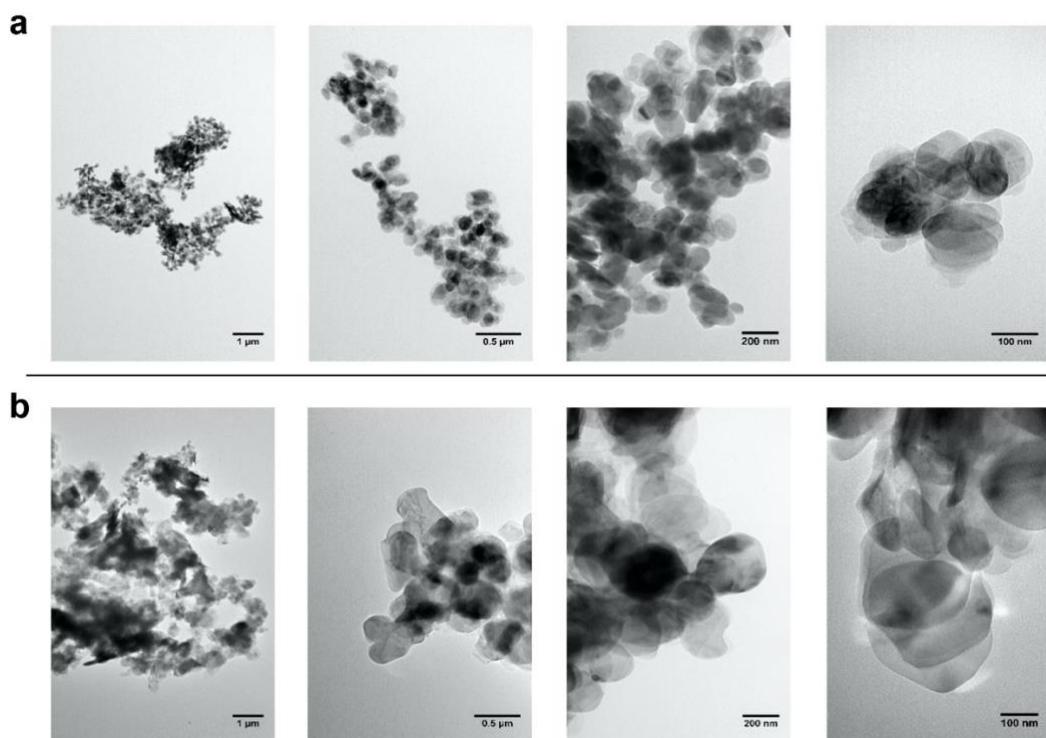


Figure 3: TEM images of BN nanopowder (a) and BN nanoplatelets (b). BN dispersions with a concentration of 20 mg L^{-1} were deposited by drop casting on carbon-coated copper grids.

XPS and RAMAN analysis

To analyze the surface chemistry (stoichiometry) and the atomic structure of the materials, XP and Raman spectra were collected and analyzed. Figure 4 shows the B1s and N1s XP spectra of BN-PW (black line) and BN-PL (red line) samples. For both samples, the B1s peak is centered at $190.6 \pm 0.1 \text{ eV}$ and N1s peak is located at $398.1 \pm 0.1 \text{ eV}$, which are in concordance with the binding energies of the hexagonal BN (h-BN) compound (Guimon et al., 1990). The atomic concentrations (%) of boron and nitrogen atoms in BN-PW (B: 51.00 ± 0.05 ; N: 49.00 ± 0.05) and BN-PL (B: 52.29 ± 0.06 ; N: 47.71 ± 0.06) correspond as well to those expected for BN materials.

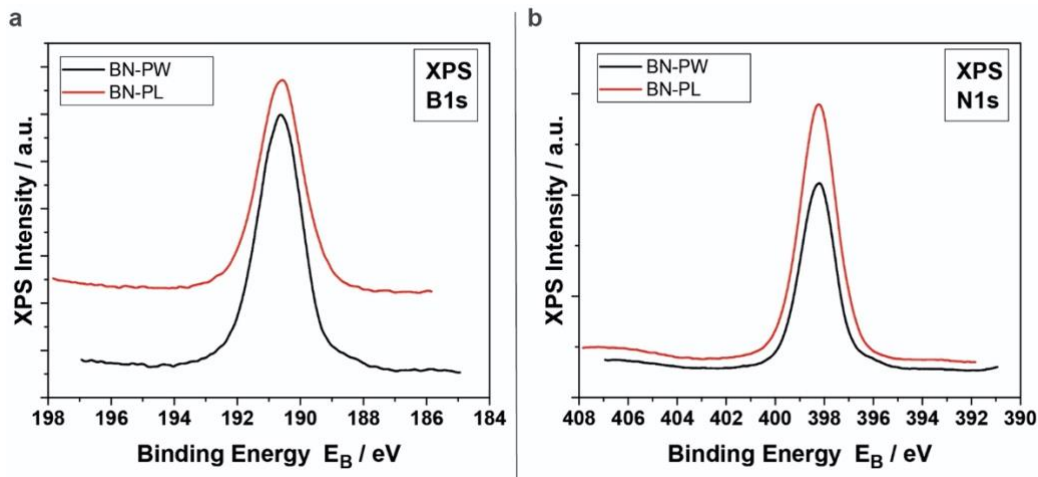


Figure 4: B1s (a) and N1s (b) XP spectra of BN-PW and BN-PL samples.

The Raman spectra shown in Figure 5 also demonstrate the existence of the h-BN crystal phase. Fitting the spectra with Lorentzian lines revealed that the E_{2g} mode is located at 1367.5 and 1367.7 cm^{-1} for the BN-PL (blue line) and BN-PW (red line), respectively. Their half width at half maximum are 12.7 (BN-PL) and 14.7 cm^{-1} (BN-PW). Based on a correlation by Nemanich *et al.* (Nemanich *et al.*, 1981), among the crystallite sizes and the Raman shift and width of the E_{2g} mode (the mode frequency shifted to higher energies and the width increased as the crystallite size decreased), the bandwidths of both BN samples indicate a slightly smaller crystallite size for BN-PW, which is in concordance to the observations in the performed microscopy analyses. The thickness dependence of the Raman spectra was first studied by Gorbachev *et al.* (Gorbachev *et al.*, 2010) who reported that the E_{2g} band of atomically thin BN flakes on Si/SiO₂ substrates shifts with thickness. The monolayer exhibits blue-shift of the order of $2\text{-}4$ cm^{-1} , whereas for more layers a red-shift was observed by $1\text{-}2$ cm^{-1} , in relation to the E_{2g} energy of the bulk h-BN. Contrasting results were reported by Li *et al.* (Li *et al.*, 2014), who found that mono- and few-layer h-BN mechanically

exfoliated flakes exhibit systematically blue shift in the E_{2g} mode in comparison to the bulk energy. More recently, Cai *et al.* (Cai et al., 2017) found that in the absence of interactions with the substrate, mono- and few-layer BN flakes show no measurable shift in relation to the bulk. They suggested that the observed Raman shift in such studies arises from strain induced by substrate. Based on these findings, and considering that the particles of BN in our case are not free standing, we conclude that the observed shift in BN-PW and BN-PL might be indicative of three-layers particles.

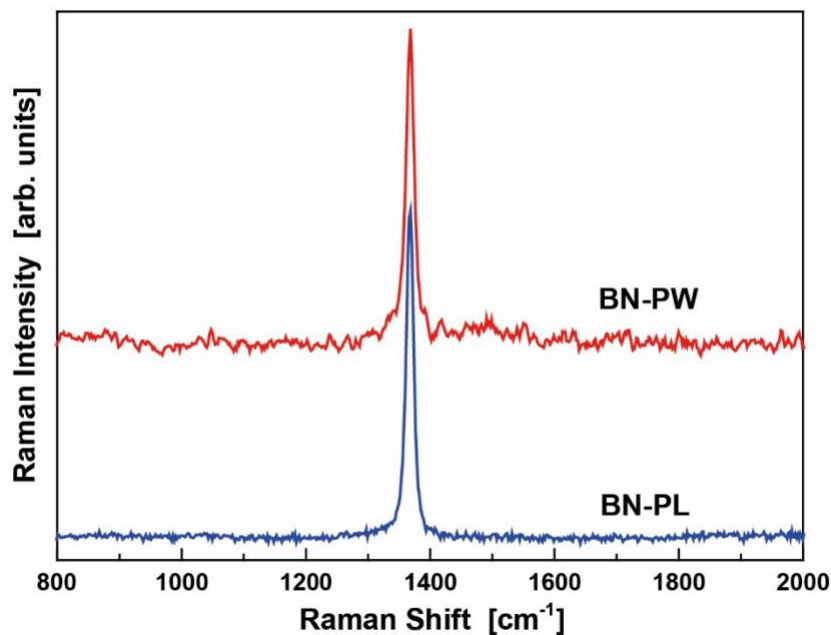


Figure 5: Raman spectra of BN powder and platelets

Toxicology assessment using adenocarcinoma A549 human cells

To assess the potential cytotoxic effects of commercial BN nanoforms, we selected the human lung carcinoma cell line (A549) as a cellular model to study possible adverse effects in human health via inhalation exposure of

nanoparticles (Visalli et al., 2015). Hence, cells were exposed to different concentrations (20, 40, 80, 160 mg L⁻¹) of both commercial BN-PW and BN-PL samples for a period of 24 hours. To determine the percentage of living cells after the BN exposure, we performed the Neutral Red assay, one of the most used protocols in nanotoxicological studies (Repetto et al., 2008). In the follow assay, the dye can enter inside the cells and it is adsorbed by the lysosomes in living cells, consenting the quantitative valuation of the number of alive cells after the exposure to the nanomaterials. As shown in Figure 6, after 24 h exposure to BN-PW and BN-PL, for all concentrations tested, the viability of the cells was not reduced, indicating the absence of cytotoxicity in the conditions tested towards the selected model. Although BN nanomaterials are generally considered highly biocompatible (Emanet et al., 2019), various recent reports indicate that 2D BN toxicity depends on cell type, dosage, and aspect ratio. For instance, Liu *et al.* observed that human hepatoma HepG2 cells viability was significantly reduced in the presence of 30 mg L⁻¹ BN sheet-like structured nanoparticles (Liu et al., 2017), while BN nanosheets changed from non-toxic to toxic towards SaOS2 cells when their diameters were reduced from the micro to nanometer range (Mateti et al., 2018). In a more recent study, *in vivo* and *in vitro* studies employing insect haemocytes, L929 mouse cells and human erythrocytes showed that h-BN nanosheets functionalized with hydroxyl groups had low cytotoxicity, although the behavior of the insect immunocompetent cells was found to be altered (Czarniewska et al., 2019).

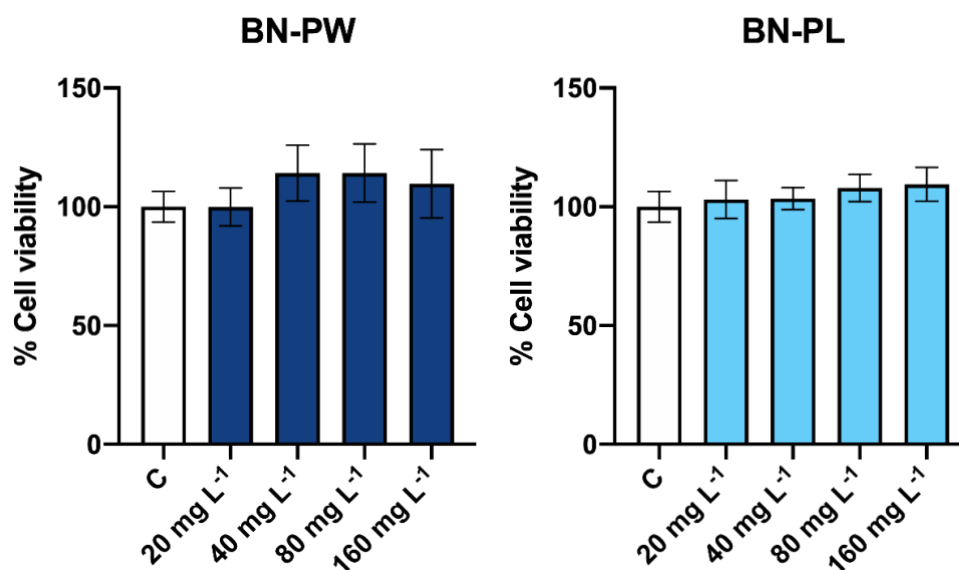


Figure 6: Viability of A549 cells (Neutral Red assay) treated with different concentrations of BN-PW (a) and BN-PL (b). Results are expressed as % of control (untreated cells). Data represent the mean (\pm standard deviation, SD) of two independent experiments. Differences were established using a One-way ANOVA followed by Dunnett *post hoc* test to compare every mean with the control, and considered significant at $P \leq 0.05$.

Despite the absence of cell death after exposure to selected BN samples, potential adverse effects on human cells following nanoparticles exposure could still occur due to the induction of oxidative stress (Domi et al., 2019). It is well known that many different nanoparticle types can induce significant levels of reactive oxygen species (ROS), resulting in cells inability to preserve normal physiological redox-regulated functions (Fu et al., 2014). Due to their high oxidation potential, the overproduction of intracellular ROS can result in the damage of biomolecules and organelles, leading to necrosis, apoptosis or even mutagenesis (Fu et al., 2014). Even though the molecular and cellular mechanisms correlated to the biotoxicity of NP-

induced ROS are still uncertain, it is important to investigate the oxidative stress production to further search the mechanisms related with the formation of ROS by NPs, which would specify more information to modify the physico-chemical features of BN nanomaterial to control the ROS generation. Therefore, to understand the possible presence of adverse effects at sublethal level, we investigated the possible intracellular increase of ROS. A549 cells were exposed to 20, and 40 mg L⁻¹ of BN-PW and BN-PL for 1 h incubation, and as displayed in Figure 7, the obtained results showed no ROS over production under the studied conditions.

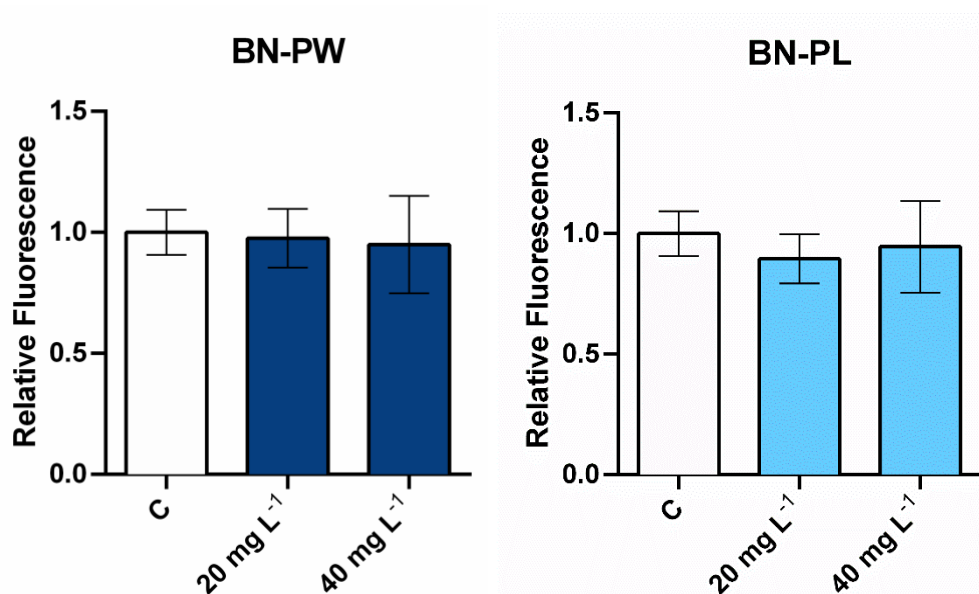


Figure 7: ROS production of A549 cells treated with different concentrations of BN-PW (a) and BN-PL (b). The reported values are expressed in arbitrary units and correspond to the averages of two biological replicates per culture condition. Data represent the mean of two independent experiments (\pm standard deviation, SD). Differences were established using a One-way ANOVA followed by Dunnett *post hoc* test to compare every mean with the control, and considered significant at $P \leq 0.05$.

Data available on oxidative stress production by BN nanosheets exposure in human cells is scarce, and the reported results, in the few available studies, are conflicting or difficult to compare. BN nanosheets in the concentration range 10-50 mg L⁻¹ did not induce ROS production in osteoblast cells exposed for 24 h (Rasel et al., 2015). However, in a more recent study, Mateti *et al.* reported a possible increase of ROS levels in osteoblast-like cells (SaOS2) exposed to BN nanosheets, although the nanomaterials concentration used was remarkably higher (1000 mg L⁻¹) (Mateti et al., 2018). Sheet-like BN nanoparticles also induced ROS formation in human hepatoma HepG2 cells exposed to relatively low concentrations (2-20 mg L⁻¹) (Liu et al., 2017). Similarly, in a more recent study, DU145 and PNT1A prostate cells were exposed to 22 to 176 mg L⁻¹ of BN nanoparticles, and an increase in ROS levels was observed in all cases (Emanet Ciofani et al., 2020).

Toxicology assessment using *Saccharomyces cerevisiae*

The yeast *S. cerevisiae* is an extensively used eukaryotic model to comprehend fundamental molecular processes in humans and other higher eukaryotes, being widely used as well for the toxicity assessment of substances, such as engineered nanomaterials (Braconi et al., 2016; Michels, 2003). Therefore, to evaluate the potential environmental impact of BN, we exposed yeast cells to two different concentrations (160 and 800 mg L⁻¹) and exposure times (2 and 24 h) of BN-PW and BN-PL, and subsequently their viability was assessed through colony forming units (CFUs) determination. As shown in Figure 8, only a small decrease on the

cell's viability was observed in the studied conditions after 24 h exposure. Although the antimicrobial properties of BN nanosheets has been explored, most of the studies performed have focused on bacteria, and data available on their antifungal potential is very low. A study performed by Kivanç *et al.* reported a MIC value of hBN nanoparticles against the yeast *Candida* sp. M25 of 3.25 mg L⁻¹ (Kivanç *et al.*, 2018). This result contrasts with our observations, as *S. cerevisiae* cells proliferation was only slightly reduced, even in the presence of 800 mg L⁻¹ of the nanomaterial. In a recent study, pristine BN films composed by spherical nanoparticles formed by nanosheets and nanoneedles did not show antifungal capacity against *Neurospora crassa* spores from different strains (Gudz *et al.*, 2020). Further studies are necessary to clarify the potential toxicity of BN nanomaterials against different fungal species.

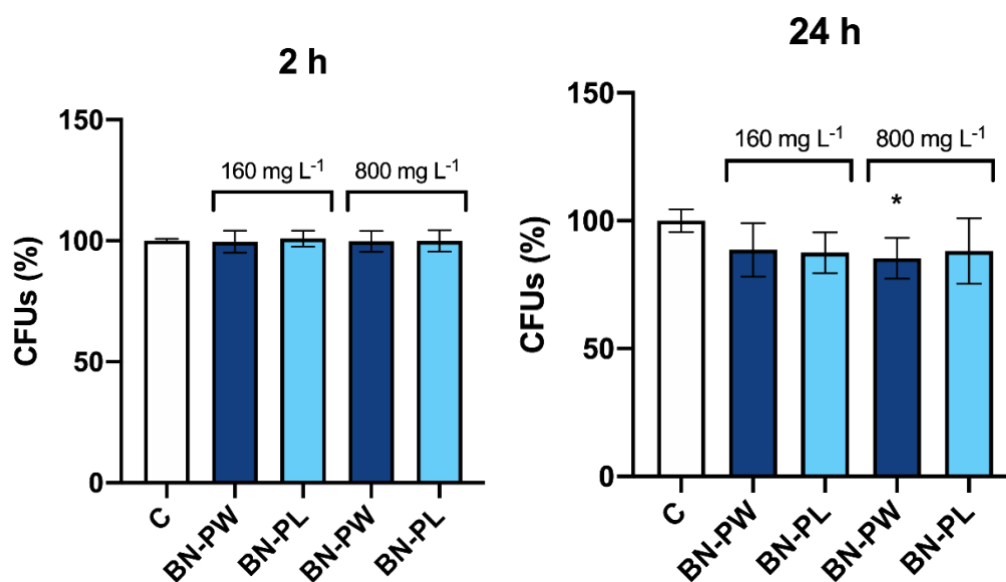


Figure 8: Colony forming units (CFUs) determination of *S. cerevisiae* cells exposed to 160 and 800 mg L⁻¹ of BN-PW and BN-PL during 2 hours (a) and 24 hours (b). The reported values are the averages of two independent

experiments. Differences were established using a One-way ANOVA followed by Dunnett *post hoc* test to compare every mean with the control, and considered significant at $P \leq 0.05$. * $P \leq 0.05$.

As mentioned above, the evaluation of the potential ROS induction in cells is performed in toxicology studies to study cell damage, which can end up in cell death and apoptosis. The accumulation of ROS in yeast usually originates from internal metabolic processes connected to cell respiration, however it can be similarly activated by environmental stress stimuli, such as nanoparticles exposure (Perrone et al., 2008; Suarez-Diez et al., 2020). In yeast species, including *S. cerevisiae*, the consequences of ROS accumulation are programmed cell death, autophagy, necrosis and upregulation of antioxidants mediated by complex transcriptional changes (Farrugia and Balzan, 2012). Hence, to evaluate whether BN-PW and BN-PL were able to induce oxidative stress in *S. cerevisiae*, cells growing at exponential phase were exposed to BN dispersion with concentration 160 and 800 mg L⁻¹ for 2 and 24 h. As shown in Figure 9, the oxidative stress levels of yeast cells exposed for 2 h to BN-PW and BN-PL were slightly higher than those observed in the negative control. Specifically, the fluorescence signal increased 0.2 and 0.4 times more in the BN-PW and BN-PL samples at 800 mg L⁻¹. However, after 24 h exposure no statistically augmented ROS production could be observed for both nanomaterials. The ROS induction caused by the presence of both BN nanoparticles samples was lower than that produced by other 2D nanomaterials, such as graphene oxide and molybdenum disulphide, when yeast cells were exposed to them in comparable conditions (Domi et al., 2020, 2019).

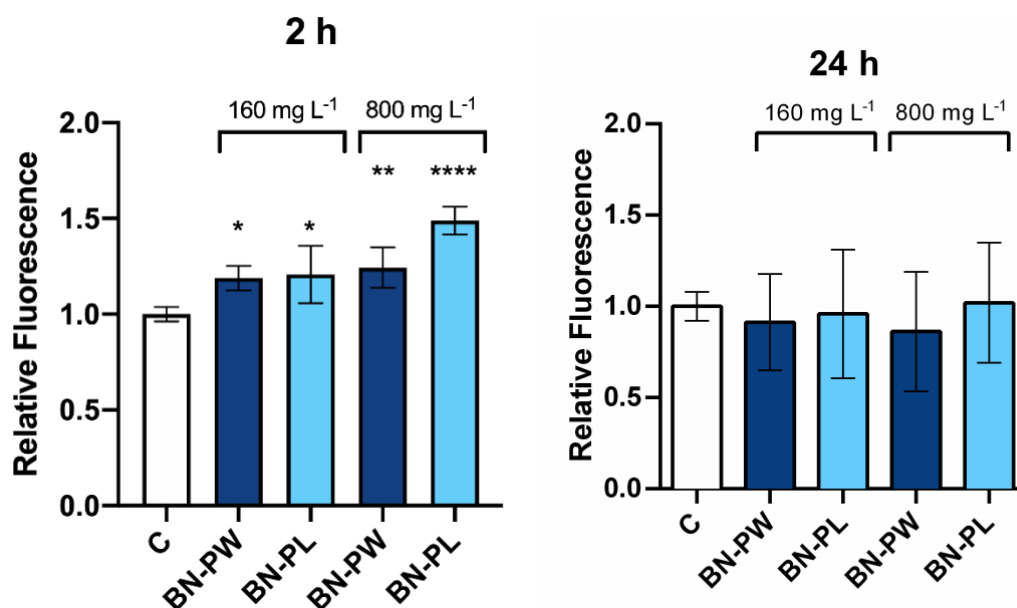


Figure 9: Oxidative stress (ROS) determination of *S. cerevisiae* cells exposed to 160 and 800 mg L⁻¹ of BN-PW and BN-PL during 2 hours (a) and 24 hours (b). The reported values are expressed in arbitrary units and correspond to the averages of two independent experiments. Differences were established using a One-way ANOVA followed by Dunnett *post hoc* test to compare every mean with the control, and considered significant at $P \leq 0.05$. * $P \leq 0.05$, ** $P \leq 0.01$, **** $P \leq 0.0001$.

Conclusion

The results obtained in the present work provide novel insights on the physico-chemical characteristics and the toxicological impact of commercial BN nanomaterials on different eukaryotic models. The morphological analysis of commercial nanopowder and nanoplatelets determined a lateral size in the nanoscale range for both products, while the analysis of their structure and stoichiometry through Raman spectroscopy and XPS revealed characteristics in concordance with those of hexagonal BN (h-BN).

The exposure analyses performed in human lung adenocarcinomic cells and the yeast *S. cerevisiae* indicate that both BN-PW and BN-PL have a low toxicological impact in the studied conditions. No reduction in cellular viability, nor oxidative stress production could be observed in exposed human cells, while minor effects were observed in exposed yeast cells. These results support the suitability of BN nanomaterials as 2D material to develop future biomedical and environmental applications.

Conflict of Interest

The authors declare that they have no conflict of interests.

AUTHOR INFORMATION

Corresponding Author

Juan Antonio Tamayo-Ramos

International Research Centre in Critical Raw Materials-ICCRAM,
Universidad de Burgos, Plaza Misael Banuelos s/n, 09001 Burgos, Spain

e-mail: ja.tamayoramos@gmail.com

Funding Sources

This work was supported by the European Union's H2020 research and innovation programme under the Marie Skłodowska-Curie grant agreement N° 721642.

ACKNOWLEDGMENTS

We would like to thank Dr. V. Dracopoulos (FORTH/ICE-HT) for recoding SEM images and Javier Gutierrez Reguera for his valuable contribution during the AFM analysis process.

References

- Braconi, D., Bernardini, G., Santucci, A., 2016. *Saccharomyces cerevisiae* as a model in ecotoxicological studies: A post-genomics perspective. *J. Proteomics* 137, 19–34. <https://doi.org/10.1016/j.jprot.2015.09.001>
- Cai, Q., Scullion, D., Falin, A., Watanabe, K., Taniguchi, T., Chen, Y., Santos, E.J.G., Li, L.H., 2017. Raman signature and phonon dispersion of atomically thin boron nitride. *Nanoscale* 9, 3059–3067. <https://doi.org/10.1039/c6nr09312d>
- Chen, X., Wu, P., Rouseas, M., Okawa, D., Gartner, Z., Zettl, A., Bertozzi, C.R., 2009. Boron nitride nanotubes are noncytotoxic and can be functionalized for interaction with proteins and cells. *J. Am. Chem. Soc.* 131, 890–891. <https://doi.org/10.1021/ja807334b>
- Czarniewska, E., Mrówczyńska, L., Jędrzejczak-Silicka, M., Nowicki, P., Trukawka, M., Mijowska, E., 2019. Non-cytotoxic hydroxyl-functionalized exfoliated boron nitride nanoflakes impair the immunological function of insect haemocytes in vivo. *Sci. Rep.* 9. <https://doi.org/10.1038/s41598-019-50097-0>
- Domi, B., Bhorkar, K., Rumbo, C., Sygellou, L., Yannopoulos, S.N., Quesada, R., Tamayo-Ramos, J.A., 2020. Fate assessment of

commercial 2D MoS₂ aqueous dispersions at physicochemical and toxicological level. *Nanotechnology* 31, 445101.

<https://doi.org/10.1088/1361-6528/aba6b3>

Domi, B., Rumbo, C., García-Tojal, J., Elena Sima, L., Negroiu, G., Tamayo-Ramos, J.A., 2019. Interaction Analysis of Commercial Graphene Oxide Nanoparticles with Unicellular Systems and Biomolecules. *Int. J. Mol. Sci.* 21, 205.

<https://doi.org/10.3390/ijms21010205>

Emanet Ciofani, M., Şen, Ö., Çulha, M., 2020. Hexagonal Boron Nitride Nanoparticles for Prostate Cancer Treatment. *ACS Appl. Nano Mater.* 3, 2364–2372. <https://doi.org/10.1021/acsanm.9b02486>

Emanet, M., Sen, Ö., Taşkin, I.Ç., Çulha, M., 2019. Synthesis, Functionalization, and Bioapplications of Two-Dimensional Boron Nitride Nanomaterials. *Front. Bioeng. Biotechnol.*

<https://doi.org/10.3389/fbioe.2019.00363>

Farrugia, G., Balzan, R., 2012. Oxidative stress and programmed cell death in yeast. *Front. Oncol.* <https://doi.org/10.3389/fonc.2012.00064>

Fiume, M.M., Bergfeld, W.F., Belsito, D. V., Hill, R.A., Klaassen, C.D., Liebler, D.C., Marks, J.G., Shank, R.C., Slaga, T.J., Snyder, P.W., Andersen, F.A., Gill, L.J., 2015. Safety Assessment of Boron Nitride as Used in Cosmetics. *Int. J. Toxicol.*

<https://doi.org/10.1177/1091581815617793>

Fu, P.P., Xia, Q., Hwang, H.M., Ray, P.C., Yu, H., 2014. Mechanisms of nanotoxicity: Generation of reactive oxygen species. *J. Food Drug*

Anal. <https://doi.org/10.1016/j.jfda.2014.01.005>

Gorbachev, R. V., Riaz, I., Nair, R.R., Jalil, R., Britnell, L., Belle, B.D., Hill, E.W., Novoselov, K.S., Watanabe, K., Taniguchi, T., Geim, A.K., Blake, P., 2010. Hunting for Monolayer Boron Nitride: Optical and Raman Signatures. *Small* 7, 465–468.
<https://doi.org/10.1002/sml.201001628>

Gudz, K.Y., Permyakova, E.S., Matveev, A.T., Bondarev, A. V., Manakhov, A.M., Sidorenko, D.A., Filippovich, S.Y., Brouchkov, A. V., Golberg, D. V., Ignatov, S.G., Shtansky, D. V., 2020. Pristine and Antibiotic-Loaded Nanosheets/Nanoneedles-Based Boron Nitride Films as a Promising Platform to Suppress Bacterial and Fungal Infections. *ACS Appl. Mater. Interfaces* 12, 42485–42498.
<https://doi.org/10.1021/acsami.0c10169>

Guimon, C., Gonbeau, D., Pfister-Guillouzo, G., Dugne, O., Guette, A., Naslain, R., Lahaye, M., 1990. XPS study of BN thin films deposited by CVD on SiC plane substrates. *Surf. Interface Anal.* 16, 440–445.
<https://doi.org/10.1002/sia.740160191>

Kıvanç, M., Barutca, B., Kopalal, A.T., Göncü, Y., Bostancı, S.H., Ay, N., 2018. Effects of hexagonal boron nitride nanoparticles on antimicrobial and antibiofilm activities, cell viability. *Mater. Sci. Eng. C* 91, 115–124. <https://doi.org/10.1016/j.msec.2018.05.028>

Li, L.H., Cervenka, J., Watanabe, K., Taniguchi, T., Chen, Y., 2014. Strong oxidation resistance of atomically thin boron nitride nanosheets. *ACS Nano* 8, 1457–1462. <https://doi.org/10.1021/nn500059s>

- Li, X., Wang, Xiupeng, Zhang, J., Hanagata, N., Wang, Xuebin, Weng, Q., Ito, A., Bando, Y., Golberg, D., 2017. Hollow boron nitride nanospheres as boron reservoir for prostate cancer treatment. *Nat. Commun.* 8, 1–12. <https://doi.org/10.1038/ncomms13936>
- Liu, S., Shen, Z., Wu, B., Yu, Y., Hou, H., Zhang, X.X., Ren, H.Q., 2017. Cytotoxicity and Efflux Pump Inhibition Induced by Molybdenum Disulfide and Boron Nitride Nanomaterials with Sheetlike Structure. *Environ. Sci. Technol.* 51, 10834–10842. <https://doi.org/10.1021/acs.est.7b02463>
- Mateti, S., Wong, C.S., Liu, Z., Yang, W., Li, Y., Li, L.H., Chen, Y., 2018. Biocompatibility of boron nitride nanosheets. *Nano Res.* 11, 334–342. <https://doi.org/10.1007/s12274-017-1635-y>
- Michels, C.A., 2003. *Saccharomyces cerevisiae* as a Genetic Model Organism. *Genet. Tech. Biol. Res.* 6, 1–22. <https://doi.org/10.1002/0470846623.ch1>
- Mukheem, A., Shahabuddin, S., Akbar, N., Miskon, A., Sarih, N.M., Sudesh, K., Khan, N.A., Saidur, R., Sridewi, N., 2019. Boron nitride doped polyhydroxyalkanoate/chitosan nanocomposite for antibacterial and biological applications. *Nanomaterials* 9. <https://doi.org/10.3390/nano9040645>
- Nemanich, R.J., Solin, S.A., Martin, R.M., 1981. Light scattering study of boron nitride microcrystals. *Phys. Rev. B* 23, 6348–6356. <https://doi.org/10.1103/PhysRevB.23.6348>
- Pakdel, A., Zhi, C., Bando, Y., Golberg, D., 2012. Low-dimensional boron

nitride nanomaterials. *Mater. Today*. [https://doi.org/10.1016/S1369-7021\(12\)70116-5](https://doi.org/10.1016/S1369-7021(12)70116-5)

Pandit, S., Gaska, K., Mokkaapati, V.R.S.S., Forsberg, S., Svensson, M., Kádár, R., Mijakovic, I., 2019. Antibacterial effect of boron nitride flakes with controlled orientation in polymer composites. *RSC Adv.* 9, 33454–33459. <https://doi.org/10.1039/c9ra06773f>

Perrone, G.G., Tan, S.X., Dawes, I.W., 2008. Reactive oxygen species and yeast apoptosis. *Biochim. Biophys. Acta - Mol. Cell Res.* 1783, 1354–1368. <https://doi.org/10.1016/j.bbamcr.2008.01.023>

Rasel, M.A.I., Li, T., Nguyen, T.D., Singh, S., Zhou, Y., Xiao, Y., Gu, Y.T., 2015. Biophysical response of living cells to boron nitride nanoparticles: uptake mechanism and bio-mechanical characterization. *J. Nanoparticle Res.* 17. <https://doi.org/10.1007/s11051-015-3248-2>

Repetto, G., del Peso, A., Zurita, J.L., 2008. Neutral red uptake assay for the estimation of cell viability/cytotoxicity. *Nat. Protoc.* 3, 1125–31. <https://doi.org/10.1038/nprot.2008.75>

Salvetti, A., Rossi, L., Iacopetti, P., Li, X., Nitti, S., Pellegrino, T., Mattoli, V., Golberg, D., Ciofani, G., 2015. In vivo biocompatibility of boron nitride nanotubes: Effects on stem cell biology and tissue regeneration in planarians. *Nanomedicine* 10, 1911–1922. <https://doi.org/10.2217/nnm.15.46>

Suarez-Diez, M., Porras, S., Laguna-Teno, F., Schaap, P.J., Tamayo-Ramos, J.A., 2020. Toxicological response of the model fungus

Saccharomyces cerevisiae to different concentrations of commercial graphene nanoplatelets. *Sci. Rep.* 10, 1–12.

<https://doi.org/10.1038/s41598-020-60101-7>

Visalli, G., Bertuccio, M.P., Iannazzo, D., Piperno, A., Pistone, A., Di Pietro, A., 2015. Toxicological assessment of multi-walled carbon nanotubes on A549 human lung epithelial cells. *Toxicol. Vitro.* 29, 352–362. <https://doi.org/10.1016/J.TIV.2014.12.004>

Xu, M., Liang, T., Shi, M., Chen, H., 2013. Graphene-like two-dimensional materials. *Chem. Rev.* 113, 3766–3798.

<https://doi.org/10.1021/cr300263a>

Zhang, H., 2015. Ultrathin Two-Dimensional Nanomaterials. *ACS Nano* 9, 9451–9469. <https://doi.org/10.1021/acsnano.5b05040>

Zhang, Y., Chan, C., Li, Z., Ma, J., Meng, Q., Zhi, C., Sun, H., Fan, J., 2019. Nanotoxicity of Boron Nitride Nanosheet to Bacterial Membranes. *Langmuir* 35, 6179–6187.

<https://doi.org/10.1021/acs.langmuir.9b00025>

Chapter 5

General Discussion and Conclusion

General Discussion

With so many applications of 2D nanomaterials, the increase in their production has been prolonged globally. Consequently, potentials for both environmental deposition of these layered nanomaterials and exposure of different living organisms are also growing and rises concerns about public and environmental health and safety. The reason of the intense research interest of the potential nanotoxicological impact of nanomaterials, it is mainly because of the innovative physical and chemical properties. As discussed in the previous chapters of this thesis, there are various physico-chemical properties of NPs that could affect the biological interaction such as size, shape, hydrophobicity, surface chemistry as charge, stability, agglomeration and aggregation and so on(nota). In addition, it is important to notice that the fate and effects of NPs might be influenced by both intrinsic (particle-related) factors, as well as factors related with the exposure matrix. Moreover, most of the works on 2D materials have concentrated on the basic synthesis and characterization of their fundamental behaviors (like photonic, electronic and catalytic). The study of biological and environmental interactions is necessary to understand and achieve development risks, which is equivalently important for biomedical and nonbiomedical fields. Therefore, the evaluation of the potential adverse effects of 2D nanomaterial family, should be an indispensable task along the development pathway for altogether new chemical- and material-based technologies, involving the 2D material field. Hence, due to the lack in the scientific literature of commercial NPs' biological effects related to specific

physico-chemical factors, we decided to deep our research using *in vitro* assays, to provide new scientific results for the product safety.

The aim of this PhD thesis was:

1. To investigate whether different commercial 2D materials (rather than lab made nanoparticles) could show adverse responses toward eukaryotic and prokaryotic cells;

2. To explore and deal with the complex physico-chemical factors (such as oxidation and degradation in water) as a potential factor influencing the biological responses;

3. To provide new insights of the possible differences in the toxicological potential of toward different cellular models, identifying cellular-type toxicity related.

To achieve these goals, we firstly focused on the physico-chemical characterization of the nanomaterials because of the importance of the investigation of the intrinsic proprieties of 2D materials. Hence, we decided to use several analysis such as:

AFM:

Atomic Force Microscopy, to determine the shape, size and size distribution of nanoparticles¹⁰⁹.

¹⁰⁹ Rao, A.; Schoenenberger, M.; Gnecco, E.; Glatzel, T.; Meyer, E.; Brändlin, D.; Scandella, L. Characterization of Nanoparticles Using Atomic Force Microscopy. *J. Phys. Conf. Ser.* 2007, 61 (1), 971–976.

TEM:

Transition Electron Microscopy, for studying the structure of nanomaterials and to determine quantitative measures of particle size, size homogeneity, morphological information and so on¹¹⁰.

Raman spectroscopy:

Vibrational spectroscopy utilized to categorize the vibrational, rotational, and other low-frequency modes of molecules in the TMDs samples used. Raman spectroscopy it has been used to identify the phases of the various 2D nanoparticles and which regions of the samples are amorphous or crystalline, and also the presence of other chemical elements such as impurities of the samples¹¹¹.

XPS:

X-ray photoelectron spectroscopy, a very efficient technique used to evaluate the electronic structure, elemental composition and oxidation state¹¹².

¹¹⁰ Asadabad, M. A.; Eskandari, M. J. Transmission Electron Microscopy as Best Technique for Characterization in Nanotechnology. *Synth. React. Inorganic, Met. Nano-Metal Chem.* 2015, 45 (3), 323–326.

¹¹¹ Koniakhin, S. V.; Utesov, O. I.; Terterov, I.; Siklitskaya, A.; Utesov, O. I.; Terterov, I. N.; Siklitskaya, A. V.; Solnyshkov, D.; Yashenkin, A. G. Raman Spectra of Crystalline Nanoparticles: Replacement for the Phonon Confinement Model Raman Spectra of Crystalline Nanoparticles View Project Drag of Electrons in Supported Graphene by Phonons View Project Novel Approach to Raman Spectra of Nanoparticles. *Artic. J. Phys. Chem. C* 2018, 122 (33), 19219–19229.

¹¹² Sublemontier, O.; Nicolas, C.; Aureau, D.; Patanen, M.; Kintz, H.; Liu, X.; Le Garrec, J.-L.; Robert, E.; Barreda, F.-A.; Etcheberry, A.; et al. X-Ray Photoelectron Spectroscopy of Isolated Nanoparticles. 2014.

FTIR spectra:

Fourier transform infrared spectroscopy, used to value insight into the diverse functional groups that are present in the commercial samples, by assessing the vibrational frequencies of the chemical bonds involved¹¹³.

ICP-MS:

Inductive coupled plasma mass spectroscopy, provides information on nanoparticle size and elemental composition in a single and rapid analysis. Moreover, leads to a particularly high signal to noise ratio for metal nanoparticles (i.e., low detection limits)¹¹⁴.

Once we determined the physicochemical factors of the commercial samples used on this PhD thesis, we selected several cellular models to identify possible alteration and dissimilarities in the adverse effects in relation to the cellular type used.

We decided to use both eukaryotic and prokaryotic cells, such as:

A549 cells

Adenocarcinomic human alveolar basal epithelial cells are a cell line developed through culturing of carcinogenic lung tissue in the explanted tumor of a 58-year-old caucasian male. A549 cells, are squamous, adherent and they grow as a monolayer attaching to the culture flask. This cell line is

¹¹³ López-Lorente, Á. I.; Mizaikoff, B. Recent Advances on the Characterization of Nanoparticles Using Infrared Spectroscopy. *TrAC - Trends in Analytical Chemistry*. Elsevier B.V. November 1, 2016, pp 97–106.

¹¹⁴ Laborda, F.; Bolea, E.; Jiménez-Lamana, J. Single Particle Inductively Coupled Plasma Mass Spectrometry for the Analysis of Inorganic Engineered Nanoparticles in Environmental Samples. *Trends in Environmental Analytical Chemistry*. Elsevier B.V. January 1, 2016, pp 15–23.

widely used as a type II pulmonary epithelial cell model for the evaluation of nanoparticles toxicity toward human health via inhalation exposure¹¹⁵.

Saccharomyces cerevisiae

The single-celled fungus *S. cerevisiae*, is one of the most intensively studied species of yeast as a eukaryotic model organism in several toxicological studies. *S. cerevisiae* cells shares several molecular pathways with mammalian cells, are easy to manipulate and non-expensive. Therefore, it is widely used also in the research of the molecular biology field¹¹⁶.

Vibrio fischeri

The Gram-negative *V. fischeri*, is a bioluminescent bacterium found in marine environments. This bacterium is used in several research studies such as the examination of microbial bioluminescence, bacterial-animal symbiosis, quorum sensing, and it is globally used as an ecotoxicological cellular model¹¹⁷.

Consequently, after the evaluation of the selected cellular models, we decide to focus on the toxicological assays. One of the crucial factors that can alter the biological results after the NPs exposure, is the use of several and different assay in the scientific literature. It is known that some assay

¹¹⁵ Cooper, J. R.; Abdullatif, M. B.; Burnett, E. C.; Kempell, K. E.; Conforti, F.; Tolley, H.; Collins, J. E.; Davies, D. E. Long Term Culture of the A549 Cancer Cell Line Promotes Multilamellar Body Formation and Differentiation towards an Alveolar Type II Pneumocyte Phenotype. *PLoS One* 2016, *11* (10).

¹¹⁶ Parapouli, M.; Vasileiadis, A.; Afendra, A. S.; Hatziloukas, E. *Saccharomyces Cerevisiae* and Its Industrial Applications. *AIMS Microbiology*. AIMS Press 2020, pp 1–31.

¹¹⁷ Visick, K. L.; Foster, J.; Doino, J.; McFall-Ngai, M.; Ruby, E. G. *Vibrio Fischeri* Lux Genes Play an Important Role in Colonization and Development of the Host Light Organ. *J. Bacteriol.* 2000, *182* (16), 4578–4586.

can interfere with NPs and as a consequence bringing false or non-representative results.

After a carefully study of the most used assays in nanoparticles toxicity, we selected the follow protocols:

Neutral Red:

The neutral red uptake assay is one of the most used tests in many biomedical and environmental research. This assay provides a quantitative estimation of the number of viable cells after the exposure with nanomaterials (as shown in Figure 8). In fact, living cells are able to absorb and bind the neutral red supravital dye in the lysosomes. The specific protocol is well described in the section “materials and methods” of the scientific articles present in this thesis¹¹⁸.

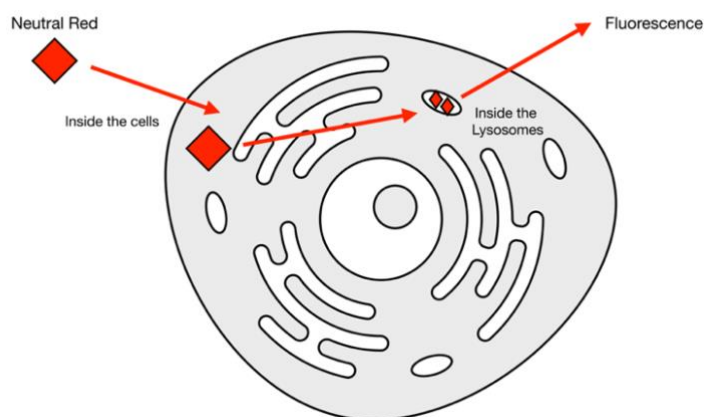


Figure 8: Schematic representation of the Neutral Red Assay.

¹¹⁸ Hu, W.; Culloty, S.; Darmody, G.; Lynch, S.; Davenport, J.; Ramirez-Garcia, S.; Dawson, K.; Lynch, I.; Doyle, H.; Sheehan, D. Neutral Red Retention Time Assay in Determination of Toxicity of Nanoparticles. *Mar. Environ. Res.* 2015, *111*, 158–161.

MTT:

Another well-known assay for assessing cell metabolic activity, is the colorimetric assay MTT (3-(4,5-dimethylthiazol-2-yl)-2,5-diphenyltetrazolium bromide) which is reduced by NAD(P)H-dependent cellular oxidoreductase enzymes into insoluble formazan in living cells (Figure 9). Tetrazolium dye assays are used to quantify cytotoxicity (loss of cellular viability) or cytostatic activity (quiescence) of possible drug agents and toxic nanomaterials¹¹⁹.

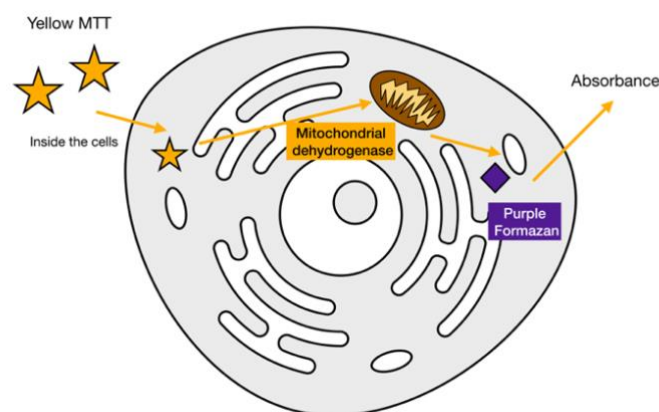


Figure 9: Schematic representation of the MTT Assay.

Flow cytometry:

Flow cytometry (FCM) (Figure 10) is globally technique used to identify and quantify physical and chemical characteristics of a population of cells or particles. For instance, it is also utilized to study the morphological changes

¹¹⁹Popescu, T.; Lupu, A. R.; Raditoiu, V.; Purcar, V.; Teodorescu, V. S. On the Photocatalytic Reduction of MTT Tetrazolium Salt on the Surface of TiO₂ Nanoparticles: Formazan Production Kinetics and Mechanism. *J. Colloid Interface Sci.* 2015, 457, 108–120.

(like blebbing, cell shrinkage and so on) during the activation of apoptosis pathway. For example, one important cellular change during the programmed cell death is the appearance of phosphatidylserine (PS) on the extracellular surface of cellular membrane (in healthy cells, PS is located on the cytoplasmic side). Hence, a fluorescein isothiocyanate (FITC) conjugated form of Annexin V is used to detect PS exposed, allowing the detections and measurement of apoptotic cells. However, due to membrane disintegration during necrosis, Annexin V can similarly bind to intracellularly located PS in necrotic cells¹²⁰.

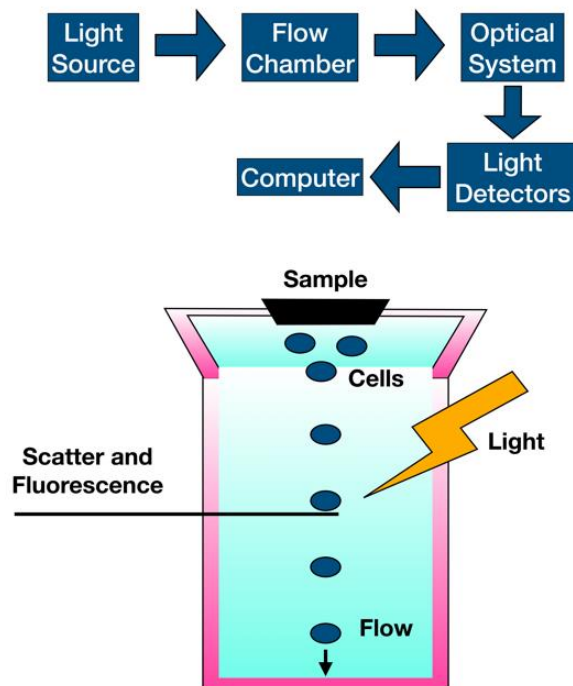


Figure 10: Schematic representation of the Flow cytometry Assay.

¹²⁰ Wlodkowic, D.; Skommer, J.; Darzynkiewicz, Z. Flow Cytometry-Based Apoptosis Detection. *Methods Mol. Biol.* 2009, 559, 19–32.

DCFH-DA assay:

One of the most widely used assay to detect intracellular ROS and oxidative stress, is the DCFH-DA probe. The probe is cell-permeable and intracellularly is hydrolyzed to the DCFH carboxylate anion, a non-fluorescent compound. In the presence of ROS, there is the oxidation of DCFH into a fluorescent product, dichlorofluorescein (DCF), which can be observed by numerous fluorescence-based techniques¹²¹ (Figure 11).

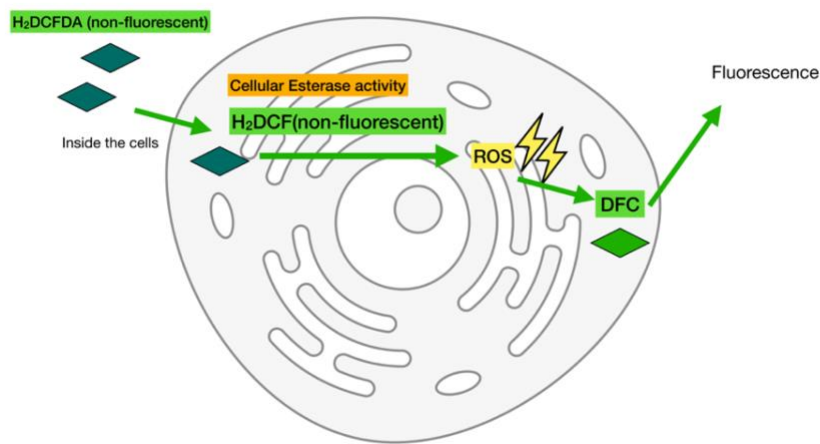


Figure 11: Schematic representation of the DCFH-DA Assay.

CFU:

The colony-forming unit (CFU) assay is generally used to evaluate the number of viable bacteria or fungal cells in a sample (Figure 12). Specifically, the cellular viability is defined as the ability to multiply via binary

¹²¹ randa, A.; Sequedo, L.; Tolosa, L.; Quintas, G.; Burello, E.; Castell, J. V.; Gombau, L. Dichloro-Dihydro-Fluorescein Diacetate (DCFH-DA) Assay: A Quantitative Method for Oxidative Stress Assessment of Nanoparticle-Treated Cells. *Toxicol. Vitro*. 2013, 27 (2), 954–963.

fission. A colony forming unit (CFU), present on an agar plate can be multiplied by the dilution factor to provide a CFU/ml result¹²².

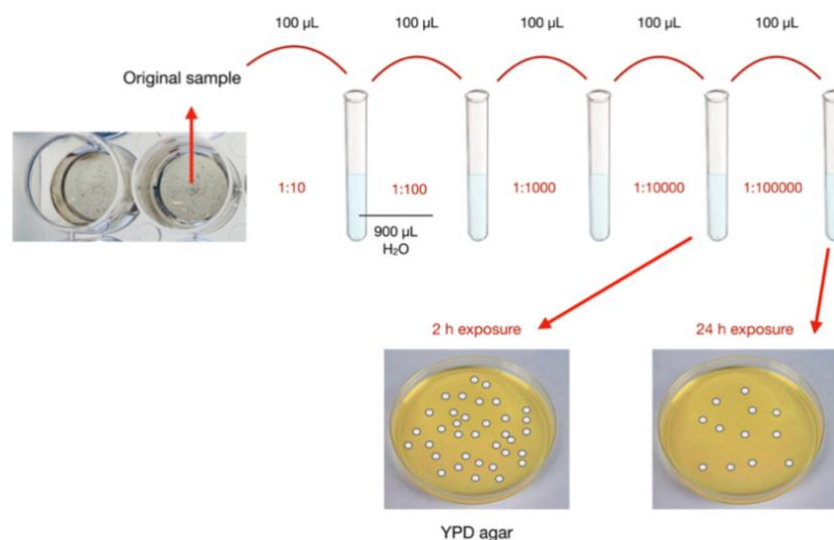


Figure 12: Schematic representation of the CFU Assay with yeast.

Bioluminescence inhibition:

Vibrio fischeri bioluminescence inhibition bioassay (VFBI) has been extensively used for the toxicity monitoring and ecotoxicological screening of diverse chemical substances. The bioluminescence (Figure 13) of the bacterium is directly proportional to the metabolic activity of the bacterial population and any inhibition (such as NPs exposure) of enzymatic activity can promote the decrease of light production¹²³.

¹²² Tran, K.; Green, E. Assessing Yeast Cell Survival Following Hydrogen Peroxide Exposure. *BIO-PROTOCOL* 2019, 9 (2).

¹²³ Abbas, M.; Adil, M.; Ehtisham-ul-Haque, S.; Munir, B.; Yameen, M.; Ghaffar, A.; Shar, G. A.; Asif Tahir, M.; Iqbal, M. *Vibrio Fischeri* Bioluminescence Inhibition Assay for Ecotoxicity Assessment: A Review. *Science of the Total Environment*. Elsevier B.V. June 1, 2018, pp 1295–1309.

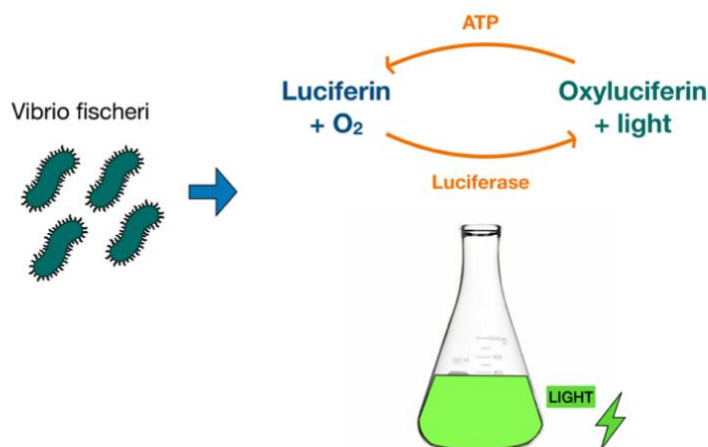


Figure 13: Schematic representation of the bioluminescence reaction.

In this PhD thesis, we focused on the possible adverse or compatible effects of commercial 2D nanomaterials, rather than laboratory made ones. In our days, the nanotoxicology is a branch of nanoscience, necessary to evaluate whether and to what extent the possible toxic effects of nanomaterial may have an impact to the environment and to human health. Specifically, the behavior of 2D nanoparticles in several environmental matrices is very complex and involves numerous processes and physico-chemical factor. For instance, the nanomaterials' properties are exclusive and distinctive from the conventional materials and the bulk counterpart. Moreover, properties such as (1) particle size, (2) solubility and (3) shape are known to affect the NP toxicity. For that reason, in Chapter 2, we focused on the study of one of the most famous nanomaterials: commercial graphene oxide (GO) and graphene oxide nanocolloids (GOC). The aim of our work was to investigate the ability of the selected commercial samples to interact with different unicellular systems such as human alveolar carcinoma epithelial cells, the yeast *Saccharomyces cerevisiae* and the bacteria *Vibrio fischeri*.

Moreover, we wanted to study the binding affinity of different microbial enzymes, like the α -l-rhamnosidase enzyme RhaB1 from the bacteria *Lactobacillus plantarum* and the AbG β -d-glucosidase from *Agrobacterium* sp. (strain ATCC 21400). To achieve these scientific purposes, we firstly characterized the nanomaterials using several techniques such as microscopy analyses using AFM and TEM instruments, showing similarity between both GO and GOC flakes, such as monolayer state and differences in the size range. Moreover, to investigate possible dissimilarities in their oxygen functional groups, we performed FTIR spectra of GO and GOC, and both nanomaterials showed to be very similar. In addition, we also have studied the possible of impurities such as trace metal in both the graphene derivatives samples, using the inductively coupled plasma mass spectrometry (ICP-MS). The presence of different metallic elements at low concentration was observed in both the samples analyzed, within significant differences in the concentration of some of the identified metals and metalloids. Hence, once the nanomaterials characterization was performed, we wanted to focus of the potential cytotoxic effects. We use eukaryotic cells (A549 cells and *S. cerevisiae*) and prokaryotic cells (*V. fischeri*), performing several cytotoxic assays to study the cell viability, oxidative stress, genotoxicity and luminescence inhibition. Furthermore, the protein binding affinity of the graphene derivatives at different oxidation levels was analyzed. The results obtained in this research article, indicate the higher capacity of GO than GOC to induce adverse effects such as significant oxidative stress production in both *S. cerevisiae* and human cells. Specifically, in A549 cells the viability after 24 h of exposure to 40, 80, and

160 mg L⁻¹ of GO and GOC was analyzed using the neutral red uptake and MTT assays. Consequently, a deeper analysis using flow cytometry with double staining of Annexin V-FTIC and propidium iodide (PI) was performed to evaluate the possible presence of apoptotic cells after the incubation with the two nanomaterials. The results related to the Neutral red assay indicate no negative effects on cellular viability in any of the concentrations tested for both GO and GOC. In contrast, the results obtained with MTT assay that A549 cells exposed to GOC present a minor decline in viability at the higher concentrations (less than 15% of decrease) and cells exposed to GO show no significant differences between controls of non-treated cells. Moreover, the quantification of the percentages of both apoptotic and necrotic cells using flow cytometry, indicated that cells treated with different GO concentrations (40, 80, 160 mg L⁻¹) revealed a constant 93-95% of viable cells, similar to the untreated control sample. However, in the case of GOC, the results obtained evidenced a stable 6-10% cell death. Hence, no significant apoptosis was induced from both the commercial samples. Nevertheless, in nanotoxicology studies, even if nanoparticles don't trigger cell death, it is possible to observe the production of oxidative stress. Hence, we also performed the DFCH-DA assay in A549 cells to investigate possible adverse effects related to the significant presence of reactive oxygen species. Thus, our results showed that ROS levels were significantly increased in after 1 hour of exposure to both nanoparticles, being this induction much higher in the case of the cells incubated with GO. Consequently, based on our results it has been evidenced that an acute GOs exposure of human cells can induce high oxidative stress levels,

however no significant decrease on cellular vitality was observed. Nevertheless, the possible adverse effects of the two commercial samples, could be different in relation to the cellular model used. For instance, the toxicological results in *S. cerevisiae* are very dissimilar to A549 cells exposed to GO and GOC in similar concentration. More specifically, the cellular viability of yeast cells was quantified using CFU assay where cells were exposed for 2 and 24 h at two concentration of 160 and 800 mg L⁻¹ to the nanomaterials. After 2h exposure, no significant differences in viability were observed in the selected conditions, except for the condition where a high GOC concentration was used. However, after 24 hours, viability issues could be observed after a longer exposure time. In case of GO, the nanomaterial reduced *S. cerevisiae* CFUs provoking a viability loss of 36.5% when the material was present at the lower concentration and 49.7% when the material was present at the higher concentration. In contrast, GOC showed no significant influence on the yeast viability at 160 mg L⁻¹, although the viability loss observed at the higher concentration was very similar for both nanomaterials. Moreover, we performed DCFH-DA assay also in yeast cells, to study the possible correlation of the cellular vitality decrease and possible oxidative stress production. We discovered that the oxidative stress levels were significantly increased in *S. cerevisiae* in the presence of both carbon nanoparticles. A similar adverse effect, was demonstrated even in the prokaryotic cellular model *V. fischeri*, where the light production of the bacterial cells was affected by the presence of both GO and GOC. Specifically, the bacteria luminescence decreased in the presence of a higher concentration of the nanomaterials, with significant difference

between both nanomaterial types. Particularly, the highest concentration of 800 mg L⁻¹ of GO induced a 100% of luminescence inhibition, already after 10 minutes of exposure. In contrast, the same concentration of GOC showed a significantly lower luminescence inhibition capacity at both exposure times of 10 and 30 minutes. Also, we have demonstrated the possible variances in the binding capacity with prokaryotic enzymes of both nanomaterials, being their maximum loading capacity different as well, in function of the enzyme tested. Specifically, the obtained result showed that the maximum loading capacity of GO and GOC was significantly higher for the α -rhamnosidase RhaB1. Hence, we have demonstrated that different enzymes could exhibit different enzyme loadings and stabilities when bound to graphene oxide due to differences in the charge status of their surface functional groups. Finally, in Table 1 it has been showed the representation of the significant results obtained in this research work.

Table 1: Schematic representation of toxicity of GO and GOC toward different unicellular systems.

Results - A549 cells	GO	GOC
Neutral Red	Not affected	Not affected
MTT	Not affected	Not affected
Flow cytometry	No significant apoptosis	6-10% cell death, irrespective of the administered dose
ROS	Significant ROS production in all concentration tested	Significant ROS production in all concentration tested

Results - Yeast	GO	GOC
CFU 2h	Not affected	Affected at 800 mg L ⁻¹ , slight decrease of cell viability
CFU 24h	Affected: ~37% cellular viability decreased at 160 mg L ⁻¹ and ~50% at 800 mg L ⁻¹	Not affected at 160 mg L ⁻¹ Similarly affected to GO at 800 mg L ⁻¹
ROS 2h	Significant oxidative stress	Significant oxidative stress
ROS 24h	Significant ROS production in all concentration tested	Significant ROS production in all concentration tested

Results – <i>V. fischeri</i>	GO	GOC
Luminescence inhibition 10 minutes	100% inhibition at 800 mg L ⁻¹	~ 30% inhibition at 800 mg L ⁻¹
Luminescence inhibition 30 minutes	100% inhibition at 800 mg L ⁻¹	~ 40% inhibition at 800 mg L ⁻¹

Due to the increasing use of Transition Metal Dichalcogenides (TMDs) in several industry fields, in chapter 3, we evaluated the potential toxicity of the rising star nanomaterials Molybdenum Disulfide (MoS₂) and Tungsten Disulfide (WS₂). Firstly, we focused on the evaluation of adverse effects of several commercial MoS₂ nanoflakes with different lateral size and different oxidation stage, using similar eukaryotic cells and cytotoxic assays performed as well in the GO and GOC work. Principally, we performed several characterization analysis to understand the physico-chemical properties of the selected MoS₂ nanoparticles and the implications in the

potential biological responses. To achieve this goal, different suspension of micro and nano MoS₂ (old sample in a higher oxidation stage and fresh sample in a lower oxidation stage), were analyzed using several techniques such as Raman spectroscopy and X-ray photoelectron spectroscopy to identify more quantitatively the nature of the formed oxidized species. Also, the possible differences in shape and size of micro and nano MoS₂ were investigated using AFM and TEM, indicating similarity between the samples. Specifically, the morphological analysis of commercial micro- MoS₂ and nano- MoS₂ determined a lateral size in the nanoscale range for both products, while the analysis of their structure and chemical composition through Raman and XPS revealed high similarity between both pristine nanomaterials, but remarkable differences in the chemical composition of fresh and old water suspensions. In particular, the sample of nano- MoS₂ stored as aqueous suspensions were degraded faster, but in both cases 10 months old suspensions were highly enriched in a mixture of defected MoS_x species, and oxysulfides MoS_xO_y. Hence, adenocarcinomic human alveolar basal epithelial cells (A549 cells) and the unicellular fungus *S. cerevisiae* were used as biological models, to study cell viability and reactive oxygen species (ROS) production after the nanomaterial's exposure. Both MoS₂ nanoparticle types (old and fresh samples) induced sublethal damage on the A549 cells though the increase of intracellular ROS levels, while comparable concentrations reduced significantly the viability of yeast cells. In particular, the old nanoparticles suspensions samples exhibited a higher toxicity for both human and yeast cells than the fresh ones. Particularly, in A549 cells we have studied both the cellular viability using the Neutral Red

(NR) assay and the oxidative stress production using the DCFH-DA protocol. Specifically, the results obtained with NR showed that cells exposed to both types of fresh and old MoS₂ nanosheets (160 mg L⁻¹) exhibited the same viability as the negative control (non-treated cells). The same result was observed for the lower concentrations tested of the different nanoparticles suspensions, indicating that the viability of A549 cells is not negatively affected in the presence of micro-MoS₂ and nano-MoS₂, nor by their transformation and degradation products, at the studied conditions. In contrast, the results obtained from DCFH-DA assay to evaluate the ROS levels, demonstrated that cells exposed to old micro- and nano-MoS₂ displayed 3.6- and 3.1-times higher ROS levels respectively, than the non-exposed cells. The significant oxidative levels induced by the old samples suggest a mixture toxicity effect derived from the MoS₂ nanosheets transformation products. Moreover, a similar toxicological effect related to the presence of the aqueous transformed products of MoS₂ was observed in yeast cells. Specifically, a clear decrease on yeast viability (CFU assay) was observed in exposures of 24 h, being more drastic when cells were exposed to the old suspensions of both nanoparticle types. The toxicity provoked by micro-MoS₂ and nano-MoS₂ was comparable. Particularly, in the presence of 160 mg L⁻¹, the fresh nanoparticles suspensions induced a decrease on yeast viability of ~40%, while the presence of 800 mg L⁻¹ reduced the CFUs around 70%. In case of the old nanoparticles suspensions, 160 mg L⁻¹ reduced the yeast cells viability 50 to 60%, while in the presence of the higher concentration only 1% of the exposed cells survived. Moreover, the oxidative stress assay confirmed the

presence of high levels of ROS that could be linked to the drastic decrease on cellular viability of yeast. Precisely, the results obtained indicate that the fresh nanoparticles have a higher capacity to induce oxidative stress in yeast cells in comparison to the old nanoparticles, indicating that are not necessarily associated to the presence of ROS, at least at an early exposure stage of 2h. Henceforth, in this work, we have showed the fate of MoS₂ nanoparticles in aqueous suspensions and their toxicological impact on different biological systems at distinct material life cycle stages. Our findings demonstrate that the fate assessment of nanomaterials is a critical aspect to increase the understanding on their characteristics and on their potential impact on biological systems along their life cycle. Hence, the presented results (schematic representation showed in Table 2) highlight the relevance of analyzing the fate of nanomaterials at physico-chemical and toxicological level to increase the understanding on their characteristics and their potential impact on biological systems along their life cycle.

Table 2: Schematic representation of the toxic effects of micro and nano MoS₂ toward A549 cells and *S. cerevisiae*.

Results - A549 cells	Fresh micro MoS₂	Old micro MoS₂	Fresh nano MoS₂	Old nano MoS₂
Neutral Red	Not affected	Not affected	Not affected	Not affected
ROS	Not affected	Affected, ~ 3 times more ROS	Not affected	Affected, ~ 3 times more ROS

Results - Yeast	Fresh micro MoS₂	Old micro MoS₂	Fresh nano MoS₂	Old nano MoS₂
CFU 2h	Not affected	Not affected	Not affected	Affected: decreased cellular viability of ~ 20% at 800 mg L ⁻¹
CFU 24h	Affected: decreased cellular viability of ~ 40% at 160 mg L ⁻¹ and ~ 70% at 800 mg L ⁻¹	Affected: decreased cellular viability of 50- 60% at 160 mg L ⁻¹ and ~ 99% at 800 mg L ⁻¹	Affected: decreased cellular viability of ~ 40% at 160 mg L ⁻¹ and ~ 70% at 800 mg L ⁻¹	Affected: decreased cellular viability of 50- 60% at 160 mg L ⁻¹ and ~ 99% at 800 mg L ⁻¹

ROS 2h	Not affected at 160 mg L ⁻¹ Affected at 800 mg L ⁻¹ , almost 3 times more ROS	Not affected	Not affected at 160 mg L ⁻¹ Affected at 800 mg L ⁻¹ , almost 3 times more ROS	Not affected
--------	--	--------------	--	--------------

In the same chapter, we also focused on another rising star TMD nanomaterial, specifically we evaluated the potential toxicological impact of different commercial WS₂ nano-samples in aqueous dispersions with distinct lateral size. Firstly, due to the importance of a well physico-chemical characterization of layered nanomaterials, we studied the structure and stoichiometry of monolayer tungsten disulfide (WS₂-ACS-M) and nano size monolayer tungsten disulfide (WS₂-ACS-N) using Raman spectroscopy, while to study the formed oxidized species in the samples we performed X-ray photoelectron spectroscopy. The results of the performed analysis showed that the stoichiometry and structure of the tested nanomaterials are principally monolayers, composed by a combination of 1T'-WS₂, 2H-WS₂, WO₃ and SO₂ species. Secondly, we used similar cellular models tested in previous works such as (A549 cells) and the ecotoxicology model *Saccharomyces cerevisiae* to evaluate the potential cytotoxicity. The toxicological results in A549 cells, showed that the cellular viability (performed using Neutral Red assay) was not significant affected by the exposure to both WS₂-ACS-M (micro range scale) and WS₂-ACS-N (nano range scale) in aqueous suspensions provided by the ACS supplier. Moreover, both the commercial samples did not increase significantly the presence of intracellular ROS in human cells. However, the toxicological

impact it is different in the yeast cellular model. Specifically, both WS₂ suspensions were able to reduce yeast cell viability (CFU) at different concentration and exposure time. In particular, after 24 h exposure, cell viability decreased about 50% at 800 mg L⁻¹ when cells were exposed to WS₂-ACS-M and 60% when exposed to WS₂-ACS-N. However, their ability to trigger ROS production in this organism was very low after 2 and 24h, indicating that the oxidative stress pathway could not be involved in cellular death. Furthermore, the toxicity of a nano size 2D WS₂ commercialized in dry form from the same provider was similarly measured, demonstrating the ability to decrease yeast cells viability as well, in a lower percentage. Specifically, the commercial dry form WS₂ (namely WS₂-ACS-N-PW) determined the decrease on yeast cellular viability of 20% decreased at 160 mg L⁻¹ and 30% at 800 mg L⁻¹ after 24 h exposure. Moreover, significant oxidative stress production could be observed in the selected conditions. In conclusion, the experimental results achieved in the present research work show the physico-chemical properties and the potential toxicity of commercial 2D WS₂ aqueous suspensions and in dry form, when interacting with distinct eukaryotic organisms, showing differences in function of the biological system exposed. In Table 3, it is possible to observe all the toxicological results of the selected WS₂ commercial samples.

Table 3: Schematic representation of the toxic effects of commercial WS₂ samples in aqueous suspensions and in dry form toward A549 cells and *S. cerevisiae*.

Results – A549 cells	WS ₂ -ACS-M	WS ₂ -ACS-N
Neutral Red	Not affected	Not affected
ROS	Slight affected at highest concentration of 160 mg L ⁻¹	Slight affected at highest concentration of 160 mg L ⁻¹

Results - Yeast	WS ₂ -ACS-M	WS ₂ -ACS-N
CFU 2h	Not affected	Not affected
CFU 24h	Affected: ~50% cell viability decreased at 800 mg L ⁻¹	Affected: ~60% cell viability decreased at 800 mg L ⁻¹
ROS 2h	Slight capability to increase ROS productions	Slight capability to increase ROS productions
ROS 24h	Slight capability to increase ROS productions	Slight capability to increase ROS productions

Results - Yeast	WS ₂ -ACS-N-PW
CFU 2h	Not affected
CFU 24h	Affected: ~20% cellular viability decreased at 160 mg L ⁻¹ and ~30% at 800 mg L ⁻¹
ROS 2h	Significant ROS production
ROS 24h	Significant ROS production

In chapter 4, we analyzed the potential biocompatibility effects of BN nanoparticle, following a similar protocol and assays of the previous research articles presented in this thesis. First, we selected two commercial BN, namely BN-nanopowder (BN-PW) and BN-nanoplatelet (BN-PL), to identify possible alterations in the toxicological behavior in relation to the size and the shape of the particles selected and comparing the biological responses toward different cellular models. The possible toxicological effects of the BN samples under physico-chemical analysis, were investigated toward A549 cells and the unicellular fungus *Saccharomyces cerevisiae* as cellular models for *in vitro* assays. As we did in other previous research using different 2D nanomaterials, we firstly studied the physico-chemical features of the selected commercial samples. The structure analysis using AFM and TEM revealed that both BN products are present in aggregates with different shape with a round shape and 2D platelet-like shape. While XPS and Raman spectra confirmed the existence of the h-BN crystal phase within three-layers particles. Secondly, we performed several *in vitro* assays to identify possible alterations in oxidative stress and cell viability in both the eukaryotic cell selected. The experimental results, showed both BN samples exhibited a very low cytotoxicity toward human cells and yeast. No significant decrease on cell viability and increase of ROS production could be observed in A549 cells exposed to BN-PW and BN-PL. Similarly, in the cellular model *S. cerevisiae*, even at the highest concentration of 800 mg L⁻¹ and exposure time of 24 h, no adverse effects on the percentage of living cells and oxidative stress production was observed. In contrast, slight increase in oxidative stress production could be

observed at 2 h exposure. In conclusion, in this research study, our results indicate no meaningful differences between BN-nanopowder and BN-nanoplatelets, representing safe products at the concentration and exposure tested for the prospective future applications in the biomedical and environmental field. The results achieved in the present work provide novel insights of the toxicological impact of commercial BN samples in hexagonal structure on different biological cellular models. In Table 4 are represented all the toxicological results.

Table 4: Schematic representation of the low toxicity of commercial BN samples toward A549 cells and *S. cerevisiae*.

Results – A549 cells	BN nanopowder	BN nanoplatelets
Neutral Red	Not affected	Not affected
ROS	Not affected	Not affected

Results – Yeast	BN nanopowder	BN nanoplatelets
CFU 2h and 24h	Not significantly affected	Not significantly affected
ROS 2h and 24h	Slightly affected at 2h, not significantly affected at 24h	Slightly affected at 2h, not significantly affected at 24h

Conclusion

Two-dimensional nanomaterials are extensively seen as having huge potential, and are interesting considerable and increasing investments from governments and from industrial companies in many parts of the world. As a consequence, the study of the interaction of 2D nanomaterials with

biological and environmental living systems is a very essential research field, with results that update human health risk assessment providing safe material development for 2D material applications. This PhD thesis focuses on commercial 2D materials, both monolayer and few-layer forms, in different shapes and synthesized in diverse methods from several providers. The biological response to 2D nanomaterials differs significantly, in relation to the cellular model used and to their chemical diversity such as physico-chemical factors and the evaluation of their nanosafety is a challenge for any comprehensive assessment of their effects. The layered two-dimensional (2D) nanomaterials used in this work, such as graphene oxide (GO), transition metal dichalcogenides (TMDs) and boron nitride (BN), have fascinated incredible interest owing to their unique structural morphologies and outstanding physicochemical properties. Consequently, these nanomaterials have been vigorously explored for several different biomedical and environmental applications. However, one of the central aspects that is of significant attention and ought to be studied in vaster depth is their nanotoxicity and biocompatibility. As such, there is an urgent need to investigate and determine the nanotoxicological profiles of these layered nanomaterials in order to optimize and develop them for several applications. Here, in this PhD work, we have provided new insights *in vitro* toxicological results of different commercial layered nano-samples. First, two different samples of Graphene Oxide and Graphene Oxide nanocolloids were actively investigated to evaluate their potential toxicity, indicating that GO induces higher toxicity in the cellular model used. Specifically, both nanomaterials did not affect the cellular vitality of A549 cells, however

oxidative stress was observed in all the concentration tested. In contrast, both the cellular model of the yeast *S. cerevisiae* and the bacterium *V. fischeri* demonstrated adverse biological responses after the exposure to GO and GOC. In particular, yeast cells produced high levels of ROS within decrease of cellular viability and the bacterium *V. fischeri* significantly inhibited the production of bioluminescence. Second, we focused on the study of the toxicological effects of micro and nano MoS₂, using similar cellular models such as A549 cells and the yeast *S. cerevisiae*, showing the higher toxic effects of oxidized MoS₂ samples toward *S. cerevisiae*. In particular, the higher the oxidation stage of both micro and nano MoS₂ and the higher the toxicological effects, particularly in yeast cells. Third, we evaluated the toxicity of WS₂, another TMD nanomaterial, toward human cells and yeast indicating differences in the biological responses in relation to the commercial samples and the preparation of the sample as a aqueous suspensions provided by the supplier or dry form prepared in our laboratory. Specifically, all the WS₂ commercial sample tested did not induce significant cellular viability in human cells. Moreover, low levels of ROS were observed in similar conditions, revealing slight dissimilarities toward the WS₂ samples tested in A549 cells. Furthermore, dissimilarities could be observed using *S. cerevisiae* as eukaryotic model. Specifically, the same commercial products of WS₂, importantly affected the cellular viability and production of ROS. And finally, we focused of the study of the biocompatibility effects of boron nitride (BN) nano-powder and nanoplatelets, showing a very negligible toxic effects toward the selected eukaryotic cells of A549 and yeast, even at the highest concentration and exposure time. Henceforth, in

this research thesis, the diverse physicochemical features determining the biocompatibility or nanotoxicological effects of these commercial nanomaterials, such as lateral size, morphology, concentration, exposure time, oxidation state, purity, method of preparation of the providers, cellular model, have been intensively evaluated. Conclusively, this work proposes new toxicological results for seeking a more understanding of the biological effects based on fundamental physico-chemical characteristics and cellular type biological response.